DEVELOPMENT OF PROTECTION SCHEMES FOR MICROGRIDS WITH INTEGRATED BATTERY ENERGY STORAGE

Thesis

Submitted in partial fulfilment of the requirements for the degree of

DOCTOR OF PHILOSOPHY

by

ANN MARY JOSHUA

DEPARTMENT OF ELECTRICAL AND ELECTRONICS ENGINEERING,

NATIONAL INSTITUTE OF TECHNOLOGY KARNATAKA,

SURATHKAL, MANGALORE - 575025

APRIL 2023

DECLARATION

by the Ph.D. Research Scholar

I hereby declare that the Research Thesis entitled **DEVELOPMENT OF PROTECTION SCHEMES FOR MICROGRIDS WITH INTEGRATED BATTERY ENERGY STORAGE** which is being submitted to the National Institute of Technology Karnataka, Surathkal in partial fulfilment of the requirements for the award of the degree of **Doctor of Philosophy** in **Electrical & Electronics Engineering** is a bonafide report of the research work carried out by me. The material contained in this Research Thesis has not been submitted to any University or Institution for the award of any degree.

Register Number: 187085EE003, Ann Mary Joshua

Department of Electrical & Electronics Engineering

Place: NITK-Surathkal

Date: 12-04-2023

CERTIFICATE

This is to certify that the Research Thesis entitled **DEVELOPMENT OF PROTECTION SCHEMES FOR MICROGRIDS WITH INTEGRATED BATTERY ENERGY STORAGE** submitted by **Ann Mary Joshua** (Register Number: **187085EE003**) as the record of the research work carried out by her, is accepted as *the Research Thesis submission* in partial fulfilment of the requirements for the award of the degree of **Doctor of Philosophy**.

12/4/2023

Dr. K. Panduranga Vittal
(Research Guide)

13/4/2023

Dr. Dattatraya N. Gaonkar
(Chairman-DRPC)

ASSOC. PROFESSOR & HEAD
DEPT. OF ELECTRICAL & ELECTRONICS ENGINEERING
NATIONAL INSTITUTE OF TECHNOLOGY KARNATAKA
SURATHKAL SRINIVASNAGAR P.O., MANGALORE-575025

Acknowledgement

First of all, I thank Lord Almighty for his countless blessings, granting me knowledge and perseverance in accomplishing this thesis.

I offer my sincere gratitude to my research supervisor Prof. K. Panduranga Vittal, for giving me an opportunity to pursue the Ph.D. degree under his supervision. I am deeply indebted to him for his unrelenting support, encouragement and counsel throughout this process. I also thank him and Prof. K. Manjunatha Sharma for the Centre of Excellence in Smart Grid Technologies(COE-SGT) facilities.

I extend my sincere gratitude to the Department of Technical Education (DTE), Kerala for granting me three years of leave under QIP and AICTE for the financial assistance.

My heartfelt thanks to the research progress assessment committee (RPAC) members, Dr. Prajof P and Dr. Rathnamala Rao, for their constructive comments, support and encouragement. I fondly acknowledge the help from Dr. Dattatraya N. Gaonkar, Prof. Gururaj S Punekar, Prof. Shubhanga K N and Prof. Venkatesa Perumal during their tenure as the Head of the Department. I am grateful to all teaching and non-teaching faculty of EEE department, NITK for their assistance.

I acknowledge the help received from my fellow research scholars at NITK. I am immensely thankful to my friend Mr. James Antony Pinto for his help, discussions, and valuable suggestions. Thanks to my seniors, Dr. M. Mohan, Dr. Prakash Pawar and Dr. Nisha B Kumar, for their timely advice and help. I also thank my M.Tech friends Mr. Poirei, Ms. Pooja, Mr. Ravi Teja and Mr. Sayantan for their cooperation.

I am deeply indebted to my parents, Joshua George and Annamma Kurien, whose love, care and words of encouragement keep my spirits high throughout. I thank my in-laws and siblings for standing by me throughout this journey. I also express my love and thanks to my children, Johan and Jiya. I thank my husband, Mobby Thomas, for his patience, support and continuous encouragement throughout this journey.

Abstract

Energy storage is a vital component of a resilient microgrid. Though storage will solve all problems related to power mismatches between generation and loads, it brings additional challenges. Due to the bidirectional power flows, control and protection become complicated. The control, as well as the fault behaviour of the microgrid, varies with microgrid mode of operation, demanding adoption of new control and protection strategies.

The initial part of the thesis focus on transient behavioural modelling of a LV microgrid with a centralised battery energy storage system (BESS). All the inverters are operated in grid following mode in the grid connected mode of microgrid operation. In the islanded operation, the BESS will act as the grid forming inverter. Consequently, AC fault analysis of the microgrid is carried out. The magnitude and direction of fault current from microgrid feeders are seen to vary and is influenced by the following factors: (i) inverter controller (ii) microgrid mode of operation (grid connected or islanded) (iii) BESS mode (charging or discharging) (iv) fault resistance (v) DERs connected (vi) fault distance (vii) loading level and (viii) fault type. Due to the restrictions imposed by power electronic switches, the fault currents in Inverter Interfaced Distributed Generators(IIDGs) are limited. The non-linear controllers of inverters alter the fault responses in many ways. The stringent PQ controller of BESS will not allow it to dissipate into a fault during its charging mode, causing the conventional directional schemes to maloperate. Hence, legacy protection schemes are not suitable for microgrids.

Later chapters attempted to develop protection strategies for AC microgrid feeders that are not impacted by the above factors. Adaptive protection strategies and differential schemes that do not require adaptive settings are proposed in this thesis. The performance of proposed strategies are tested for different fault scenarios by carrying out simulations in MATLAB/SIMULINK software.

The final part of this thesis investigated the fault characteristics of a ring type LVDC microgrid. In the transient stage of DC faults, there can be very high currents and severe dc link voltage variations. The dc link capacitors of the Voltage Source Inverters or DC-DC converters may discharge quickly leading to collapse of dc link voltage. Though the self protection circuits in DC-DC converters can lock the gate pulses to IGBT switches, large currents will freewheel through the antiparallel diodes. This is then followed by grid or source feeding stage (steady state) that will cause grid or other sources to feed large fault currents through antiparallel diodes in the VSI or DC-DC converters. The protection devices (PD) at AC side can access fault currents only at this stage. Hence it is imperative that DC network protection act in the transient stage itself to avoid damages to the converter. A fault localisation scheme based on transient signals is also proposed for ring type DC microgrids. This scheme can interrupt the faulty section accurately in the transient stage itself. The efficacy of proposed schemes are validated by extensive simulations.

Keywords: Battery Energy Storage Systems, Microgrid, Fault Detection, Differential, Directional, Adaptive

Contents

List of Figures v

List of Tables ix

List of Abbreviations xi

1 Introduction 1

1.1 Overview 1
1.2 Microgrid Architectures 2
1.2.1 Role of Energy Storage Systems (ESS) in Microgrids: 3
1.3 Microgrid Control 4
1.3.1 State of the art on Inverter Control Strategies 4
1.4 Research Motivation 6
1.5 Research Objectives 7
1.6 Organisation of the thesis 7

2 Literature Survey 11

2.1 Introduction 11
2.2 Review of challenges in AC microgrid protection 11
2.3 Review of AC microgrid protection solutions 14
2.3.1 Adaptive protection: 14
2.3.2 Overcurrent protection: 16
2.3.3 Directional protection: 17
2.3.4 Voltage based protection: 19

2.3.5 Differential protection: 19
2.3.6 Hybrid protection schemes: 21
2.4 Review of challenges in DC microgrid protection 22
2.5 Review of DC microgrid protection solutions 24
2.5.1 Unit protection methods 25
2.5.2 Local measurement methods 26
2.6 Inferences 27

3 Transient Behavioural Modelling of Microgrids supported by Battery Energy Storage System 29
3.1 Introduction 29
3.2 Microgrid Topology 29
3.3 Simulation Studies 32
3.3.1 System Response under different loads 32
3.3.2 Fault Analysis 35
3.4 Inferences 41

4 Development of Protection Schemes for an AC microgrid 43
4.1 Introduction 43
4.2 Adaptive Protection Schemes 44
4.2.1 Protection Principle 44
4.2.2 Proposed Protection Schemes 46
4.2.3 Results and Discussions 49
4.3 Superimposed Current Based Differential Protection Scheme 64
4.3.1 Protection Principle 64
4.3.2 Proposed Protection Scheme 67
4.3.3 Results and Discussions 71
4.4 Inferences 84

5 Development of an Incremental Transient Power Based Protection Scheme for a DC Microgrid 87
5.1 Introduction 87

5.2 Microgrid Topology 88
5.3 Fault Analysis 88
5.4 Proposed Protection Scheme 91
    5.4.1 Startup Unit 91
    5.4.2 Direction Identification Unit 92
    5.4.3 Fault Localisation 94
5.5 Results and Discussions 96
    5.5.1 Selection of Inc. Transient Power Threshold 96
    5.5.2 Effect of fault on various line segments 96
    5.5.3 Performance under Close-In Faults 98
    5.5.4 Performance under High Impedance Faults (HIF) 99
    5.5.5 Performance with Noisy Signals 100
    5.5.6 Performance under External Faults 101
    5.5.7 Performance under No Fault cases 102
    5.5.8 Comparative evaluation of the proposed scheme with existing methods 103
5.6 Inferences 104

6 Conclusive Remarks and Scope for Future Work 107
6.1 Key points emphasized in the thesis 107
6.2 Major contributions 109
6.3 Scope of future work 110

Appendix A AC Microgrid Parameters 127

Appendix B DC Microgrid Parameters 129

Appendix C List of Publications 131

List of Figures

1.1 Simplified representation of grid connected inverters 5

2.1 Schematic of differential protection. 20

3.1 Microgrid topology. 30
3.2 BESS components and its control. 31
3.3 DC link voltage / PQ control 31
3.4 V/F control 32
3.5 Case 1: $P_L > P_{PV}$ 33
3.6 Case 2: $P_L < P_{PV}$ 34
3.7 Test microgrid for fault study. 35
3.8 LL fault performance when BESS is charging 36
3.9 LL fault performance when BESS is discharging 37
3.10 SLG fault performance when BESS is discharging 38
3.11 LLLG fault performance when BESS is charging 39
3.12 AG fault response of PQ controlled BESS 41
3.13 Phasor plots for AG fault 41

4.1 Positive sequence networks 45
4.2 Proposed logic of MPU 47
4.3 Test microgrid - 1. 50
4.4 Case1: MPU performance for a LLLG fault in GCM 52
4.5 Case2: MPU performance for an SLG fault in IM 53

4.6 Case3: MPU performance for a LLLG fault in GCM and BESS voltage controlled . . . 54
4.7 Case4: Performance in the presence of decaying DC component 55
4.8 Case5: Performance under far and near end faults . . . 56
4.9 Test microgrid - 2. . . . 57
4.10 The Emmanuel arc model. . . . 57
4.11 Case 6: Performance under HIF . . . 58
4.12 Adaptive settings of relay R13 . . . 59
4.13 R31 pickup adapting to system changes in AOC scheme. . . . 60
4.14 Performance of TE based schemes . . . 63
4.15 Internal fault in a microgrid feeder. . . . 65
4.16 Locus diagram of an unbalanced system in rotating dq0 coordinates. . . 66
4.17 dq currents under HIF . . . 67
4.18 Schematic of proposed differential protection. . . . 68
4.19 IED relay hardware architecture. . . . 69
4.20 Microgrid topology. . . . 71
4.21 Case1: Internal BC fault in GCM . . . 72
4.21 Internal BC fault in GCM . . . 73
4.22 Case2: Internal AG fault in IM . . . 74
4.22 Case2: Internal AG fault in IM . . . 75
4.23 Case3: Internal ABCG fault when BESS is voltage controlled and grid connected . . . 76
4.24 Case4: Performance in the presence of decaying DC component 77
4.25 Case5: Performance under far and near end faults . . . 78
4.26 Case6: Performance under HIF . . . 79
4.27 External fault with CT saturation . . . 80
4.28 Internal AG fault with different inception angles. . . . 81
4.29 Internal AG fault with varying PV penetration levels. . . . 81
4.30 Non-fault disturbances . . . 82
4.31 Operating currents with different window lengths. . . . 84

5.1 DC Microgrid Topology. 88

5.2 Equivalent Circuit of a VSC under fault. 89

5.3 DC Fault Response of VSC 90

5.4 Fault responses at various DG buses for F1 fault 91

5.5 Forward Fault with respect to IED 1.2.p. 92

5.6 Reverse Fault with respect to IED 1.2.p. 93

5.7 Schematic of the feeder protection scheme. 94

5.8 Flow chart of the local measurement scheme. 95

5.9 $|\Delta P|$ computed by IED 3.4 for various disturbances. 97

5.10 I,V and ΔP seen by various relays for a PP fault at F1 97

5.10 I,V and ΔP seen by various relays for a PP fault at F1 98

5.11 Forward Close-in Faults: (a) & (b) and Reverse Close-in Faults: (c) & (d) 99

5.12 High Impedance Faults. 99

5.13 Effect of noisy signals. 101

5.14 ΔP of IEDs 3.2.p and 3.4.p for F3 (External) fault. 102

5.15 Validation of proposed scheme. 104

List of Tables

2.1 Adaptive Overcurrent, Directional and Differential protection solutions . 18

4.1 Performance of the proposed schemes for various faults 61
4.2 Direction Assesed for Internal Fault (F1) - Comparison 62
4.3 Comparative Assessment for F1 fault with $R_f = 0.05\Omega$ 64
4.4 Comparison of differential schemes 83

5.1 Performance of the proposed scheme with different fault types and fault resistances 100
5.2 Performance of the proposed scheme with different fault distances . . . 100
5.3 Performance of the proposed schemes for faults at various locations . . 102
5.4 Comparison of proposed method with existing protection schemes . . . 104

List of Abbreviations

AC	Alternating Current
AOCR	Adaptive Over Current Relays
BESS	Battery Energy Storage System
CB	Circuit Breaker
CCU	Central Computation Unit
CHP	Combined Heat and Power
CMV	Common Mode Voltage
CSI	Current Source Inverter
DC	Direct Current
DER	Distributed Energy Resource
DG	Distributed Generator
DMS	Distribution Management System
DOCR	Directional Over Current Relays
EMTDC	Electro Magnetic Transients including DC
GCM	Grid Connected Mode
GPS	Global Positioning System
HIF	High Impedance Fault
HVDC	High Voltage Direct Current
IC	Interlinking Converter
IEC	International Electrotechnical Commission
IEEE	Institute of Electrical and Electronics Engineers
IIDG	Inverter Interfaced Distributed Generator

IM	Islanded Mode
LIF	Low Impedance Fault
LL	Line to Line
LLG	Double Line to Ground
LV	Low Voltage
LVDC	Low Voltage Direct Current
LVRT	Low Voltage Ride Through
MCPU	Main Central Protection Unit
MGCC	Microgrid Central Controller
MMS	Microgrid Management System
MPR	Microgrid Protection Relay
MPU	Main Protection Unit
MV	Medium Voltage
NPG	Negative Pole-Ground
NPS	Negative Phase Sequence
NSIA	Negative Sequence Impedance Angle
NSQ	Negative Sequence
OC	Over Current
PCC	Point of Common Coupling
PD	Protection Device
PG	Pole-Ground
PLL	Phase Locked Loop
PMU	Phasor Measurement Unit
PP	Pole-Pole
PPG	Positive Pole-Ground
PPS	Positive Phase Sequence
PPU	Probe Power Unit
PSCAD	Power System Computer Aided Design
PSFC	Positive Sequence Fault Current
PSQ	Positive Sequence

PV	Photovoltaic
RES	Renewable Energy Resource
SG	Synchronous Generator
SLG	Single Line to Ground
SOC	State of Charge
SRE	Superimposed Reactive Energy
SSCB	Solid State Circuit Breaker
STG	Setting Groups
TE	Transient Energy
VPP	Virtual Power Plants
VSM	Virtual Synchronous Machine
VSI	Voltage Source Inverter
WTG	Wind Turbine Generator
ZSQ	Zero Sequence

List of Nomenclature

List of Symbols

i	Instantaneous currents
v	Instantaneous voltages
I	Current phasor
V	Voltage phasor
R	Resistance
L	Inductance
C	Capacitance
P	Output active power
Q	Output reactive power
f	Frequency
w	Angular frequency
t	Sampling time
T	Time period
Δ	Incremental or Superimposed
η	Turbine efficiency (%)

List of Subscript

d	Variables in d axis in dq frame
q	Variables in q axis in dq frame
F	Fault variable
pre	Pre-fault variable

ref	Reference values
abc	Three phase variables in phase a, b and c
s	sampling/switching variable
th	threshold variable
g	Variables related to PCC
mov-av	Moving average
1	Variables in positive sequence network
2	Variables in negative sequence network
0	Variables in zero sequence network
N	Number of samples per cycle
op	Operating
res	Restraining

Chapter 1

Introduction

1.1 OVERVIEW

Microgrids are the building blocks of future power grids or smart grids. The US Department of Energy (DOE) defines a microgrid as “a group of interconnected loads and distributed energy resources (DER) with clearly defined electrical boundaries that acts as a single controllable entity with respect to the grid. It can connect and disconnect from the grid to enable operation in both grid-connected or island modes”.

The microgrid is an evolving concept that has led to many paradigm shifts. One is centralised to decentralised generation. A microgrid facilitates the integration of distributed generators(DG) and cogeneration. Large scale integration of renewable energy resources will contribute to the reduction of greenhouse gases. The generation will not follow load in a microgrid as in traditional grids. Instead, consumption will follow generation. The utility will attempt to maximise the generation using available assets, conserve them (energy storage) and manages the load demand at peak (load control). The legacy grid has a top down architecture with power flowing from the generation side to distribution systems. But with the evolution of microgrids, the distribution side becomes active. Since the DGs are connected close to the load, the transmission losses and network congestions will be reduced. The possibility of power supply interruptions of end consumers connected to a low voltage (LV) distribution grid diminishes as the microgrids can operate in islanded mode at the time of power system. Thus, microgrids can increase reliability and resilience of the grid. Digitilaised controls and communication are other hallmarks of a microgrid.

Many microgrid projects have been deployed around the world over the last few years. Some examples are Illinois Institute of Technology Microgrid, USA [Shahidehpour (2014)], Sendai Microgrid, Japan [Hirose (2013)], off-grid microgrids: Gaidouromantra Microgrid in Kythnos island, Greece [Tselepis (2012)] and Isle of Eigg Microgrid in Scotland [Chmiel and Bhattacharyya (2015)].

1.2 MICROGRID ARCHITECTURES

The major components of microgrids are DERs, loads(critical or non-critical) and controllers. The DERs include distributed generators such as wind turbines, photovoltaic arrays, fuel cells, and distributed energy storage devices like flywheels, batteries, supercapacitors, compressed-air systems. There are mainly three categories of microgrid architectures in distribution [Patrao et al. (2015)]. They are AC microgrids, DC microgrids and Hybrid AC-DC microgrids.

AC microgrids: These microgrids consist of AC feeders only; hence compatible with existing distribution grid. All DGs, ESS and loads are integrated into the microgrid using an AC interface (inverters and back-back converters). The microgrid is connected to the main grid at the point of common coupling (PCC) via a static switch.

DC microgrids: These microgrids support only DC loads and if AC loads are to be connected, it requires an additional converter. They are connected to grid through a bidirectional DC/AC converter. If there is excess power at DC microgrid, it can be exported to grid and vice-versa. The Distributed Generators (DGs) and storage units can be easily integrated in to DC microgrids with reduced power conversion stages. The main disadvantage of DC microgrid is that the series connected IC has to handle the whole power flow between dc microgrid and grid; thus reliability is reduced. The present distribution grids are not compatible with DC microgrids. A DC microgrid can be interfaced to an AC grid in different architectures[Kumar et al. (2017)].

- Radial Configuration
- Ring or Loop Configuration
- Interconnected Configuration - DC microgrid is connected to AC supply at multiple points

Depending on the voltage polarity, DC microgrids are further classified as Unipolar and Bipolar microgrids. In unipolar microgrids, power is transmitted at one voltage level. Whereas bipolar DC microgrids give the flexibility to connect the consumer loads to three voltage levels +V_{dc}, -V_{dc} and 2 V_{dc}.

Hybrid AC-DC microgrids: Hybrid microgrids integrate both DC and AC feeders. They combine the advantages of AC and DC microgrids. ESS/DGs can be integrated to either AC or DC feeder, so that power conversion stages are reduced. It can support both AC and DC loads. However, maintaining power balance between ac and dc networks is challenging and there are many roadblocks to its practical implementation.

1.2.1 Role of Energy Storage Systems (ESS) in Microgrids:

Energy Storage Systems are crucial elements for a resilient microgrid. During the transition to islanded mode at grid outages, ESS can provide instant power and thus regulate voltage and frequency and maintain power quality. In standalone mode, the ESS strives to maximise the microgrid's operating duration. Incorporating a storage system with DGs will create a dispatchable source that can follow commands of MGCC to contribute additional generation (discharging), or balance generation with electricity demand (charging). Apart from providing ancillary services, the benefits of incorporating ESS [Kocer et al. (2019), Sufyan et al. (2019)] are peak shaving, energy management, load levelling, transmission and distribution(T&D) upgrade deferral, frequency regulation, voltage regulation, Low Voltage Ride Through (LVRT), reactive power support, demand response, reliability improvement and energy arbitrage. In islanded microgrids, ESS increases the fault current feeding capability [Laaksonen (2010)].

Tesla's grid level energy storage (150MW/194MWh, Li-ion battery) at Hornsdale Power Reserve (HPR), South Australia and Vistra Energy's (300MW/1200MWh, Li-ion battery) Moss landing energy storage facility at California are some representative examples.

1.3 MICROGRID CONTROL

There are two approaches for microgrid control - Centralised and Decentralised. Centralised control relies on data gathered in a dedicated central controller that performs required control actions for all units at a single point, requiring extensive communication between central controller (CC) and controlled units. In a decentralised control, each unit is controlled by its local controller (LC). It receives only local information and is not aware of system vide variables or other controllers action. Due to the extensive communication and computation needs, a fully centralised approach is not feasible for interconnected power systems. A fully decentralised approach is also not preferred due to strong coupling between operation of various units in a power system. A compromise between these two approaches is achieved by hierarchial control scheme consisting of three levels. The primary control stabilises the voltage and frequency after an islanding event, offers plug and play capability for DERs and shares active and reactive power. The main objectives of the secondary control are to restore the microgrid voltage and frequency, power quality improvement and synchronization between the microgrid and main network. The tertiary control manages power flow between microgrid and main grid and is responsible for coordinating the operation of multiple microgrids[Fathima et al. (2018)].

1.3.1 State of the art on Inverter Control Strategies

There are two common control modes for Inverter Interfaced Distributed Generators (IIDGs): grid following (current control) and grid forming (voltage control). Grid following inverters are synchronised with the grid through PLL. The voltage and frequency are dictated by the grid and microgrid performs only ancillary services. They export active and reactive power as specified by the power references [Rocabert et al. (2012), de Souza and Castilla (2019), Zuo et al. (2021)]. Hence they behave as power controlled current sources as represented in Fig. 1.1a.

The grid forming control finds application in islanded mode of operation. In the absence of grid, the grid forming inverter will determine the voltage and frequency.

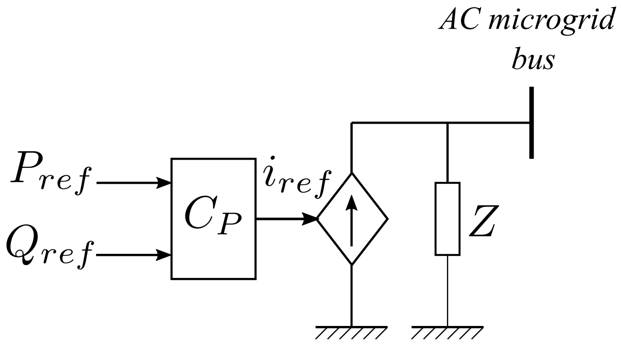
AC microgrid bus
P_{ref}
Q_{ref}
C_P
i_{ref}
Z

(a) Grid following (PQ control)

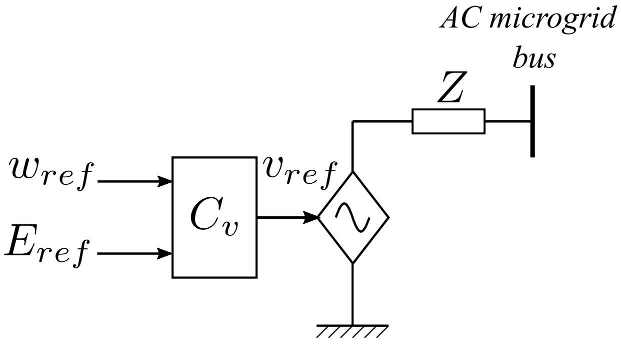
AC microgrid bus
Z
w_{ref}
E_{ref}
C_v
v_{ref}

(b) Grid forming (V/F control)

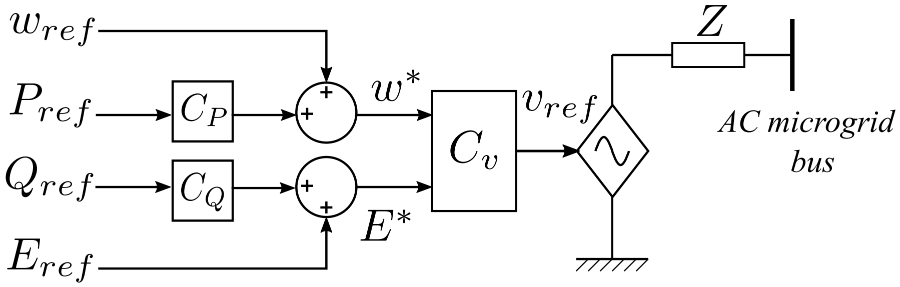
w_{ref}
P_{ref}
Q_{ref}
E_{ref}
C_P
C_Q
+
+
+
+
w^*
E^*
C_v
v_{ref}
Z
AC microgrid bus

(c) Grid forming (Droop control)

Figure 1.1: Simplified representation of grid connected inverters

They are represented in steady state by an ideal voltage source with a low output impedance as in Fig. 1.1b. A grid following inverter cannot energise an islanded microgrid because they require grid frequency. Whereas, grid forming inverters in Fig. 1.1b are specifically designed for islanded mode of operation.

In Droop control, each DG will deliver active and reactive power based on frequency and voltage droop characteristics and thus contribute to grid frequency and voltage regulation. Grid forming inverters with droop control are represented by an ideal voltage source in series with a link impedance in steady state as shown in Fig. 1.1c. Virtual impedance can be included in the voltage references initially generated by the droop characteristics to impart inertia to the grid forming inverters. These inverters mimic the behaviour of synchronous machines and are hence called Virtual Synchronous Generators [Liu et al. (2016)].

1.4 RESEARCH MOTIVATION

The performance of implemented projects ascertains that microgrids improve resilience, reliability, generation flexibility, energy security and efficiency. Renewable energy and storage technologies have witnessed tremendous growth in recent years. The cost of renewable energy and battery technologies is dwindling. The coming years will witness large scale deployment of community microgrids. However, microgrids affect the operating pattern of power system scenario. With large scale penetration of renewables, which are mostly stochastic, maintaining power balances is difficult in islanded mode. As a majority of the DERs are electronically interfaced, system inertia is much lower in microgrids than in traditional power systems, leading to control, stability, and protection issues.

The microgrids are mostly installed at the distribution level. The protection devices (PDs) conventionally used in distribution grids are fuses and reclosers based on current magnitude. These devices are unreliable, as a microgrid is susceptible to dynamic changes and there can be large variations in the short circuit current. The distribution side becomes active with bidirectional power flows. The fault behaviour of microgrids with IIDGs is significantly different from traditional grids which are dominated by synchronous machine based generation.

Many researchers have addressed the above concerns by proposing new protection schemes. Nevertheless, no commercial relay is available for microgrid protection [Hooshyar and Iravani (2017)]. Further, most of these schemes were validated on feeders integrating PV or machine based DGs. These schemes have not analysed their performance when IIDGs are PQ controlled and reference power is negative. There are very few protection studies on microgrids integrating Battery Energy Storage Systems(BESS). Considering this, a BESS based microgrid with different inverter controller strategies is used in this study.

Low voltage DC (LVDC) microgrids possess numerous benefits compared to AC microgrids. However, their application is restricted due to many challenges; mainly related to protection. During faults, DC microgrids are exposed to severe transients. Unlike AC which uses phasors, DC system uses sampled values. Hence, determination of exact fault location and its selective isolation in the transient period itself is challenging.

The research methodology adopted in this thesis is as follows. Fault behavioural studies are performed on AC and DC microgrids using PSCAD/EMTDC models. Based on the transient studies, reliable protection schemes are proposed for fault location in AC and DC microgrids. The performance of proposed method is tested for different fault scenarios by carrying out simulations in MATLAB/SIMULINK software. The proposed schemes require low bandwidth communication and are driven by cost factor, as it is not economical to invest in distribution networks like in transmission networks.

1.5 RESEARCH OBJECTIVES

Based on the literature survey and assessed research gaps (presented in the upcoming chapter), the goals of the research work are listed below

- To model a low voltage microgrid with a centralised Battery Energy Storage System and to investigate its transient behaviour under AC and DC faults
- To investigate the impact of existing relaying schemes on the microgrid and propose practical protection strategies for microgrid feeders that are effective in both operational modes of the microgrid.
- To develop transient signal based protection schemes for VSC based DC microgrids.

1.6 ORGANISATION OF THE THESIS

This thesis is organized into seven chapters. The contents of each chapter is briefly outlined in this section.

- **Chapter 1:** This introductory chapter presents an overview of microgrid systems - architectures and control strategies. The motivation for the research, objectives and the structure of the thesis is also discussed.

- **Chapter 2:** This chapter presents a review of challenges associated with the protection of AC and DC microgrids. Also includes a survey of literature in AC and DC microgrid protection.

- **Chapter 3:** This chapter elaborates on the modeling and control of studied microgrid topology. Simulation studies are conducted at steady state and transient conditions. The role of BESS in mitigating microgrid power fluctuations is highlighted by case studies. This chapter also discusses the fault behaviour of IIDG feeders with different control strategies. Simulation studies affirm the inability of traditional schemes to offer reliable microgrid protection.

- **Chapter 4:** Adaptive protection strategies for microgrids are proposed in this chapter. The simulation studies in the previous chapter showed that conventional direction assessment methods fail with BESS integration. A direction estimation scheme is proposed for microgrid feeders with integrated storage. The assessed direction at either end of feeder is compared in the main protection unit (MPU) to detect a fault. This scheme mainly relies on the magnitude and phase angle of superimposed positive sequence impedance. An adaptive backup overcurrent relay is also proposed in this chapter.

  This chapter also presents a current only differential protection scheme for microgrids that does not require any adaptive settings. The operating phasor is computed from dq components of superimposed currents; instead of conventional Fourier algorithms.

- **Chapter 5:** In this chapter, fault analysis of an LVDC microgrid is presented. This chapter demonstrates the need for interrupting DC faults in the transient stage itself. An incremental transient power based protection scheme that effectively isolates the faulty section is presented and validated on a ring type DC microgrid.

- **Chapter 6:** This chapter draws together the conclusions and scope for future work. The contributions of the thesis are highlighted again in this chapter.

Chapter 2

Literature Survey

2.1 INTRODUCTION

This chapter presents a detailed review of the challenges in protection of AC and DC microgrids. A comprehensive review of the available protection solutions for AC and DC microgrids is also presented. The research gaps are identified and the need for further studies in microgrid protection is presented in Section. 2.6.

2.2 REVIEW OF CHALLENGES IN AC MICROGRID PROTECTION

Traditional protection schemes assumed radial network structure with unidirectional power flows and large fault currents. However, with the integration of DERs, the network configurations have become complex. Traditional devices like fuses, reclosers and overcurrent relays are no longer applicable. The protection schemes must be capable of detecting faults in both modes of microgrid operation - grid connected mode(GCM) and islanded mode(IM). Identifying the exact location of fault is critical in microgrids. If the fault is within the microgrid, the faulty section must be isolated at the earliest. For external faults, microgrids are required to abide by the LVRT requirements. As per IEEE 1547 (2018), DERs outside the fault zone need a minimum ride-through programmed ($\geq$160 ms).

Variations in fault current level: In GCM, grid will provide sufficient fault current to activate the overcurrent relays. But in standalone mode, the fault current is contributed by low capacity DERs only. The synchronous generator based DGs can contribute five times the rated current. Whereas the fault current in IIDGs is limited to twice the rated current due to the restrictions imposed by power electronic switches [Zamani et al. (2014), Nimpitiwan et al. (2007)].

There are several other factors like microgrid mode of operation, inverter control strategy, DER penetration, battery state of charge (SOC) [Manson and McCullough (2021)], fault resistance and location of grid forming DERs which affect the fault current[Jain et al. (2019), Laaksonen (2010)]. Overcurrent relays find limitations, as the settings have to be varied with different operation modes. Even with adaptive settings, the chances of nondetection of faults are high.

Bidirectional flow of current: Directional Over Current Relays (DOCR) are normally employed for fault location identification. With the integration of multiple DGs and BESS in a microgrid, power can flow in either direction. The direction reversal can occur during mode switchings as well (from grid connected to standalone mode or vice versa)[Jain et al. (2019)]. Hence fault identification using directional relays is challenging.

Dynamic changes in microgrid architecture: A microgrid is susceptible to dynamic changes as it supports plug and play feature of DGs and loads connection/disconnection. The protection system must not act during these changes.

Protection Miscoordinations: Integration of a DG in a conventional grid can lead to many protection miscoordinations such as

1. Sympathetic/false tripping - When a DG tries to feed an outside fault via a healthy feeder, the relay in a healthy feeder can trip [Papaspiliotopoulos et al. (2014)].

2. Protection blinding - Due to the fault contribution from a DG, the fault current seen by the relay in fault path reduces. Thus fault may remain undetected [Naveen and Jena (2017)]

3. Coordination issues - DGs will affect the maximum and minimum fault currents, leading to coordination issues between PDs[Brahma and Girgis (2004)].

Effect of inverter controllers: In current mode, controllers maintain the output current at target level by adjusting the internal voltages of inverters. Hence the fault current from current controlled inverters will be limited and balanced even during an asymmetrical fault. Whereas in voltage mode, the fault behaviour is similar to synchronous alternators[Shuai et al. (2018)]. The effect of current controlled inverters can be summed up as

- Reduction in fault current level.
- Absence of negative sequence components in fault current even during asymmetrical faults
- The phase angle of fault currents is determined by the inverter controller. During faults in GCM, as grid provides voltage support, DG units operate with a power factor close to unity. Whereas in IM, DGs may be required to provide reactive power support and operate with a lower power factor [Hooshyar and Iravani (2017)].

Fault Classification: The conventional fault classification techniques are based on current magnitude and sequence components. Since the output currents from current controlled inverters are balanced and lack negative sequence components, fault type identification is challenging. Many of the present day controllers suppress negative sequence components intentionally to improve the transient response.

When IIDGs are interfaced via a dYg isolation transformer, the faulted phase current may be lower than the healthy phase. This is because the zero sequence components add up with the respective positive sequence components [Hooshyar and Iravani (2017)]. The net current is determined by the angle between sequence components, which depends on the operating power factor of IIDG. Mishra et al. (2020) has demonstrated a BC-G fault case in which the faulted phase(B) current is lower than the healthy phase (A) for upf operation. Whereas, for zpf operation, the faulted phases have higher currents.

Effect of Grounding: There are ungrounded, unigrounded and multi grounded microgrid configurations. Zero sequence components will be available in IM only if the microgrid is grounded. If there are multiple DERs interfaced to microgrid via grounded transformer, zero sequence currents may circulate in the microgrid leading to protection mis-coordinations [Moon et al. (2013)]. The fault current is thus dependent on the interconnecting transformer configurations.

Lack of inertia: Integration of many converter-based renewable sources in a power system reduces system inertia significantly [Yap et al. (2019), Teimourzadeh et al. (2019)] and may be an issue to traditional power swing blocking settings/ principles.

Effect of renewable infeeds and short feeder lengths: The accuracy of impedance calculations and consequently the reach of distance relays may get affected by intermediate renewable infeeds [Voima and Kauhaniemi (2014),Telukunta et al. (2017)]. As converter interfaced DGs lack inertia and feeder lengths are short, the apparent impedance seen by the distance relay may get affected, hindering the application of distance relays [Fang et al. (2019)]. Application of distance relays requires restrictions on the number and locations of the DGs that can be connected to the microgrid.

2.3 REVIEW OF AC MICROGRID PROTECTION SOLUTIONS

The conventional protection devices and schemes like overcurrent, directional and distance relays may fail in microgrids. Researchers have proposed several solutions for microgrid protection. This section briefly reviews the available protection solutions in AC microgrids.

2.3.1 Adaptive protection:

Adaptive protection adapts the protection functions or relay settings of PDs according to the system operating state. For instance, in IIT microgrid [Che et al. (2014)] adaptive settings are adopted to respond to higher fault currents in GCM and lower currents in IM. Further, the OC relay characteristics shift from inverse time in GCM to instantaneous or definite time OC settings in IM. The settings can be calculated online or stored in a database according to the network topology. There are mainly two schemes - centralised and decentralised. Adaptive schemes heavily rely on communication infrastructure and hence associated challenges are present [Voima et al. (2014)].

Centralised adaptation scheme: A centralised controller polls each PD, analyse the circuit state and if necessary adapts the settings to new network configuration. The new settings are then sent to PDs. For example, Laaksonen (2010) proposed a Microgrid Management System (MMS) which changes the settings and limits of PDs when microgrid configuration changes from normal to islanded mode of operation. MMS also acts as an interface agent between individual grid components and DMS(Distribution Management System). DMS takes part in higher levels of cooperation such as VPP(Virtual Power Plants) or Energy Markets. However specific details of protection devices, coordination and operating algorithms are not mentioned.

Similarly, Zamani et al. (2014) presented a communication assisted microgrid protection relay (MPR) consisting of five modules: 1) the directional module that determines the correct direction of the fault; 2) the islanded module which provides protection (based on voltage dip) in the islanded mode; 3) the grid-connected module which ensures protection (Over current) in the grid-connected mode; 4) the interface module which is designed for the relay installed at the electrical boundary; and 5) the tripping module that decides whether a trip signal should be issued. The interface module embeds functions such as neutral voltage displacement for activating islanded mode under grid faults and grid synchronism check function for reconnection.

Ustun et al. (2013) proposed an adaptive overcurrent relay which is based on a Microgrid Central Protection Unit (MCPU). The MCPU communicates with every single relay and distributed generator in the microgrid to ascertain whether it is ON/OFF. With these inputs, the MCPU calculates the tripping current value for each relay. Another adaptive scheme is proposed in Brahma and Girgis (2004), which performs offline short circuit calculations to calculate the protection and coordination settings. This method requires extensive communication and a model of the network.

Decentralised adaptation scheme: Centralised schemes become complicated for large microgrids with many network configurations. Besides, it increases the computational burden on the central controller. If the main controller fails, it can lead to catastrophic conditions. Decentralised schemes [Mahat et al. (2011)] uses local controllers or relays to monitor the status of various CBs, ascertain the microgrid operating mode and choose appropriate settings. Bui et al. (2017) suggests traditional overcurrent protection in GCM and negative sequence current/voltage component based protection as primary protection in IM for an ungrounded system. But, under unbalanced load conditions, the fault tripping thresholds of negative sequence current should consider the effect of neutral point shift of phase currents or voltages. THD of phase currents or voltages is used for backup protection in IM. Singh and Basak (2019) suggests an adaptive scheme that uses time derivative of quadrature and zero sequence components for assessing fault nature and location.

2.3.2 Overcurrent protection:

Traditional inverse time overcurrent relays face many challenges in the microgrid scenario. Hence, researchers have proposed many techniques based on adaptive overcurrent protection. Pre-defined setting groups (STG) can be stored in relays or local controllers for different operating conditions [Mahat et al. (2011), Naveen and Jena (2021)]. But modern relays can store only a limited number of STGs. Moreover, while changing the setting group, the relay disables itself (all its functionalities) for a short period. To overcome this limitation, dynamic relays that computes the new settings online are proposed.

One method is to adjust the fault current seen by the relay. The fault current of different DGs are multiplied by various impact factors to increase the fault current magnitude. Muda and Jena (2017b) used superimposed sequence components for impact factor calculations. But, this may lead to unnecessary tripping of PDs at mode transitions, as a considerable amount of sequence components are present during microgrid transitions.

Another approach is to adjust the pickup or operating current of relay depending on the presence or absence of grid and different DGs [Ustun et al. (2013)]. A minimum fault current is assigned to each DG, and if present, this current is used to estimate pickup current, irrespective of the controller type or microgrid mode.

Jain et al. (2019) presents a dynamic AOCR relay that computes pickup current locally using moving average of line load estimate and DER status. Kavi et al. (2018) proposed a multistage morphological fault detector that analyzes sudden change in current magnitude to update the threshold settings.

2.3.3 Directional protection:

Adding direction feature will improve the sensitivity and selectivity of protection schemes. Commercially available directional overcurrent relays (DOCR) are 67 NEG and 67 POS. But these may malfunction in IIDG feeders due to the lack of negative sequence components and sources with large fault current [Hooshyar and Iravani (2018)]. The influence of IIDGs on fault component based directional relays are presented in Jia et al. (2019b). As IIDGs possess variable impedance characteristics, the superimposed impedance phase angle does not stay constant at 90^0 and hence mal-operate.

Different types of relays that depend only on current for direction detection are reported in the literature. The advantage of such relays is that voltage sensors or potential transformers are not required, and hence the cost of protection strategy is reduced. The phase difference between the post fault current and prefault current is used in Ukil et al. (2010) to detect whether the fault is in forward or reverse direction. Muda and Jena (2017a) and Muda and Jena (2017b) have used phase angle difference between superimposed positive/negative sequence current and positive/negative sequence pre-fault current for direction assesment. The limitations of these methods are that pre fault current status (whether current is flowing upstream or downstream) needs to be updated every time, which in turn may require voltage measurement. Moreover, direction assessment criteria are not the same for downstream and upstream power flow. Hooshyar and Iravani (2018) proposed a new directional element that uses different features for directional detection of symmetrical and asymmetrical faults. A protection scheme for

Table 2.1: Adaptive Overcurrent, Directional and Differential protection solutions

Reference	Features	Microgrid		Limitations
		Mode	DGs	
Adaptive over current				
Ustun et al. (2013)	Centralised	GCM & IM	VSI	• Complicated for large microgrids • Computational burden on MGCC • Extensive communication requirement
Mahat et al. (2011)	Different STGs stored in relays Determine system status & update relay settings locally	GCM & IM	WTG, CHP	• Validated for 3 phase faults only • Limited STGs in modern relays •Relay disables while STGs are flashed
Naveen and Jena (2021)	Provision for offline and online relay setting	GCM & IM	PV, SG & WTG	”
Singh and Basak (2019)	Uses time derivative of q0 current components	GCM & IM	SG	•Threshold setting is difficult • Requires grid status
Jain et al. (2019)	Dynamic AOCR without external controllers	GCM & IM	PV	• Relay adaptability not verified for complex microgrids
Directional (DOCR)				
Ukil et al. (2012)	Current only Angle between I_F and I_{pre}	GCM	SG	• Prefault current status required
Muda and Jena (2017b), Muda and Jena (2017a)	Adaptive DOCR Based on +ve and -ve sequence superimposed currents	GCM & IM	PV, SG	• Different direction assessment criteria • Complex computations • Mal-operation at microgrid transitions
Basit et al. (2017)	SRE & Hilbert transforms	GCM & IM	PV, SG & WTG	• Mal-operate with IIDGs only
Hooshyar and Iravani (2018)	New directional element	GCM & IM	PV, SG & WTG	• Requires multiple features extraction
Mahamedi et al. (2018)	Zero sequence reactive power based	GCM	VSI	• Requires IIDGs to be integrated by a dYg transformer • Limited to ground faults
Differential				
Phase currents based				• Due to IIDG controllers, magnitude and phase jumps occurs in healthy phases causing mal-operation
a) Dewadasa et al. (2011)	Compares current phasor	GCM & IM	SG,PV	
b) Halabi et al. (2011)	Compares phase angle	GCM	WTG	• Needs communication of three phasors, making them costly.
Gao et al. (2017)	Positive sequence fault current component based	GCM	VSI	• Needs communication of single phasor; but may not detect HIF
Dubey and Jena (2020)	Uses cumulative sum of diff NSQ impedance angle	GCM	PV, WTG	• Cannot detect three phase faults
Time frequency transform				• Spectral energy of fault current signals are extracted to obtain differential energy
a)Kar and Samantaray (2014)	S-transform	GCM & IM	SG,PV	• Different settings for GCM & IM
b)Gururani et al. (2016)	Hilbert Huang (HHT)	GCM & IM	WTG	• High computational burden
Data mining based				• Requires huge data sets for training & testing
a) Casagrande et al. (2014)	Random Forest	IM	VSI	•Requires multiple sensors for extracting different features
b)Kar et al. (2017)	Decision Tree	GCM & IM	SG	•Complex structure
Singh and Basak (2019)	Park’s transformation(q and 0 components) based	GCM	SG	• Requires adaptive settings
Nsengiyaremye et al. (2020)	Low cost communication assisted	IM	VSI	•Not applicable for PQ IIDGs with $-P_{ref}$

microgrids using Hilbert transforms and Superimposed Reactive Energy (SRE) is proposed in Basit et al. (2017). As the healthy phases are also affected by the fault in IIDG interfaced feeders, this method may mal-operate. A PMU assisted centralised protection scheme which uses Integrated Impedance Angle (IIA) for detection of internal faults is proposed in Sharma and Samantaray (2020).This scheme requires the application of several synchrophasors and their communication, which increases the cost.

2.3.4 Voltage based protection:

The scheme proposed by Al-Nasseri et al. (2005) converts the DG output voltage to dc quantities in dq reference frame. The faults will be reflected as disturbances in dq values. Dang et al. (2011) proposed a similar scheme using dq components of voltage and current. Adaptive voltage based primary and backup protection schemes were proposed by Ma et al. (2013). The settings adjust with different operation modes and its calculation relies on before-and-after-fault phase voltage difference and the phase current.

- These schemes are not capable of detecting high impedance faults (HIF)
- The magnitude of voltage dip during faults will be the same in different locations due to small feeder lengths; therefore determining fault location will be difficult [Zamani (2012)]
- The inverter terminal voltage can change in normal operation due to load switching, capacitor switching etc. Hence special measures should be taken to avoid erroneous tripping

2.3.5 Differential protection:

Differential protection schemes have more prospects in microgrid protection as they are not affected by bidirectional powerflow, changing current levels, number of distributed energy resources (DERs) in the microgrid, microgrid operation mode and weak infeed. However, they require time synchronised communication and doesn't have a provision for back up. The schematic of current differential protection is shown in Fig. 2.1.

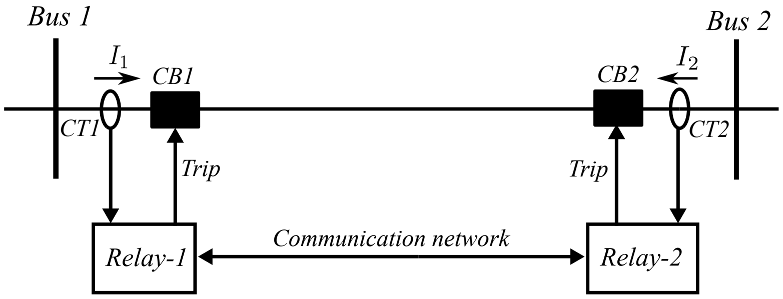

Figure 2.1: Schematic of differential protection.

The differential relay in Dewadasa et al. (2011) has five elements - three elements for each phase, negative sequence and zero sequence elements. Another scheme that uses current phase jumps for zone protection is presented in Halabi et al. (2011). These schemes require communication of at least three phasors, making them costly. Due to the impact of controllers in IIDGs, there can be magnitude and phase jumps in healthy phases as well and hence these schemes may mal-operate.

Gao et al. (2017) presented a differential protection scheme using positive sequence fault component (PSFC) instead of phase currents. As this scheme requires communication of a single phasor (superimposed positive sequence current) between terminals, the communication load is reduced. However, this protection scheme may fail under high impedance asymmetrical faults, as changes in positive sequence components are negligible.

Dubey and Jena (2020) utilised the cumulative sum value of the differential negative-sequence impedance angle (DNSIA) as the fault detection parameter for generating the trip signal. This scheme is capable of detecting both HIFs and LIFs. As negative sequence components are absent in symmetrical faults, this scheme finds limitations in detecting three phase faults.

Casagrande et al. (2014) developed a fault classifier based on Random Forest algorithm. Among different features, this study has identified that differential positive and negative sequence currents as the most suited features. Kar et al. (2017) preprocesses the faulted current and voltage signals using discrete Fourier transform and derives features at both ends of the feeder for building the Decision Tree based data mining model. The features extracted for final relaying decision are differential rate of change of frequency, rate of change of voltage, rate of change of power angle difference, active power change with time, reactive power change with time, rate of change of negative sequence voltage and rate of change of negative sequence current. But these schemes require large datasets for training and testing.

Time frequency transform based differential protection schemes [Kar and Samantaray (2014), Gururani et al. (2016)] retrieve current signals at both ends of feeder to compute spectral energy content using S-transform or Hilbert Huang transform (HHT). If the differential energy exceeds a threshold, trip signals are issued. These methods are less sensitive to synchronisation errors; but requires different settings for grid connected and islanded modes. Moreover, computational burden is high, leading to a slower response time.

Nsengiyaremye et al. (2020) proposed a low cost scheme that compares the direction of current at both ends of relay. Instead of comparing the directions at the same instant [Ukil (2016)], this method ascertains the current direction at two successive instants and then compares the transition patterns at both ends of line. Since the current directions are indicated as 1 or 0, the communication load is heavily reduced. However, this scheme is validated on a microgrid with current controlled IIDGs and reference currents set to positive values only.

2.3.6 Hybrid protection schemes:

Schemes that employ advanced signal processing, neural networks and machine learning techniques are reported in the literature. A combined wavelet and data mining based intelligent protection is described in Mishra et al. (2016). The effective features of current signals such as change in energy, entropy, and standard deviation are derived using wavelet coefficients. Once the features are extracted against faulted and unfaulted situations for each-phase, the data set is built to train the decision tree (DT). Wavelet decomposition provides scaling coefficients in addition to wavelet coefficients. Costa et al. (2017) reproduced overcurrent functions through the scaling coefficient energy, whereas the wavelet coefficient energy provided the real-time detection of the fault. The disadvantage of ANN based schemes are that they require multiple sensors at different locations, complex structure and huge data sets for training. To overcome these limitations, a Taguchi based ANN that extracts the signals at the static switch for fault diagnosis is presented in Hong and Cabatac (2020). However, this method is applicable only when grid contributes to the fault.

2.4 REVIEW OF CHALLENGES IN DC MICROGRID PROTECTION

Voltage Source Converter (VSC) based DC microgrids are gaining interest in recent years as many consumer loads have shifted to DC. Compared to AC systems, DC offers many advantages like higher power transfer capacity, low cost, reduced power conversion stages, absence of reactive power and harmonics. Moreover, the Distributed Generators (DGs) and storage units can be easily integrated in to DC microgrids. Despite these advantages, LVDC and MVDC microgrids are still in infancy stage at the implementation level. There are many challenges concerning protection [Bayati et al. (2018), Park and Candelaria (2013), Beheshtaein et al. (2019)].

Fault Interruption: Fault interruption is a major concern due to the absence of zero current crossing in DC[Cuzner and Venkataramanan (2008)]. Fuses that were conventionally used in dc systems are not preferred in microgrids due to their slow response, requirement for replacement after each operation and inability to distinguish between momentary and permanent faults. Several researchers are attempting to develop a DCCB with the following features - a) reliability b) low power losses c) low cost d) high current rating e) fast response f) high breaking current and g) long lifetime.

Non-standardisation of DC microgrid system: Many national and international organisations like International Electrotechnical Commission (IEC) has started working toward standardisation of voltages. However, there is no consensus on DC voltage level, communication protocols, grounding and safety regulations to date.

Sudden rise time of DC fault current: Due to low line impedance and presence of large dc link capacitors, the fault current rises rapidly[Beheshtaein et al. (2019), Monadi et al. (2015)]. If the fault is not interrupted quickly, it may lead to a system breakdown. Several solutions are reported in the literature to avoid sudden current build up. Mohan and Vittal (2019) designed fault current limiters using external reactors. Some power converters like boost converters are vulnerable to faults. But some other converters like buck, buck boost isolated converter known as Dual Active Bridge (DAB) can inherently limit the fault current [Beheshtaein et al. (2019)]. This is because of the inductance in the freewheeling diode path. Multimode control schemes which switch to a different control during a fault to limit the fault current are also proposed [Augustine et al. (2020)].

Relay Setting using current magnitude: There are two types of faults in the DC side; pole to pole (PP) and pole to ground (PG). In the PG faults, one or both conductors fall to the ground. The fault current in PG faults is affected by the grounding system. The conductors comes in direct contact with each other in PP faults. Hence, the PG faults are classified as high-impedance and PP faults as low-impedance faults. A lower current setting may affect the system reliability and a higher current setting might affect its sensitivity.

Bidirectional flow of currents: The integration of DGs and ESS via bidirectional converters and different DC microgrid configurations such as ring and mesh results in bidirectional current flows.

Selectivity: Due to dc link capacitors, all the DGs, ESS and loads contribute to a fault in DC cable or bus almost simultaneously. Though DC-DC converters can detect faults instantaneously, their sudden disconnection is not an appropriate solution as it will prevent them from being used for fault ride through. But the transient currents can be very high up to 15 times the rated current. Hence it is necessary to isolate the faulty section quickly to avoid damage to converters diodes. The faulty location must be isolated in µs.

Relay coordination: Available time for fault isolation is very less, coordination between relays is difficult [Cuzner et al. (2017)].

Fault type identification: There are positive pole to ground (PPG), negative pole to ground (NPG) and pole to pole (PP) faults. Identification and isolation of faulty pole in micro time scale is required to maintain supply in healthy lines.

Impact of high bandwidth ESS: Rakhra (2017) discusses the impact of high bandwidth energy storage integrated with an aircraft application. The energy storage responds rapidly when there is a voltage drop and contributes a large fault current. If the protection settings are done under this assumption, it may lead to blinding under HIF when ESS is offline. This is because under HIF, primary sources may reduce their contribution.

Grounding issues: The grounding in DC microgrids is complex than AC systems due to integration of PE converters and their interface with AC network. The DC microgrid side grounding arrangements should be chosen considering AC side (utility) grounding schemes [Carminati et al. (2014), Beheshtaein et al. (2019)]. Grounding design must accomplish prospectives of facilitating fault detection, protection requirements, safety for equipment and individuals (reduce touch voltage), minimize stray currents (earth current from the conductor) and reduction in CMV level [Mobarrez et al. (2017)].

2.5 REVIEW OF DC MICROGRID PROTECTION SOLUTIONS

The fault detection and localisation is not established in LVDC microgrids, as in AC or HVDC systems. Lack of frequency and phasor information limits the conventional fault detection methods in AC microgrids [Salomonsson et al. (2009)]. Travelling wave based methods are mostly proposed for fault detection in HVDC systems. Due to shorter feeder lengths, segregating the second travelling wave is not easy and feasible in LVDC microgrids. TW-based fault location requires high-performance data acquisition equipment.

Recently, many advanced signal processing techniques like Wavelet (WT) [Yeap et al. (2017)], Short Term Fourier (STFT) [Satpathi et al. (2018)] and Stockwell(ST) [Kar and Samantaray (2014)] transforms were proposed for HVDC systems. High frequency components are superimposed in the fault currents during the transient period.

The above methods determine high frequency components and thus detect the fault very fastly. However, these methods are computationally complex, require high sampling frequency, sensitive to noise and costly. These methods are therefore not a good option for LVDC microgrids. Protection schemes based on transient energy for fault identification are also reported for HVDC systems. Dai et al. (2020) uses transient energy ratio for fault location selectivity. Mohan and Vittal (2019) proposed a single ended protection scheme that uses variation in DC voltage, current and transient energy to discriminate external and internal faults.

The fault detection techniques in LVDC microgrids can be broadly classified as local measurement and unit protection methods. The advantage of local measurement methods is that they have an inherent capability of backup protection. However, the device threshold setting is challenging for accurate fault discriminations and if relay coordination are to be met [Fletcher et al. (2012)]. Whereas unit protection schemes offers bounded protection to a part of power system with no provision for backup.

2.5.1 Unit protection methods

Differential protection: These methods compare currents [Park and Candelaria (2013), Fletcher et al. (2014))] or voltages between two boundaries in a unit and if this difference exceeds the threshold, a trip signal is issued to the breakers. Though this method is very selective and sensitive, it requires high bandwidth communication and time synchronised measurements. Unlike AC which uses phasors, DC system uses sampled values and is exposed to severe transients. A micro time scale change in measurements can lead to protection failure.

Current direction based protection: A current direction based protection scheme for radial microgrids, which selectively trip the faulty portion, is described in Emhemed et al. (2017). This direction assessment will make a correct decision, only if the fault current is greater than the prefault current. These methods thus find limitations under HIF. Similarly, a superimposed current-based scheme for faulty feeder identification is proposed in Mohanty and Pradhan (2018b). The works reported in Jia et al. (2019a) and Mohanty et al. (2021) utilise similarity of current waveforms at feeder ends for fault detection. These current-based techniques rely on communication between relays at feeder ends for locating internal faults. These schemes cannot assess the fault direction (Forward or Reverse) locally and hence does not have any scope for offering backup protection.

2.5.2 Local measurement methods

Current derivative based protection: Protection methods based on first and second current derivatives are proposed in Meghwani et al. (2020), Meghwani et al. (2017). The current derivative depends on several parameters like cable characteristics, fault resistance and line loading. Choosing a suitable threshold is difficult and may lead to false triggerings during other system disturbances like load changes or DG switchings. Moreover, the derivative calculation requires a high sampling frequency which amplifies noise and hence may lead to false tripping [Beheshtaein et al. (2019)]. Mohanty and Pradhan (2019) proposed a novel method that depends on oscillation frequency and transient power for trip decision. These schemes do not offer selectivity and the decision time is affected by the damping level, distributed energy resource (DER) response and fault resistance.

Parameter estimation based methods: Several methods that estimate line parameters to identify fault are also reported. A Least Square based method is used in Mohanty and Pradhan (2018a) to compute the line inductance using local voltage and current samples. The sign of seen inductance is used to determine whether the fault is forward or reverse. However, this method is computationally complex. If the estimated inductance of a line falls below a threshold value, a fault is identified in Feng et al. (2017) and Shamsoddini et al. (2020). But for detecting high impedance faults, these methods require the insertion of an artificial line inductance. Moreover, the protection devices (PDs) in healthy lines may maloperate immediately after de-energisation of adjacent faulty lines with parameter based techniques. Therefore, Bhargav et al. (2020) relies on threshold values of pole voltages and currents for fault detection and line parameters only for assessing fault location. Another method that locates fault by comparing the actual fault current with analytically derived current (using an iterative method) is presented in Bhargav et al. (2019).

Injection based methods: Park et al. (2013) proposed a fault location algorithm using a probe power unit (PPU). A PPU consists of probe capacitor, probe inductor, power source, and connection switches. The probe current response is analyzed, and the fault distance is obtained in terms of damped resonant frequency. Jiang et al. (2019) suggested another method that uses terminal inductors. The voltages at either ends of the inductors are sensed to determine the fault location accurately. These methods need additional hardware units and voltage sensors.

2.6 INFERENCES

Many protection schemes were proposed for AC microgrids as shown in Section. 2.3. The summary of observations from literature review of available protection schemes in AC microgrids are as follows.

1. Majority of the schemes are limited to microgrids with rotating generators and PV. Though Energy Storage Systems are inevitable for a microgrid, the existing works have not included them. Protection of feeders integrating energy storage is more complicated as set powers can take both positive (discharging) and negative values (charging). The fault behaviour of PQ controlled IIDGs when set power is negative is not addressed in any literature.
2. Several works have employed averaged models of VSI instead of DERs for microgrid simulation and have not considered the practical constraints.
3. Few of the proposed schemes apply to a single type fault.
4. The unconventional fault signatures of IIDGs restrict traditional relays'(Overcurrent, voltage based and sequence component based relays) application in AC microgrids.
5. Distance relay may fail in microgrids due to the error in impedance calculations. This can be due to the short length of feeders, fault current variations with different modes, limited fault current of IIDGs and impact of grounding impedance.
6. Application of machine learning techniques and advanced signal processing tech-

niques in microgrid protection is trending. These methods are complex, requires multiple sensors, extensive communication and large data sets for training. The real time implementation of such schemes may not be practical considering cost factor and dynamic nature of distribution grids.

7. A comprehensive protection scheme (fault detection, location and classification of all types of fault in all modes of microgrid operation) is lacking in microgrids; hence, there is a prospect for research in AC microgrid protection.

Research on LVDC microgrids has gained momentum recently. The summary of observations from literature review on DC microgrids are as follows

1. The protection aspects of LVDC microgrids are not explored fully to date. The studies on fault location and backup protection in LVDC microgrids are limited.

2. The internal protection in DC-DC converters can act quickly during faults. However, shutdown of all DGs is not a viable option, as it will prevent them from being used for fault ride through and fault location assessment. Nevertheless, the transient currents are very high; quick disconnection of faulty section is essential.

3. Many of the proposed methods in HVDC use advanced techniques and high bandwidth communication, which makes them unfeasible for LV microgrids.

4. Differential protection schemes offer good flexibility in fault localisation. However, the precise requirements for measurements and time synchronised communication make them unfeasible for LVDC microgrids. As DC system uses sampled values and is exposed to severe transients, a slip can lead to catastrophic effects.

5. Though current derivative and voltage based methods can detect faults quickly; selectivity is not assured. Transient signal based methods are a good option, but they might appear during non-fault disturbances. Adding directional features may enhance selectivity.

Chapter 3

Transient Behavioural Modelling of Microgrids supported by Battery Energy Storage System

3.1 INTRODUCTION

This chapter presents the modelling of a microgrid supported by BESS (Battery Energy Storage System). The control strategies of BESS automatically switch between grid connected and standalone modes of operation. Section. 3.3 demonstrates how BESS mitigates the power fluctuations in a microgrid and improve the power quality indices.

This chapter will also analyse the impact of different inverter control strategies on the fault behaviour of IIDGs. A comprehensive understanding of transient behaviour is essential for an effective microgrid protection design.

3.2 MICROGRID TOPOLOGY

The studied microgrid comprises a 40 kW Solar Photovoltaic (PV) employing MPPT control, a 57 kWh centralised battery energy storage unit (BESS) and loads. All the components are connected to a 415 V busbar at the Point of Common Coupling (PCC), as shown in Fig. 3.1. The switch S facilitates the connection of microgrid to

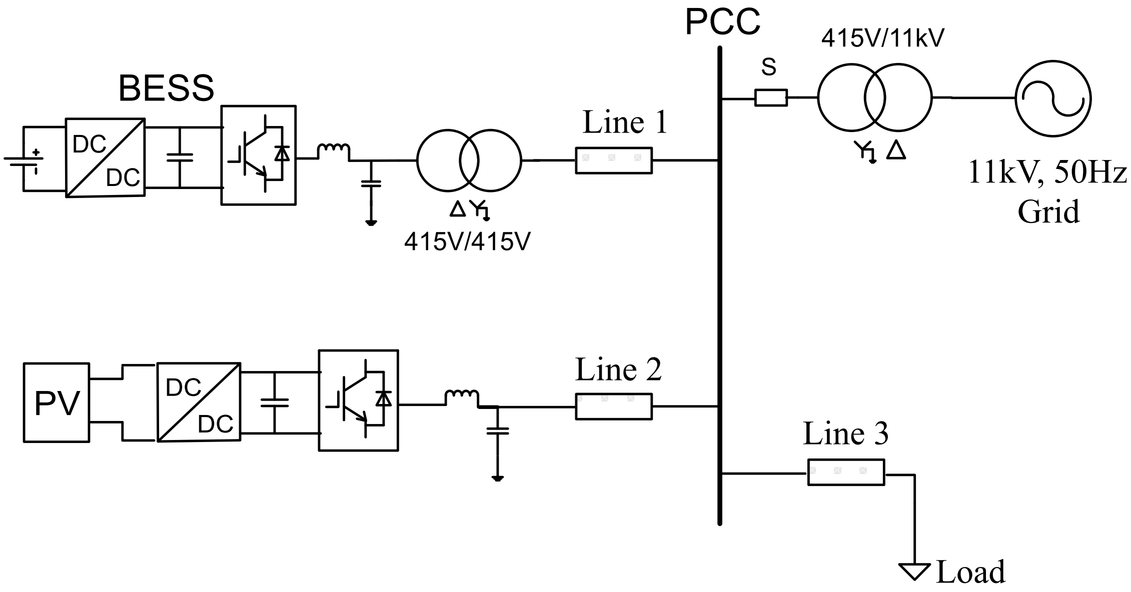

Figure 3.1: Microgrid topology.

the grid. All the DG inverters are operated in current controlled (grid following) mode during grid-connected mode. PV uses DC link voltage control to transfer maximum power and BESS employs PQ control to deliver/absorb a preset power to/from the utility grid. The parameters of the studied microgrid are listed in the Appendix A.

When the microgrid is cut off from the utility grid, fixed power control cannot maintain the voltage and frequency. A master control frame, where BESS acts as the master voltage source and PV serves as a slave is employed in islanded operation mode [Kim et al. (2010), Zhang et al. (2016)]. Control of PV remains unchanged during both modes, whereas control of BESS switches over to Voltage / Frequency (grid forming) control as in Fig. 3.2. This enables the PV to deliver maximum output power. The detailed BESS model in Fig. 3.2 [Farrokhabadi et al. (2018)] is used for the study.

The dc link voltage of the battery is regulated by the converter controller [Sagiraju et al. (2017), Alexandre et al. (2016)] of Fig. 3.2. Whenever there is a shortage of power at PCC, dc link voltage of battery inverter falls and by the control scheme, Q_2 is turned on. The inductor starts charging. Once the inductor gets fully charged, Q_1 and Q_2 are turned off and diode D_1 turns on. The converter is operating in boost mode and power is transferred from battery to dc link. The battery is in discharging mode under

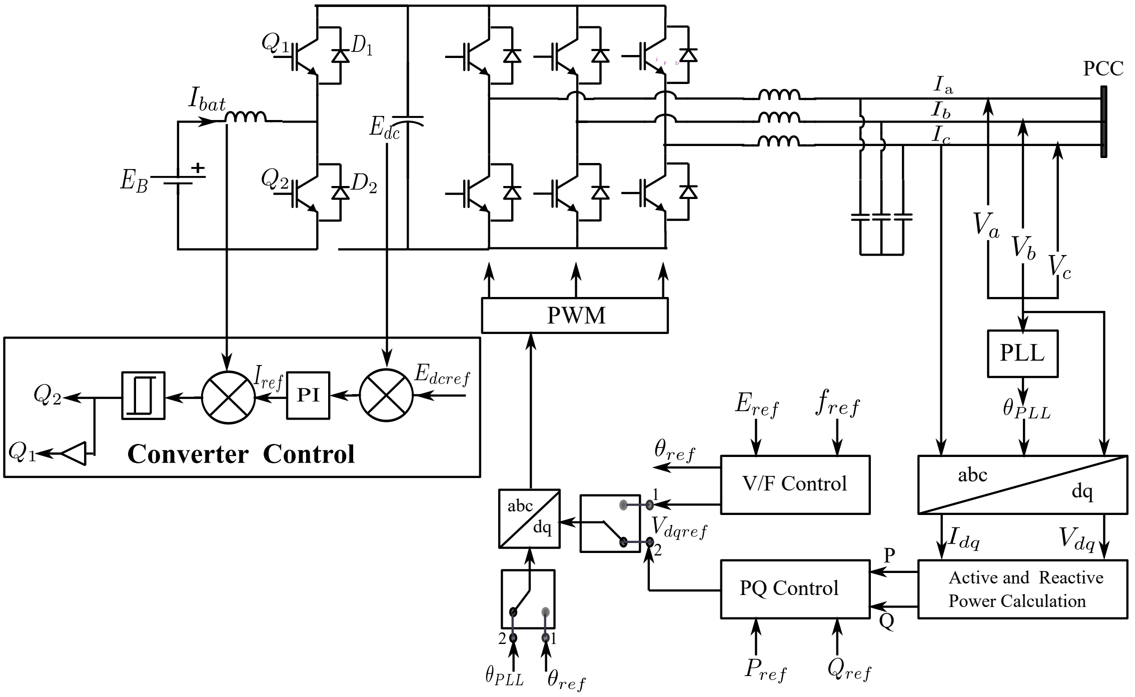
Q1
D1
Q2
D2
Ibat
EB
+
Edc
PCC
Ia
Ib
Ic
Va
Vb
Vc
PWM
PLL
θPLL
Q2
Q1
Iref
PI
Edcref
Converter Control
Eref
fref
θref
V/F Control
1
Vdqref
2
abc
dq
abc
dq
P
Q
PQ Control
Idq
Vdq
Active and Reactive
Power Calculation
2
1
θPLL
θref
Pref
Qref

Figure 3.2: BESS components and its control.

this scenario. Alternatively, when there is an excess supply of power, dc link voltage builds up and Q_1 turns on. The converter operates in buck mode and the excess power is transferred from dc link to battery. Thus, the battery is charging in this mode.

The control of all inverters is implemented in dq (synchronous reference frame). The detailed block diagrams of inverter controllers are shown in Fig. 3.3 and Fig. 3.4

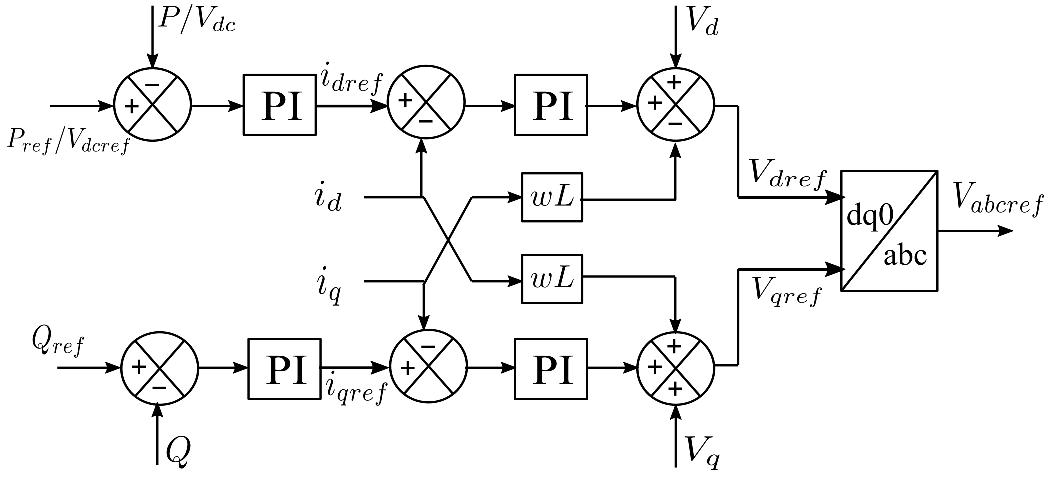
P/Vdc
Pref/Vdcref
PI
idref
PI
Vd
id
iq
wL
wL
Vdref
Vqref
dq0
abc
Vabcref
Qref
PI
iqref
PI
Q
Vq
+
−

Figure 3.3: DC link voltage / PQ control

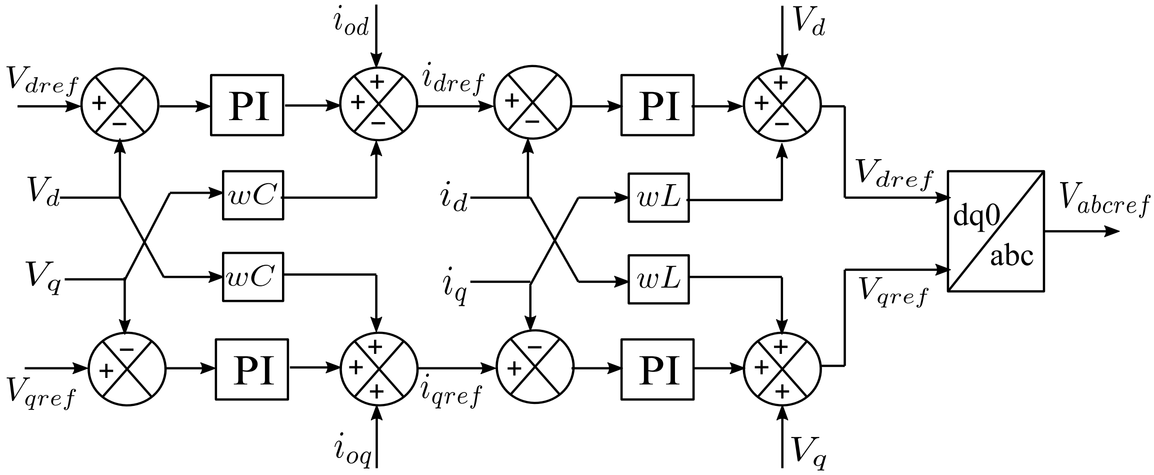

Figure 3.4: V/F control

3.3 SIMULATION STUDIES

Time domain simulations are performed to analyse the dynamic and transient behaviour of microgrid. Initially, microgrid operates in grid connected mode and at t=2s, microgrid transfers to the islanded mode of operation. The BESS is PQ controlled in GCM with reference active power (P_{ref}) set at -10 kW(charging) and reactive power (Q_{ref}) at 0 kW. Since BESS is capable of delivering (discharging) and absorbing (charging) power, the reference powers, as well as reference currents can take both positive and negative values. The control of BESS shifts to grid forming (V/F control) in IM. With this control, the battery charges or discharges depending on the voltage and frequency of AC bus. PV generation is constant in both modes at 20 kW.

3.3.1 System Response under different loads

Two cases of load are simulated as shown in Fig.3.5 and 3.6 under different modes of microgrid operation.

Case 1: P_L=30 kW+j5 kVAR; $P_L > P_{PV}$

Case 2: P_L=10 kW+j5 kVAR; $P_L < P_{PV}$

where P_L is the load power and P_{PV} is the power generated by PV.

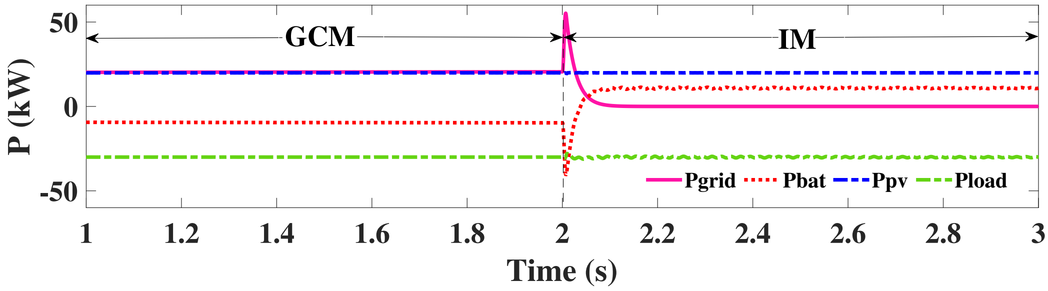

(a) Active power shared by grid and DERs

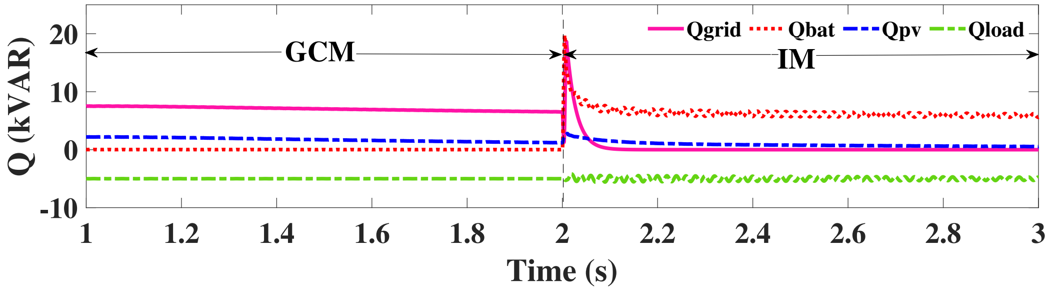

(b) Reactive power shared by grid and DERs

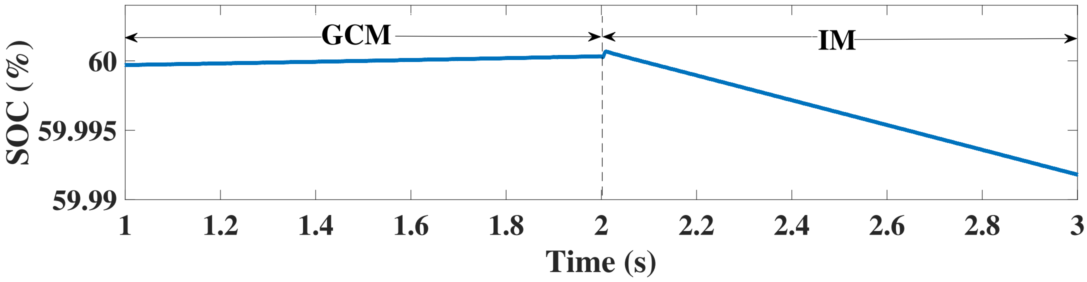

(c) State of charge of battery

Figure 3.5: Case 1: $P_L > P_{PV}$

The main observations from the study are summarised below:

- PQ controller of BESS maintains the set power references irrespective of the load conditions. This is clear from Fig. 3.5a,b and Fig. 3.6a,b as the output active and reactive power stays constant at -10 kW and 0 kW in GCM. Irrespective of the load conditions, BESS keeps charging in GCM. The surplus or deficit power is taken care of by the grid.
- V/F control targets to maintain the frequency in islanded mode of operation. During a power deficit, $P_L > P_{PV}$ (Case 1), BESS is discharging as shown in

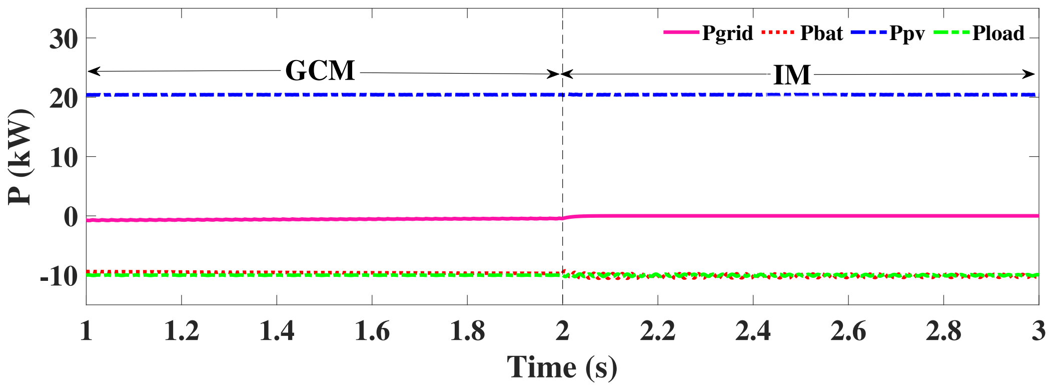

(a) Active power shared by grid and DERs

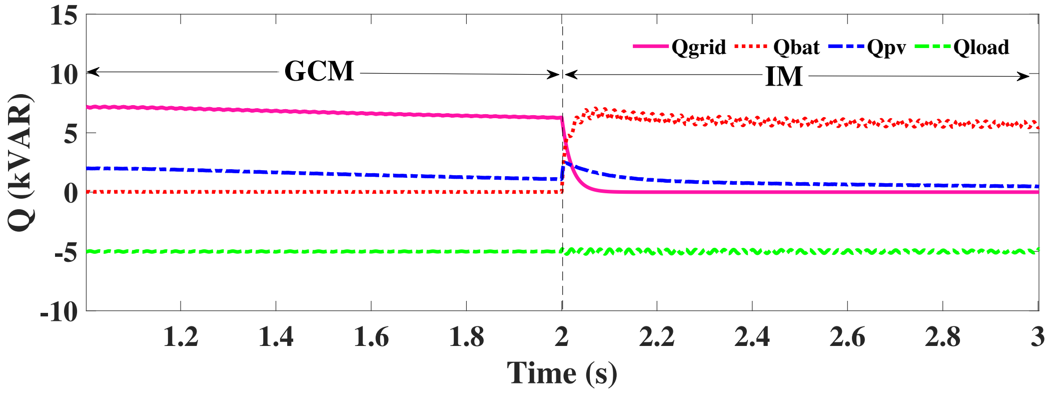

(b) Reactive power shared by grid and DERs

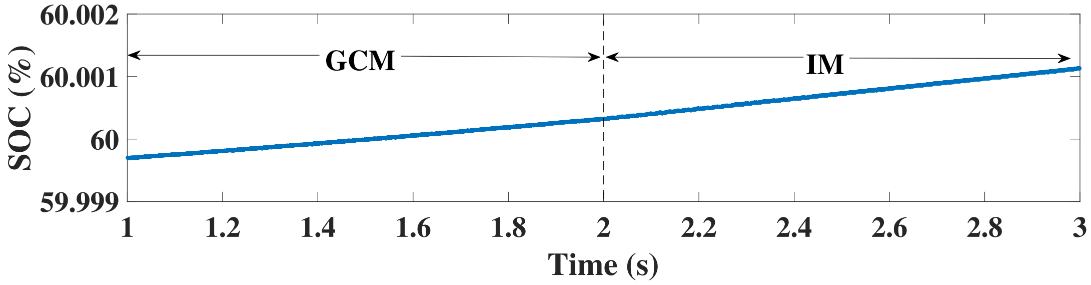

(c) State of charge of battery

Figure 3.6: Case 2: $P_L < P_{PV}$

Fig. 3.5c. When surplus power is available, $P_L < P_{PV}$ (Case 2) BESS is seen to be charging as in Fig. 3.6c.

- BESS responds very fastly to balance power at microgrid transitions as shown in Fig. 3.5a and Fig. 3.5b

- BESS is capable of providing both active and reactive power support. Referring to Fig. 3.5b and 3.6b, the reactive power is provided by the grid in grid connected mode (as Q_{ref} of BESS is 0) and battery energy storage in islanded mode.

3.3.2 Fault Analysis

To analyse the impact of different controllers on fault behaviour of IIDGs, faults are simulated as shown in Fig. 3.7. The fault characteristics of grid following and grid forming inverters are not similar. The transient response of BESS to a LL fault at location F1 in charging mode is shown in Fig. 3.8 and discharging mode in Fig. 3.9. Similarly, the fault response of BESS to a SLG fault and LLLG fault is shown in Fig. 3.10 and Fig. 3.11

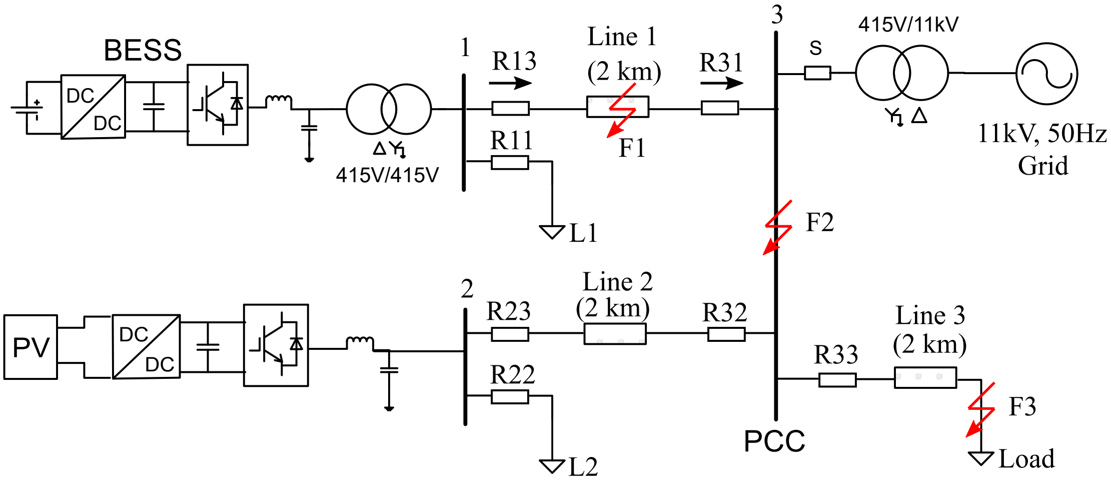

Figure 3.7: Test microgrid for fault study.

Fault current level: The fault current from PQ controlled BESS (in GCM) is limited as seen in Fig. 3.8a, 3.9a, 3.10a and 3.11a. The PQ control is briefly reviewed to understand its fault behaviour. It consists of an outer power loop that generates and limits the reference currents and an inner current control to track the reference currents. The dq axis current reference setpoints of the inner current controller [Farrokhabadi et al. (2018)] are given as

$$i_{dref} = \frac{2}{3} \frac{P_{\text{ref}}.V_{\text{gd}} + Q_{\text{ref}}.V_{\text{gq}}}{{V_{\text{gd}}}^2 + {V_{\text{gq}}}^2} \tag{3.1}$$

$$i_{qref} = \frac{2}{3} \frac{P_{\text{ref}}.V_{\text{gq}} + Q_{\text{ref}}.V_{\text{gd}}}{{V_{\text{gd}}}^2 + {V_{\text{gq}}}^2} \tag{3.2}$$

where P_{ref} and Q_{ref} are the active power and reactive power references. V_{gd} and V_{gq} corresponds to the PCC voltages in d-q axis.

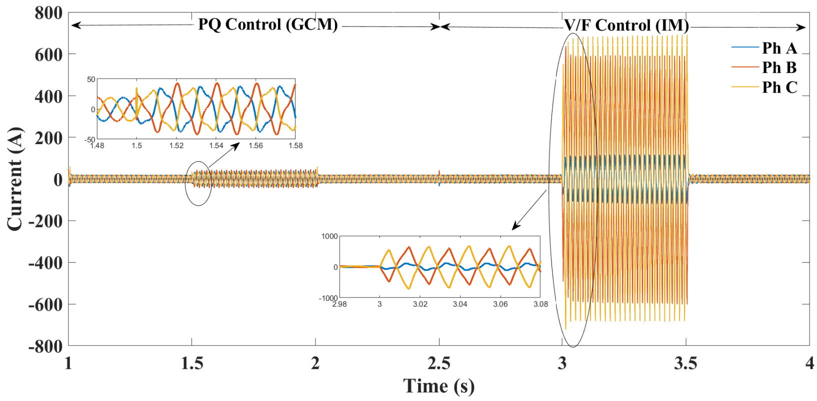

(a) BESS current

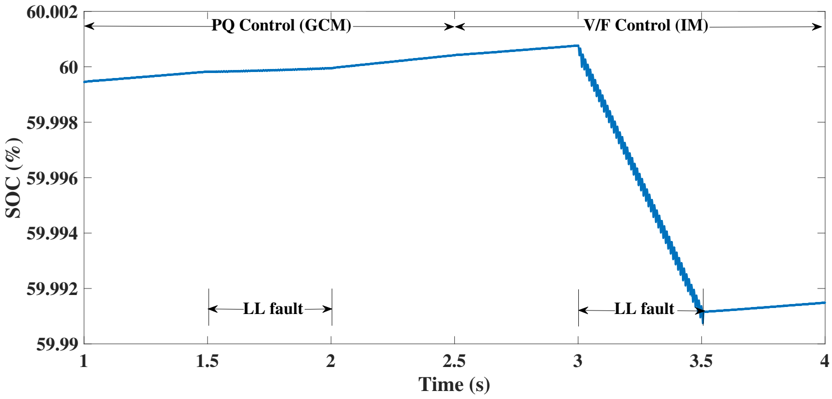

(b) State of charge of battery

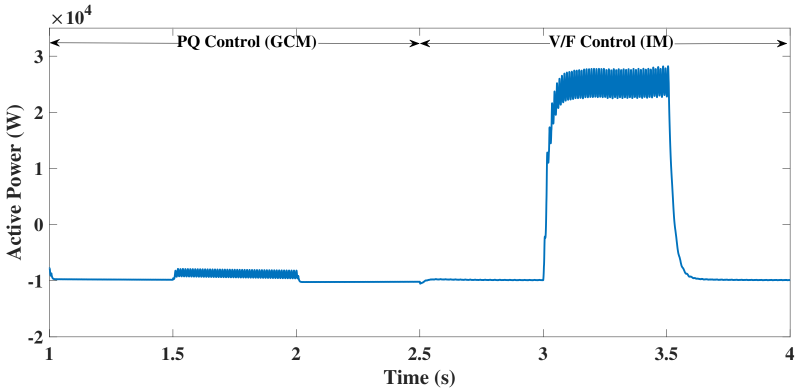

(c) Active output power

Figure 3.8: LL fault performance when BESS is charging

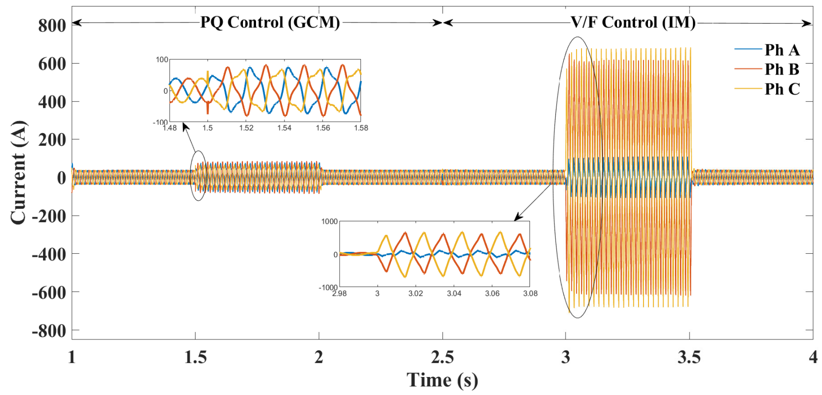

(a) BESS current

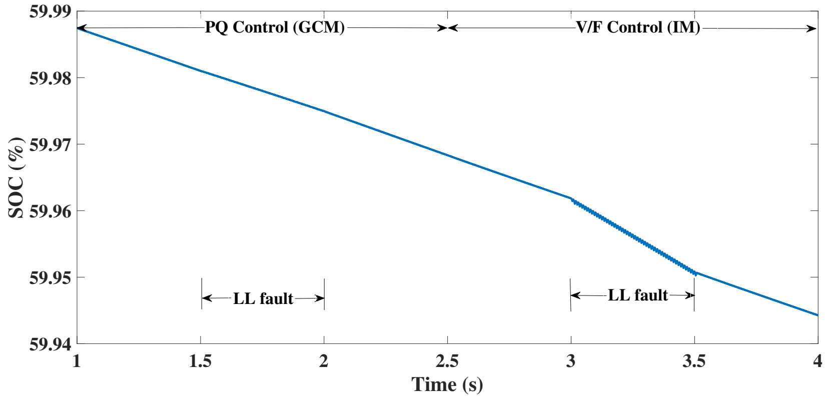

(b) State of charge of battery

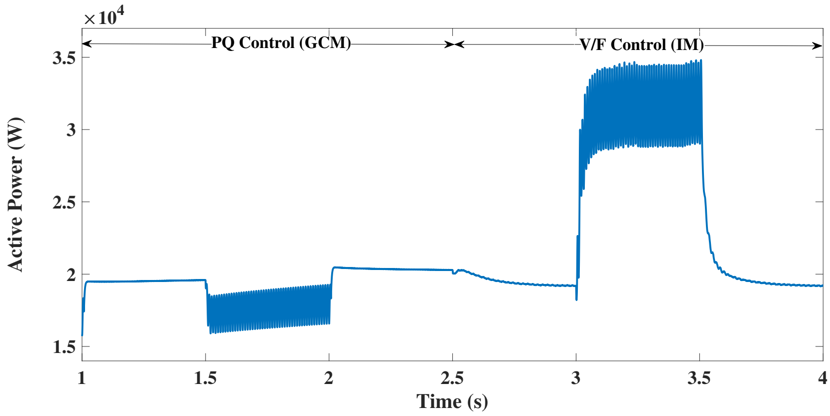

(c) Active output power

Figure 3.9: LL fault performance when BESS is discharging

When a fault occurs, the voltage drops. The fault current references as per Eqn. 3.1 and 3.2 increases to maintain the DG output power constant. Thus the fault current is proportional to the voltage dip, but limited by reference powers. Further, due to the

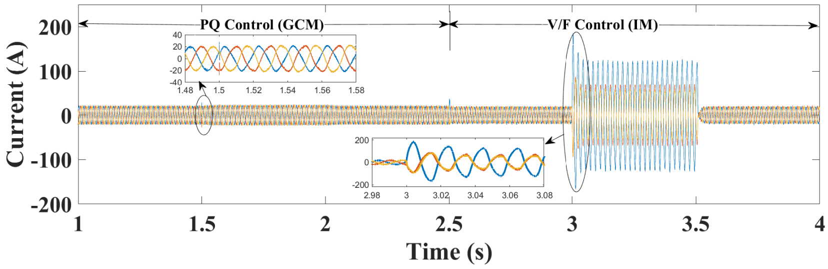

(a) BESS current

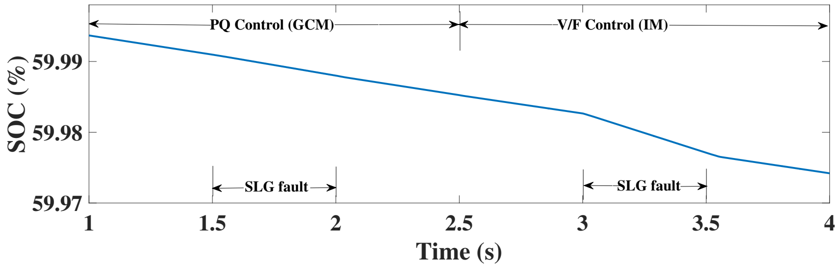

(b) State of charge of battery

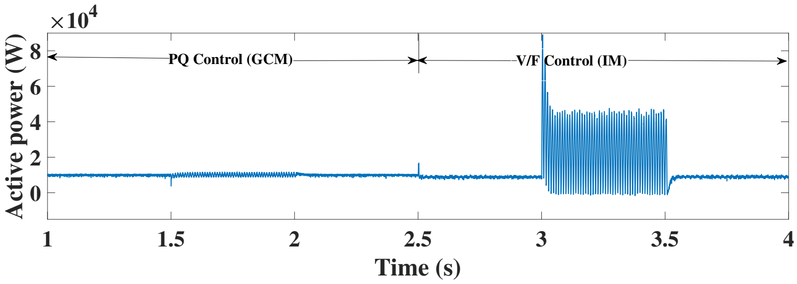

(c) Active output power

Figure 3.10: SLG fault performance when BESS is discharging

restrictions imposed by power electronic switches, the current references are limited using limiters. The controller tries to maintain the output current at the target level by adjusting internal voltage of inverters. PQ controlled inverters with current limiters are therefore modelled as controlled current sources [Shuai et al. (2018), Guo et al. (2017)].

On the other hand, V/F control attempts to maintain voltage by injecting more current into the fault (Fig. 3.8a, 3.9a, 3.10a and 3.11a). The fault response of V/F controlled IIDGs is thus similar to synchronous alternators. To accomplish fault current limiting in V/F IIDGs, some reported works modify the voltage references when a fault is detected. This adjustment of voltage references may take some time ($\approx$ 2 periods).

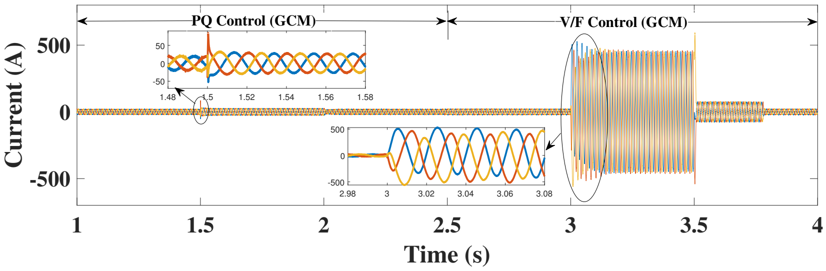

(a) BESS current

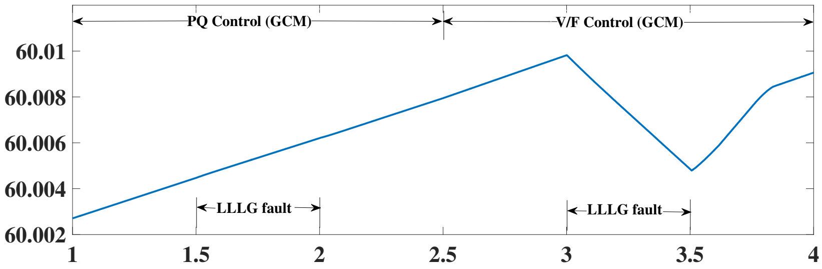

(b) State of charge of battery

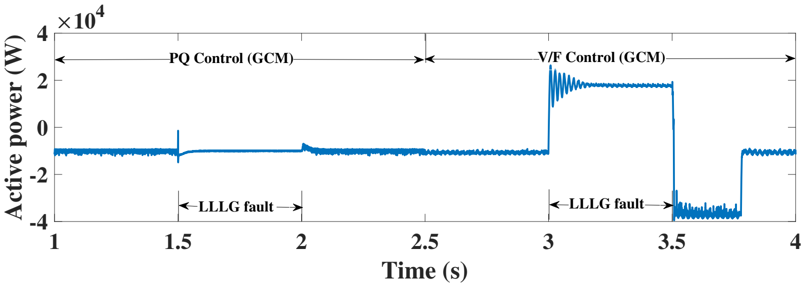

(c) Active output power

Figure 3.11: LLLG fault performance when BESS is charging

Fault current direction: Another instance where the fault behaviour of PQ controlled BESS differs from conventional sources is discussed here. Even during the fault at F1 in GCM (P_{ref} set to -10 kW), the battery continues charging as shown in Fig. 3.8b and Fig. 3.11b. This is because the PQ controller tries to maintain the same prefault power by injecting current into the battery. Whereas in IM (with V/F control), the battery is discharging during fault. Thus a PQ controlled BESS with set power negative (charging) will not dissipate in to the fault leading to mal-operation of directional relays that assumes all sources to inject current in to fault.

Output active power: The active output power of a PQ controlled DG remains constant or decreases depending on the limiter threshold. Since,the fault currents in V/F controlled inverters are high, active power output in V/F controlled IIDG increases during fault as shown in Fig. 3.8c and 3.9c.

Nature of fault response: The fault currents in GCM (from PQ controlled BESS) remains balanced even for asymmetrical faults - LL (refer Fig. 3.8a and Fig. 3.9a) and SLG (Fig. 3.10a). This affirms that fault current from current controlled inverters lack negative sequence components. PQ controlled inverter maintains the output current at target level by adjusting the internal voltage of inverter. During a fault, there are disturbances in the grid voltage. Due to the feed forward compensation technique, the imbalances in grid voltage are replicated on the terminal voltage of inverter. Thus the inverter current which is the difference between grid voltage and inverter terminal voltage is balanced. The voltage control techniques strives to maintain the inverter voltage by adjusting the current. Hence the fault currents from voltage controlled inverters are unbalanced.

Impact of interfacing transformer configuration on fault behaviour: To understand this, a fault involving ground (AG fault) is simulated at F1. The BESS is integrated via a dYg transformer. The inverter and transformer output currents when BESS is PQ controlled is shown in Fig. 3.12a and Fig. 3.12b. The faulty phase(A) current at transformer output is seen to be lower than healthy phases (B&C).

This unusual behaviour can be attributed to the absence of negative sequence components in PQ controlled IIDGs. Zero sequence components which are not affected by the control techniques, add up with the respective positive sequence components as shown in Fig. 3.13a. The net current is determined by the angle between sequence components, which in turn depends on the operating power factor of IIDG. Fig. 3.13a clearly indicates that faulty phase (A phase) current is much lower than healthy phases (B and C) with PQ control. Whereas in voltage controlled mode, phase A current is higher as shown in Fig. 3.13b due to the presence of negative sequence components.

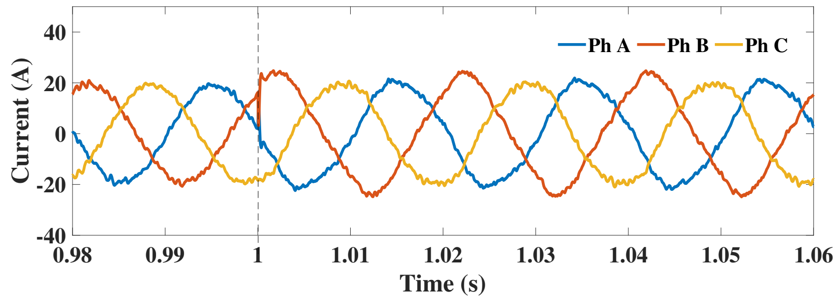

(a) Inverter output current

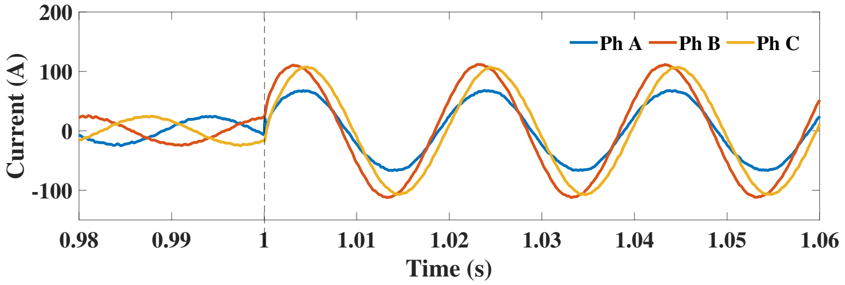

(b) Transformer output current

Figure 3.12: AG fault response of PQ controlled BESS

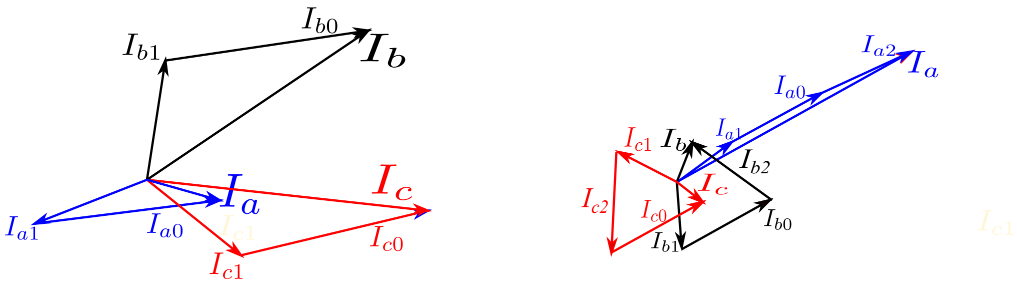
I_{b0}
I_{b1}
I_b
I_a
I_c
I_{a1}
I_{a0}
I_{c1}
I_{c0}
I_{a2}
I_a
I_{a0}
I_{a1}
I_{c1}
I_b
I_{b2}
I_c
I_{c2}
I_{c0}
I_{b0}
I_{b1}

(a) PQ controlled **(b)** V/F controlled

Figure 3.13: Phasor plots for AG fault

3.4 INFERENCES

This chapter investigated the dynamic and transient performance of a BESS based microgrid. BESS plays an important role in solving the power quality and stability issues in the microgrid by providing active and reactive power support. The fast response characteristics of BESS help to smoothen the imbalances between demand and supply at the time of transitions between microgrid modes.

Fault analysis of inverter based DERs with PQ and V/F control strategies are performed. The fault currents from grid following (PQ control) inverters are limited and lack negative sequence components, whereas the grid forming inverters (V/F control) cannot directly regulate the output current. V/F controlled inverters possess higher peak values, contain exponential damping constant and remain unbalanced for asymmetrical faults.

Further, there will be variations in the fault current with different modes of microgrid operation and topologies. Conventional overcurrent and sequence component based relays are thus not applicable for microgrids. As voltages and currents of even healthy phases are modulated by the inverter controllers, schemes based on magnitude of voltage and currents cannot be relied. Distance relays doesn't have much scope in microgrids due to short lines in distribution networks. The subsequent chapters will focus on the development of a protection schemes for microgrids.

Chapter 4

Development of Protection Schemes for an AC microgrid

4.1 INTRODUCTION

The major challenges in microgrid protection based on the transient behavioural study in the previous chapter are

- Variation in the level of short circuit current in GCM and IM. Though in GCM, contribution of short circuit current from IIDGs is less, the grid will provide high fault current.
- Bidirectional flow of current
- Lack of negative sequence components in the fault response of IIDGs with PQ/current controllers.
- PQ control will not allow DG to dissipate into a fault when the reference power is negative, leading to directional relays' mal-operation.

This chapter proposes protection schemes for microgrids that addresses the above concerns and contains main two sections. First section deals with adaptive protection schemes and second section discusses a non-adaptive differential protection scheme.

A main and backup protection scheme, capable of exact fault location is proposed in Section. 4.2. The proposed scheme uses magnitude and angle of superimposed positive sequence impedance for estimating direction. The Main Protection Unit (MPU) detects an internal fault when there is a mismatch in the direction of relays at either end of a feeder. The backup scheme uses adaptive overcurrent relay settings.

Among the conventional relays, differential protection schemes possess maximum accuracy. However, phase based differential relays cannot be adopted in microgrids due to their cost (mainly due to the communication requirements) and unconventional fault signatures of IIDGs. Section. 4.3 proposes a low cost differential protection scheme based on fundamental frequency superimposed current phasors. The phasors are extracted using dq components instead of conventional Fourier algorithms.

The performance of proposed schemes are evaluated for different fault scenarios by MATLAB/SIMULINK simulations on a test microgrid. The results confirm that internal faults are detected in a few milliseconds. At the same time, the schemes remains insensitive to external faults with CT saturation and other system disturbances. The proposed schemes are unaffected by the microgrid mode of operation, direction of power flow and DG type.

4.2 ADAPTIVE PROTECTION SCHEMES

4.2.1 Protection Principle

The basic principles and proposed algorithms for microgrid protection are elaborated in this subsection.

4.2.1.1 Superimposed positive sequence impedance

When a fault occurs, the corresponding voltages (V) and currents (I) undergoes significant changes. The post fault quantities can be obtained by adding the prefault quantities with these changes referred to as superimposed or fault imposed quantities

$$V_{post} = V_{pre} + \Delta V \tag{4.1}$$

$$I_{post} = I_{pre} + \Delta I \tag{4.2}$$

Superimposed impedance can be defined as

$$\Delta Z = \frac{\Delta V}{\Delta I} \tag{4.3}$$

Since positive sequence components exist for all types of fault, superimposed positive sequence impedance is chosen for fault direction assesment. The pre-fault positive sequence network of a simple microgrid with two sources E_A and E_B is shown in Fig. 4.1a. Relay directions (R_A and R_B) are as indicated in the figure. E_F is the voltage at the fault point prior to the fault. To obtain the superimposed network, all the prefault voltage sources are short circuited and all network components are represented by their impedances. A voltage source with magnitude equal to the pre-fault voltage and phase angle opposite to the prefault phase angle is applied at the fault. [Hashemi et al. (2013)]. The superimposed positive sequence network is obtained as shown in Fig. 4.1b

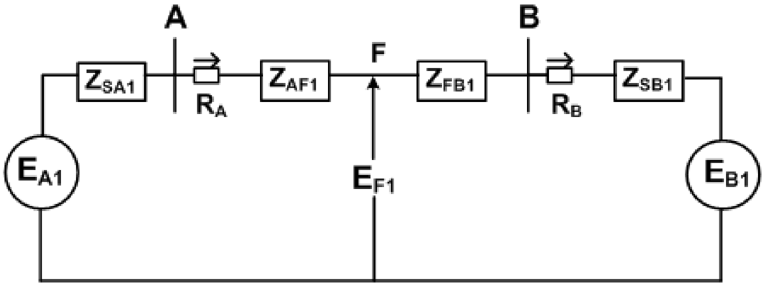

(a) Pre-fault

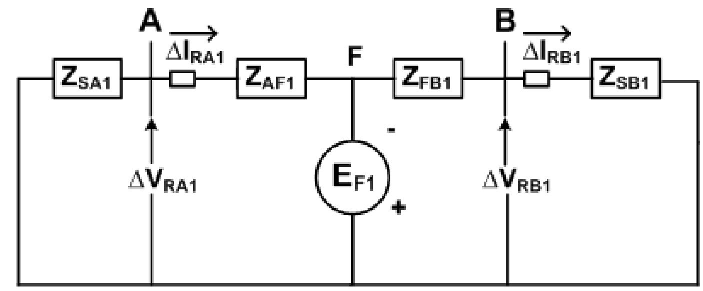

(b) Superimposed

Figure 4.1: Positive sequence networks

Forward Faults: For a fault F as shown in Fig. 4.1a, the superimposed current seen by R_A is same as the relay direction. Hence superimposed positive sequence quantities seen by relay R_A are

$$\Delta I_{RA1} = \frac{E_{F1}}{(Z_{SA1} + Z_{AF1})} \tag{4.4}$$

$$\Delta V_{RA1} = -Z_{SA1}\Delta I_{RA1} = -E_{F1}\frac{Z_{SA1}}{Z_{SA1} + Z_{AF1}} \tag{4.5}$$

Reverse Faults: The fault current and hence the superimposed current seen by relay R_B for the same fault F is opposite to the relay direction.

$$\Delta I_{RB1} = -\frac{E_{F1}}{(Z_{FB1} + Z_{SB1})} \tag{4.6}$$

$$\Delta V_{RB1} = Z_{SB1}\Delta I_{RB1} = -E_{F1}\frac{Z_{SA1}}{Z_{SB1} + Z_{FB1}} \tag{4.7}$$

The sign of superimposed positive sequence current seen by a relay is positive for a forward fault and negative for a reverse fault. Whereas the sign of superimposed positive sequence voltages are negative for both faults. Hence, the superimposed positive sequence impedance (ΔZ_1) is negative during a forward fault and positive during reverse fault. The parameter $cos\angle(\Delta Z_1)$ can be used to identify the sign of superimposed impedance. If it is positive, it implies that sign of ΔZ_1 is positive and hence a reverse fault. This criterion is valid for upstream and downstream power flows.

4.2.2 Proposed Protection Schemes

4.2.2.1 Main protection unit (MPU)

In the main protection scheme, the direction of power flow at end relays of a feeder are estimated. A sign = 1 is assigned for forward flow and a sign = -1 assigned for reverse flow. The feeder end relays are assigned same direction as shown in Fig. 4.1. When there is an internal feeder fault, the end relays show a contradiction in direction . In case of an external fault or at microgrid transitions, the end relays indicate the same direction. When a mismatch in the signs are noted, the trip signals are issued to their corresponding breakers instantaneously, without waiting for an overcurrent fault detection. This helps to isolate the faulty location very fastly. If there is any communication error between the relays or if any relay failed to operate, the adaptive overcurrent relays will offer back up protection.

An adaptive approach is proposed for ascertaining the relay direction. When the DG is PQ controlled and reference power set to negative value, the directional relay may mal-operate. To rectify this, another condition is added to identify a reverse fault in PQ controlled DGs. The magnitude of superimposed positive sequence impedance $|\Delta Z_1|$ must be less than a threshold value $|Z_{th}|$ for a RF. This threshold value is calculated by assuming the closest bolted forward fault. Since the fault current from PQ controlled

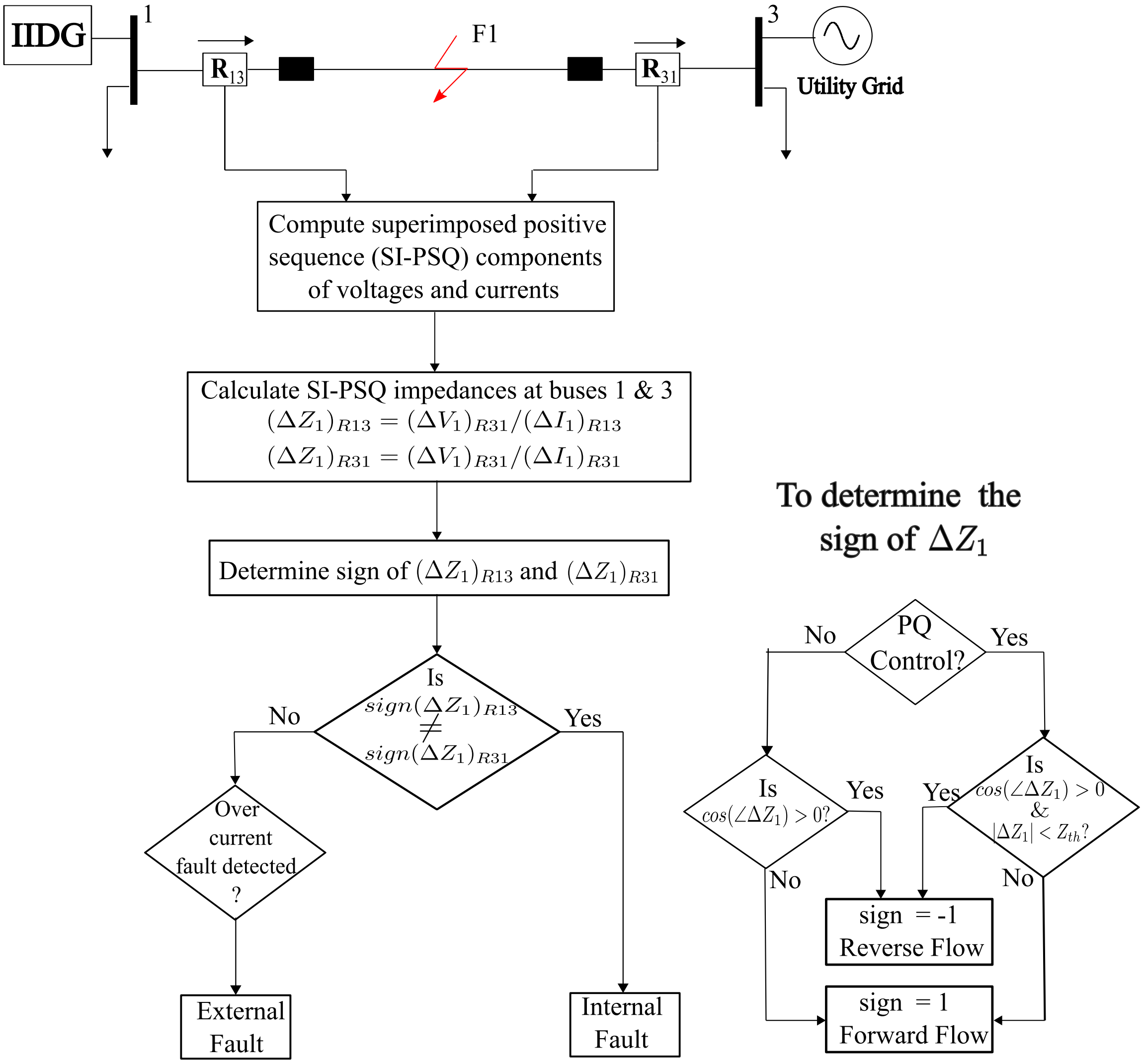
IIDG
1
R_{13}
F1
R_{31}
3
Utility Grid
Compute superimposed positive sequence (SI-PSQ) components of voltages and currents
Calculate SI-PSQ impedances at buses 1 & 3
$(\Delta Z_1)_{R13} = (\Delta V_1)_{R31}/(\Delta I_1)_{R13}$
$(\Delta Z_1)_{R31} = (\Delta V_1)_{R31}/(\Delta I_1)_{R31}$
Determine sign of $(\Delta Z_1)_{R13}$ and $(\Delta Z_1)_{R31}$
Is $sign(\Delta Z_1)_{R13} \neq sign(\Delta Z_1)_{R31}$
No
Yes
Over current fault detected ?
External Fault
Internal Fault
To determine the sign of ΔZ_1
PQ Control?
No
Yes
Is $cos(\angle \Delta Z_1) > 0$?
Yes
No
Is $cos(\angle \Delta Z_1) > 0$ & $|\Delta Z_1| < Z_{th}$?
Yes
No
sign = -1 Reverse Flow
sign = 1 Forward Flow

Figure 4.2: Proposed logic of MPU

inverters is limited, $|\Delta Z_1|$ cannot go below the threshold during forward faults. But, voltage controlled inverters possess higher fault currents and hence this magnitude criteria may fail. Hence this additional criterion is dispensed for conventional generators and IIDGs with grid forming control.

The main protection scheme and the procedure for direction estimation are shown in Fig. 4.2. The computations can be done at any particular relay by fetching data (current phasor) from the adjacent relay or at a central microgrid protection unit (which collects all relays information). As current controlled inverters experience changes in their terminal voltages due to their control, PCC voltages are used for superimposed impedance calculations. A common voltage will also ensure that the trip signals are issued only when there is a current reversal in any of the relays of the line to be protected.

4.2.2.2 Adaptive Overcurrent (AOC) Protection Strategy

The fault current contribution from IIDGs in grid following mode will be limited. Grid is the major short circuit current contributor in this mode. Whereas in grid forming mode, the fault current will be similar to that of synchronous alternators. It is proposed to calculate the pick up current dynamically when the fault contribution is only due to current controlled inverters and proceed with conventional pickup settings in the presence of voltage controlled inverters/grid. When the inverter is PQ/current controlled, the fault pickup is calculated as follows :

1. The positive sequence power at relay locations are computed using a Moving Average Window (one cycle) Filter.

$$P_{1mov-av} = \sum_{i=1}^{N} P_{1i} \tag{4.8}$$

$$P_1 = 3 \times \frac{V_1}{\sqrt{2}} \times \frac{I_1}{\sqrt{2}} \tag{4.9}$$

   $P_{1\text{mov-av}}$ is the moving average power seen by the relay in one cycle. Here i is the sample number and N the number of samples in a cycle

2. The peak value of fault pickup is then calculated as

$$I_{pickup} = a \times \frac{|P_{1mov-av}|}{\frac{3}{2} \times E_1} \tag{4.10}$$

   where a is a constant usually between 1.5 to 2, since the limiters in current controlled inverters limit the fault current to 1.5-2.0 pu. E_1 is also a constant fixed at the positive sequence PCC voltage. Since PCC voltage is 415 V L-L, E_1 is chosen as 339 V.

As mentioned earlier, if the current is limited in PQ controlled inverters, $P_{1mov-av}$ will decrease during fault. Then the pick up current will also reduce as in Eqn. 4.10, thus ensuring operation of the protection devices(PDs) during fault. Whereas synchronous alternators or voltage controlled inverters behave as constant voltage source during fault and inject high current into the fault. So in these cases, $P_{1mov-av}$ will increase and the calculated fault pickup may increase excessively. Therefore conventional pickup setting must be chosen for voltage controlled inverters.

The highlight of this method is that the pickup current adjusts automatically with the load as shown in Fig. 4.13. With the switching of new loads, $P_{1mov-av}$ will increase and hence the pickup current increases and vice versa. This method indirectly uses voltage based protection but avoids unnecessary tripping during load switching. As soon as the AOCR relay picks up, the superimposed impedance components are captured to arrive at the direction decision. However the trip signals are issued only if the fault persists one cycle after AOCR pickup. The microgrid mode of operation, which can be ascertained by the position of switch S in Fig. 3.7 should be communicated to the relays to switch between different settings.

4.2.3 Results and Discussions

The proposed schemes are implemented using MATLAB/ SIMULINK. A sampling rate of 20 samples/cycle is used for phasor estimation using DFT. Superimposed components are computed using a delta filter. In a delta filter, a delayed (by 3 cycles) input signal is subtracted from the input signal itself. The test microgrid of Fig. 4.3 is operated in GCM up to 2s and at t=2s, it transfers to IM. The test fault scenarios are

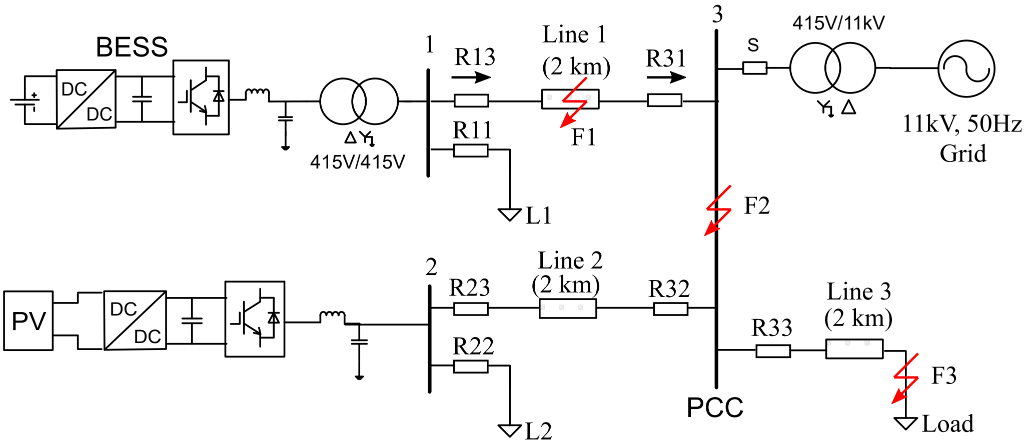
BESS
DC
DC
ΔY
415V/415V
1
R13
Line 1
(2 km)
R31
3
S
415V/11kV
YΔ
11kV, 50Hz
Grid
R11
F1
L1
F2
PV
DC
DC
2
R23
Line 2
(2 km)
R32
R22
L2
R33
Line 3
(2 km)
F3
PCC
Load

Figure 4.3: Test microgrid - 1.

listed below.

- Microgrid mode of operation: Grid connected and Islanded
- BESS modes: Charging and Discharging
- Inverter controller types: Grid following (PQ control, DC link voltage control) and Grid forming (V/F control)
- DER types: PVDG and BESS
- DERs active: BESS and PVDG, BESS only
- Fault types: Single Line to Ground (SLG), Double Line to Ground (LLG), Line to Line (LL) and Three Phase to Ground(LLLG)
- Fault locations: Feeder faults (external and internal), PCC and load terminals
- Fault impedance(ohms): 0(bolted), 0.5(low), 2(medium) and 10(high)

The BESS operates as PQ-IIDG in GCM and V/F-IIDG in IM. Reverse power flow (battery charging) is attained by setting P setpoint negative in GCM and by adjusting load L3 in IM. Some cases are demonstrated below:

4.2.3.1 Performance of Main Protection Unit

Case1: Fault performance when BESS is PQ controlled and grid-connected

A three phase to ground fault is simulated in location F1 at 1.0 s when the battery is charging ($P_{ref} = -10$ kW) and in GCM. Fault resistance is 0.05 Ω. The battery will continue charging even during the fault. Since there is no direction change associated with fault, $\angle\Delta Z_1$ of both relays R13 and R31 varies between (-90°, 90°) as in Fig. 4.4c for more than one cycle after fault inception. The conventional techniques will indicate a reverse fault in both relays. However, the superimposed impedance magnitude is more than threshold impedance in R13 and hence the proposed scheme will indicate the sign of ΔZ_1 as 1 (Forward Fault). Relay R31 gives a sign=-1 (as $|\Delta Z_1|$ is less than the threshold) indicating a reverse fault. Thus there is a mismatch in the signs of R13 and R31, and the fault is detected within half cycle.

Case2: Performance under HIF when BESS is voltage controlled in standalone mode

To assess the performance of MPU unit for a high impedance fault (HIF), the system is operated in islanded mode. Further, a single line to ground fault with a fault resistance of 10 Ω is initiated at F1 while battery is in charging mode. It is clear from Fig. 4.5a that current in relay R13 which is contributed by BESS (V/F controlled inverter in IM) is asymmetrical. In contrast, the current (Fig. 4.5b) in relay R31 contributed by PV (current controlled inverter) remains symmetrical for a SLG. Since it is a HIF, there is no significant variation in the fault current magnitude. The faulted phase current in relay R13 reverses and the argument of superimposed impedance of R13 exceeds -90° as in Fig. 4.5c. Thus the sign computed by R13 is -1 indicating a forward fault. Contrary to this, R31 calculates +1 indicating a reverse fault. The proposed MPU scheme can thus detect faults within a half cycle, excluding communication delays.

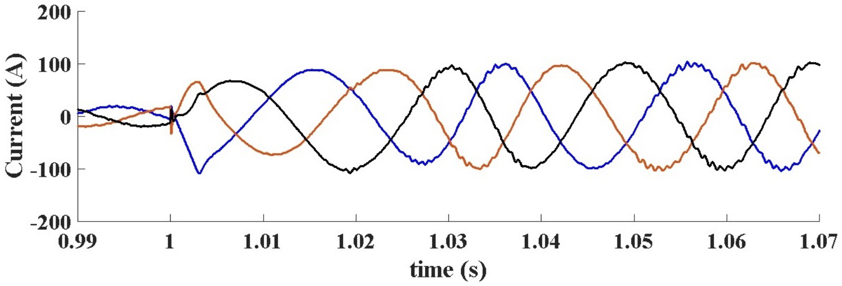

(a) R13 fault current

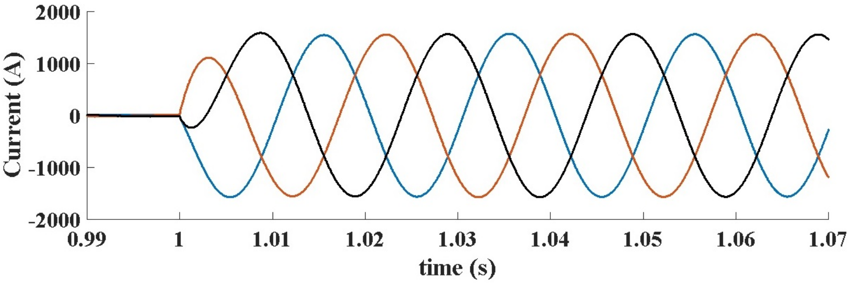

(b) R31 fault current

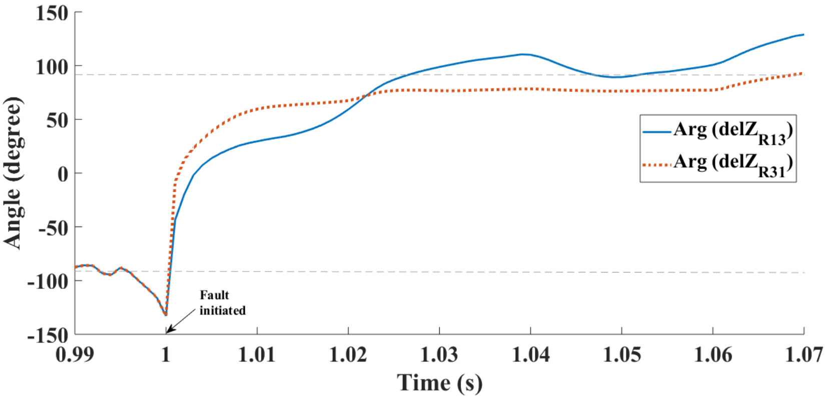

(c) $\angle \Delta Z_1$ of relays R13 and R31

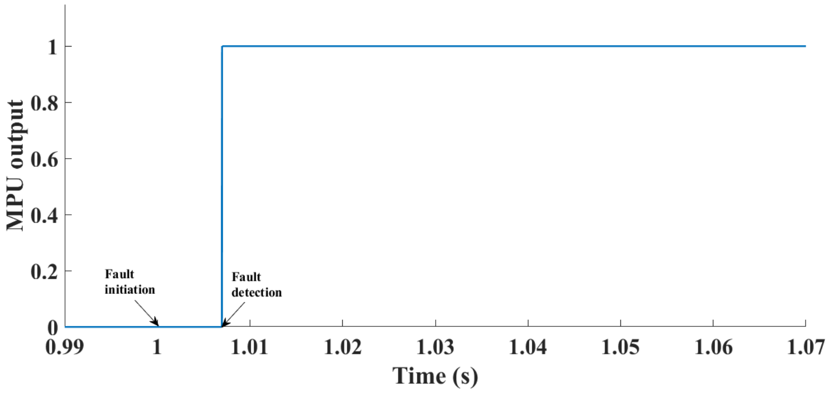

(d) MPU output

Figure 4.4: Case1: MPU performance for a LLLG fault in GCM

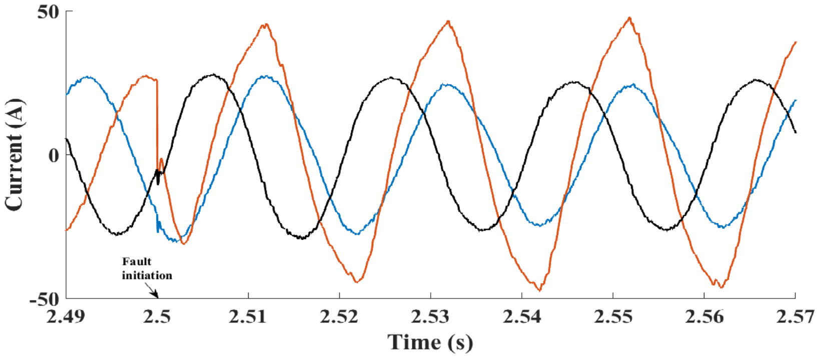

(a) R13 fault current

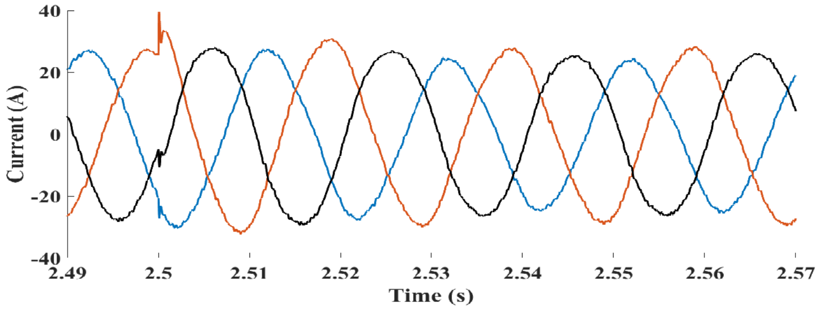

(b) R31 fault current

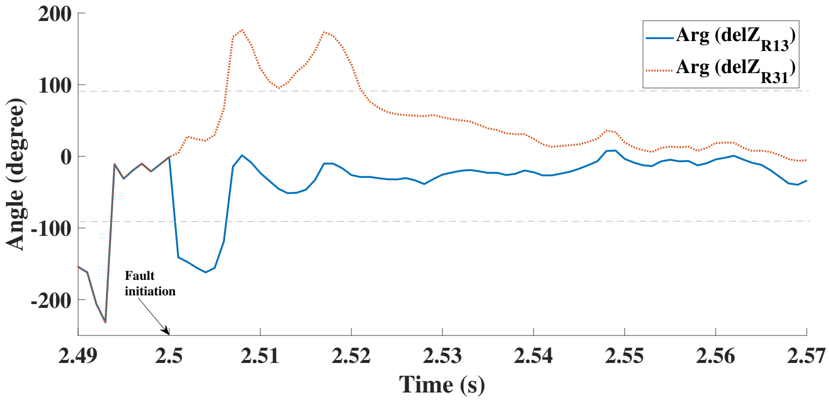

(c) $\angle \Delta Z_1$ of relays R13 and R31

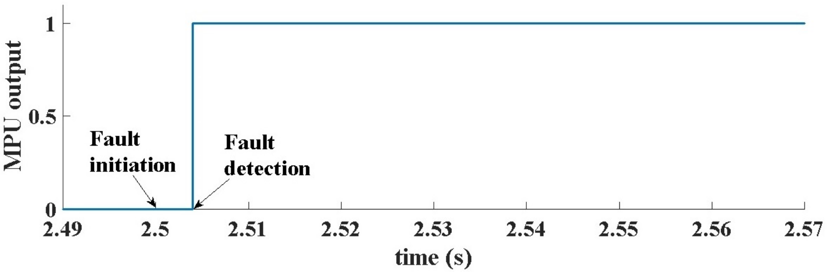

(d) MPU output

Figure 4.5: Case2: MPU performance for an SLG fault in IM

Case3: Performance when BESS is voltage controlled and grid-connected

BESS inverters with grid forming control are finding application in VSM (Virtual Synchronous Machine) technology, as it provides virtual inertia. To assess the performance of proposed protection scheme in such cases, a three phase fault is simulated at F1 with $R_f = 0.05\Omega$. Since BESS is voltage controlled, angle criterion is sufficient. When fault occurs, $\angle\Delta Z_1$ of R13 exceeds -90^0 as in Fig. 4.25c indicating a forward fault. Whereas relay R31 indicates a reverse fault and the fault is detected in 4 ms.

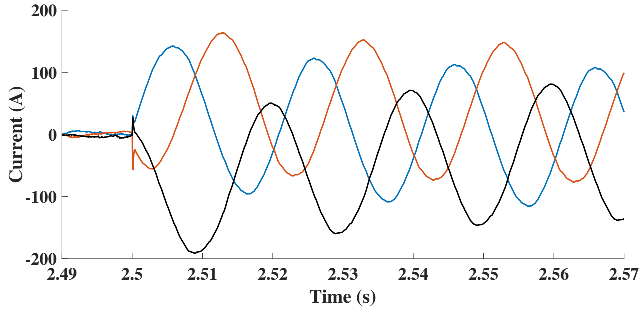

(a) R13 fault current

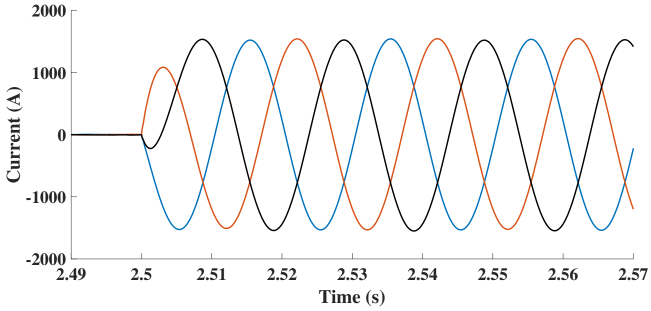

(b) R31 fault current

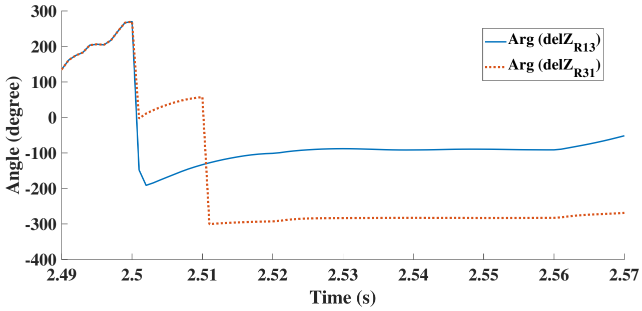

(c) $\angle\Delta Z_1$ of relays R13 and R31

Figure 4.6: Case3: MPU performance for a LLLG fault in GCM and BESS voltage controlled

Case4: Performance in the presence of decaying DC component

To illustrate the performance of the proposed scheme in the presence of a decaying DC component, a single line to ground fault with fault resistance $R_f = 0.001\Omega$ has been simulated. The BESS is charging, voltage controlled and in the islanded mode of operation. Fig. 4.7a shows the current waveforms at R13. It can be observed that a significant decaying DC component is present in the current waveform after the fault inception. The response of the MPU scheme for the aforementioned scenario is shown in Fig. 4.7b. The relay R13 registers a forward and R31 registers a reverse fault, immediately after the fault inception. Since there is a mismatch in the fault direction assessed by relays R13 and R31, the fault is confirmed within 3ms.

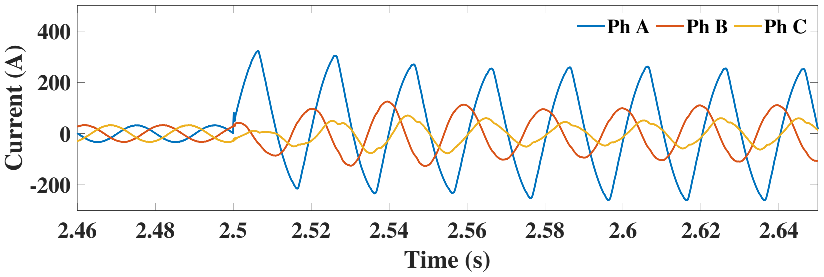

(a) R13 current waveform

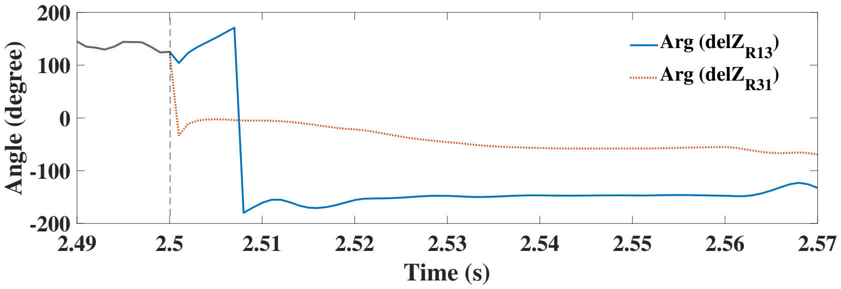

(b) $\angle \Delta Z_1$ of relays R13 and R31

Figure 4.7: Case4: Performance in the presence of decaying DC component

Case5: Performance under far and near end faults

An LLLG fault with Rf=0.05Ω is simulated on Line 1 at a distance of 10m from the relay R13. This can be considered as a near-end (close-in) fault with respect to relay R13 and a far-end (remote bus) fault for relay R31 present at the other end of the line. The BESS is PQ controlled and hence the fault current response at relay R13 is as shown in Fig. 4.25a. The current at relay R31 is mainly contributed by the grid and shown in Fig. 4.25b. When the fault occurs in Line 1, Relay R13 sees a forward fault and relay R31 sees a reverse fault. The fault is detected in 6 ms.

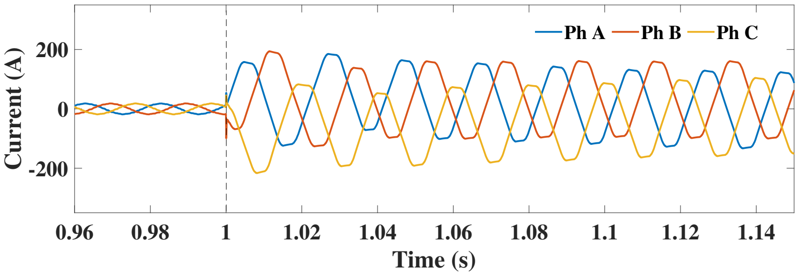

(a) R13 fault current

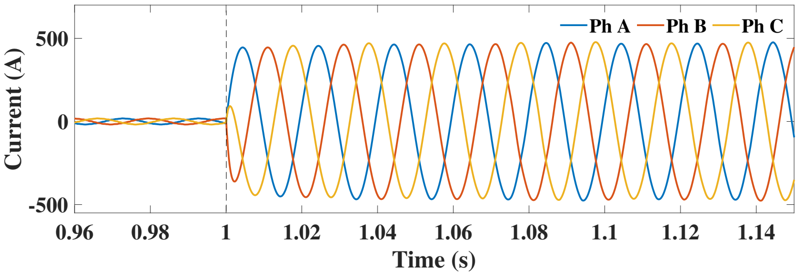

(b) R31 fault current

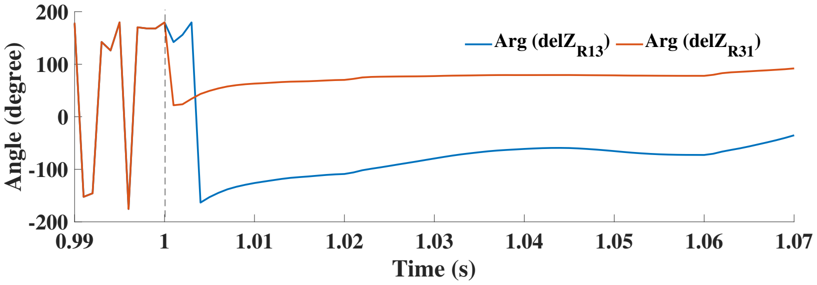

(c) $\angle\Delta Z_1$ of relays R13 and R31

Figure 4.8: Case5: Performance under far and near end faults

Case6: Performance under high resistance and high impedance faults

To validate the performance of the protection scheme under high resistance and high impedance faults, a medium-voltage (MV) microgrid as shown in Fig. 4.9 with higher penetration of PV is chosen. Relays R_M and R_N are aligned in the same direction in this scheme. A high resistance SLG fault $(R_f = 50\Omega)$ was simulated at location F. The fault was assessed by the proposed scheme in 6.67 ms.

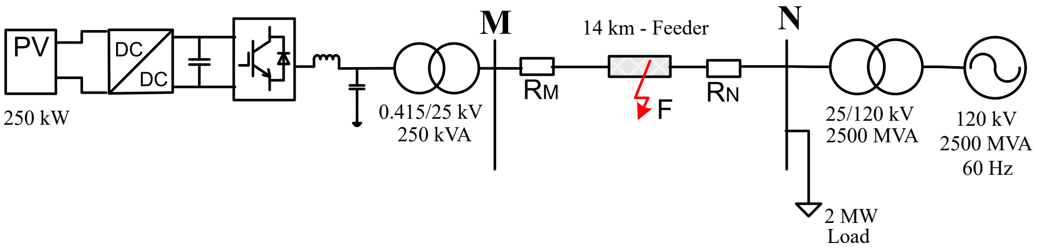

Figure 4.9: Test microgrid - 2.

HIFs are common in distribution systems. They occurs when an overhead conductor breaks or touches high impedance surfaces such as asphalt, concrete, tree, sand, cement etc. Due to the high impedance at the fault point, fault currents are restricted. These faults are often accompanied by arcing and hence their characteristics resembles a stochastic non-linear current. For simulating HIF, the Emmanuel arc model [2003] was chosen. This model has two unequal resistances that represent asymmetric fault currents and is shown in Fig. 4.10.

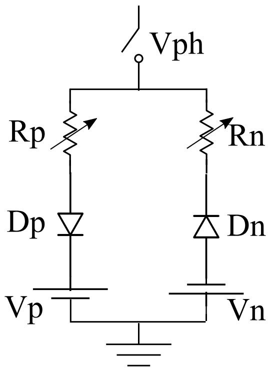

Figure 4.10: The Emmanuel arc model.

An SLG fault is initiated on the test feeder at t=1s. The parameters are Rp=1000 Ω, Rn=1050 Ω, Vp=10 kV, and Vn=10.5 kV. The relay M and relay N currents are shown in Fig. 4.11a and Fig. 4.11b below. As soon as the fault is initiated, $\angle(\Delta Z_1)$ of the relay R_M exceeds $(-90^0, 90^0)$ indicating a forward fault and relay R_N stays within $(-90^0, 90^0)$ indicating a reverse fault. Since there is a mismatch in the fault directions assessed by end relays, the fault is detected in 4 ms

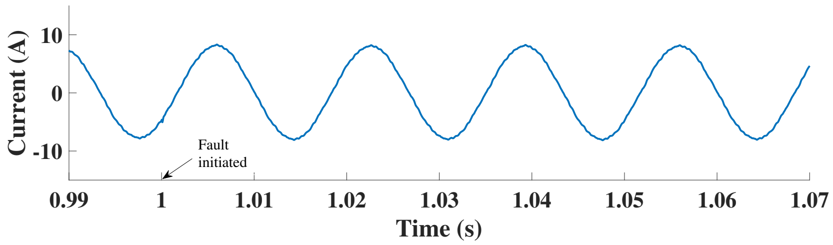

(a) R_M fault current

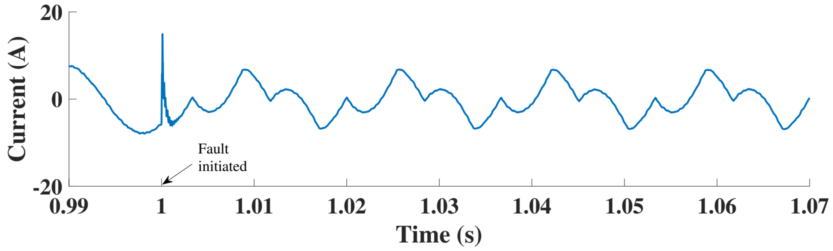

(b) R_N fault current

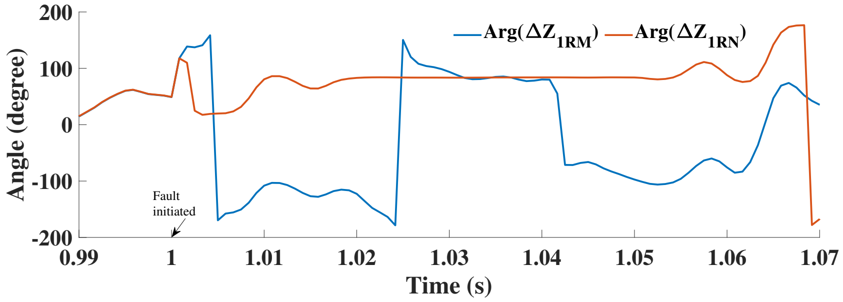

(c) $\angle\Delta Z_1$ of relays R_M and R_N

Figure 4.11: Case 6: Performance under HIF

4.2.3.2 Performance of Adaptive Overcurrent Scheme

A LL fault is simulated from 1s to 1.5s in GCM and from 2.5s to 3s in IM to evaluate the performance of proposed strategy.

Since BESS employs current controlled inverter in GCM, pickup current is calculated dynamically. As the voltage dips during fault and the fault current is limited in this mode, $P_{1\text{mov-av}}$ decreases. The computed pickup current decreases as shown in Fig. 4.12a. Since the positive sequence current seen by relay R13 exceeds the pickup, the overcurrent relay will act. When BESS employs voltage control, fixed pickup is used as shown in 4.12b.

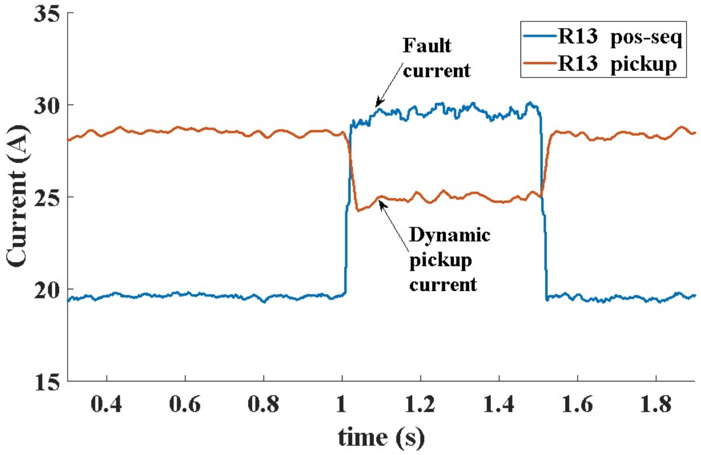

(a) Dynamic pickup setting of relay R13 in GCM (BESS inverter PQ controlled)

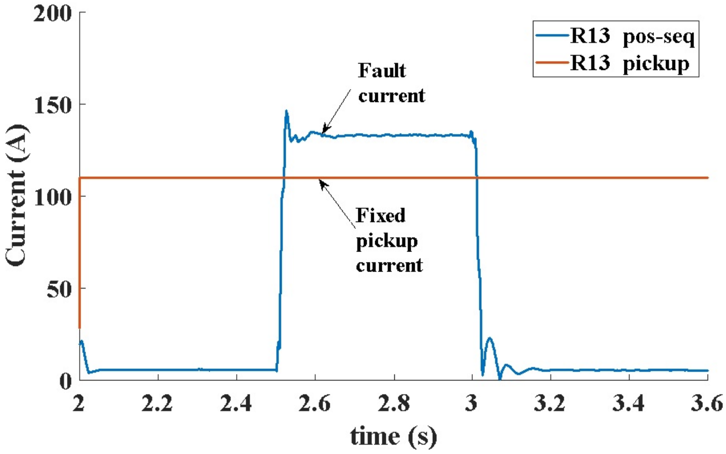

(b) Fixed pickup setting of relay R13 in IM (BESS inverter V/f controlled)

Figure 4.12: Adaptive settings of relay R13

4.2.3.3 Performance of the proposed schemes to other system disturbances

The MPU unit remains insensitive to other disturbances like microgrid transitions, DG disconnection, load switchings, variations in DG penetration level etc. The current direction seen by BESS feeder relays R13 and R31 remains same for all the above cases. These relays will witness a direction change only when an internal fault occurs.

The pickup current in proposed AOC scheme adjusts itself with changing system conditions as shown in Fig. 4.13. At t=2.0s, the microgrid transits from GCM to islanded mode and BESS shifts from charging to discharging operation. The pickup

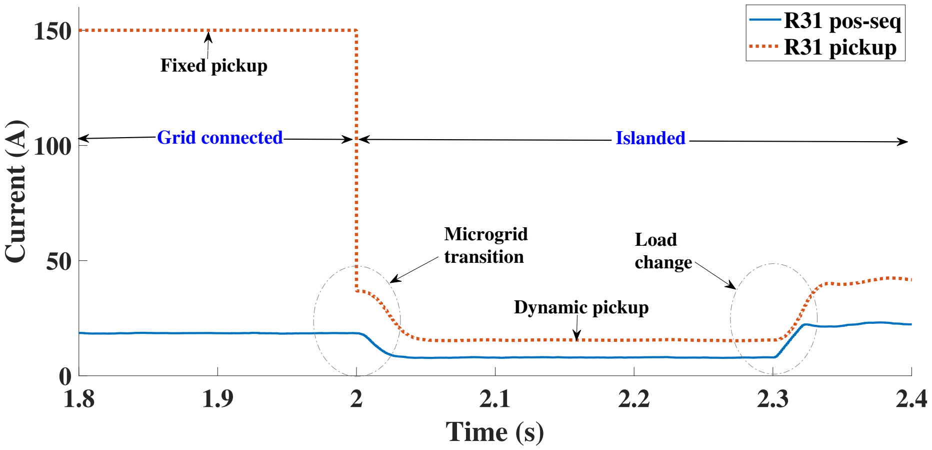

Figure 4.13: R31 pickup adapting to system changes in AOC scheme.

setting changes from fixed to dynamic when BESS shifts to V/f mode. To simulate a load change, an additional load of 15 kW and 5 kVAR is inserted at t=2.3s in L3 to an existing load of 30 kW and 5 kVAR. However, the AOC scheme may not detect single phase high resistance faults. The voltage drop will be negligible in such case and hence the positive sequence power and thus computed pickup current remains almost constant.

4.2.3.4 Relay Coordination

The proposed MPU offers high selectivity and instantaneous protection. If a fault occurs in feeder 1-3, the MPU will issue instant trip signals to breakers of R13 and R31. If MPU fails or if fault is external, the AOC scheme of R13 and R31 will offer backup protection. Time delayed definite time overcurrent relays are used for AOC scheme implementation. To validate the AOC scheme, the trip signals issued by MPU are not applied to the CBs and hence fault is remaining in the system. For relay coordination, a delay time of 0.3 s is set for R31 and 0.6 s for R13. If the fault is persisting or R31 does not operate, then R13 will offer backup. Similarly when a fault occurs at the load L3, the individual relay R33 should act first. If it fails, AOC schemes in R13 and R31 will offer backup.

Three phase faults were simulated at locations F1 (at the midpoint of BESS feeder

Table 4.1: Performance of the proposed schemes for various faults

Fault Location	Microgrid Mode	Battery Mode	Fault Initiation T_f(s)	Proposed MPU T_{trip}(s)	Proposed AOCR R13 T_{trip}(s)	Proposed AOCR R31 T_{trip}(s)
F1	GCM	Discharging	1	1.011	1.607	1.312
	GCM	Charging	1	1.011	1.615	1.311
	IM	Discharging	2.5	2.509	3.015	2.811
	IM	Charging	2.5	2.506	3.117	2.814
F2	GCM	Discharging	1	No Trip	1.619	No Trip
	GCM	Charging	1	No Trip	1.613	No Trip
	IM	Discharging	2.5	No Trip	3.119	2.806
	IM	Charging	2.5	No Trip	3.12	2.812
F3	GCM	Discharging	1	No Trip	No Trip	No Trip
	GCM	Charging	1	No Trip	No Trip	No Trip
	IM	Discharging	2.5	No Trip	3.123	2.807
	IM	Charging	2.5	No Trip	3.124	2.814

Including communication delay and relay coordination time

1-3), F2 (at PCC) and F3 (at load L3) to validate the proposed schemes. Like previous cases, the fault is simulated at 1s in GCM and at 2.5s in IM with a fault resistance of 0.05Ω. Considering a communication delay of 3ms (extreme case), the time at which trip signals are issued by primary and backup protection are tabulated in Table 4.1. The MPU will issue trip signal only if the fault is internal to the BESS feeder. If the fault is external, AOC protection scheme will issue trip signals to R13 and R31 breakers with a coordination time of 0.3 s. The fault F3 at load L3 in GCM is not detected by the relays R13 and R31. This is because in GCM, major contributor to the faults is grid. The individual relays connected at the load branch can easily detect the fault due to very high short circuit current from grid. In IM, when there is a significant contribution from BESS, the AOC protection in relays R13 and R31 will detect the fault. R13 and R31 must respond to faults in IM, because there is a significant contribution to the fault from BESS and chances of R33 not responding in IM to fault F3 due to reduced fault current is also present.

4.2.3.5 *Comparative evaluation of proposed MPU scheme with existing adaptive directional relays*

The comparison of proposed directional relay with DOCR relay [Muda and Jena (2017a)] for different modes of operation is summarised in Table. 4.2. This technique could not assess the fault direction accurately when BESS is PQ controlled and charging. Under this condition, both relays R_{13} and R_{31} assess reverse fault for feeder fault F_1 and hence method [Muda and Jena (2017a)] fails. Moreover, the direction assessment rules are different for forward power flow (BESS discharging) and reverse power flow (BESS charging). Hence directional relays based on phase angles are not suitable for BESS feeders. The proposed technique will record a reverse fault in grid following mode only when the superimposed impedance magnitude is less than threshold impedance; which is set as 0.1 Ω.

Table 4.2: Direction Assesed for Internal Fault (F1) - Comparison

		Grid Connected				Islanded Mode			
		BESS Discharging		BESS Charging		BESS Discharging		BESS Charging	
Method	Feature Used	R13	R31	R13	R31	R13	R31	R13	R31
H Muda *et al.*	Angle between SI-PSQ & prefault PSQ currents	-64.19	134.4	-39.31	-28.12	-10.3	193	111.08	-67.98
	FPF: ϕ = +ve ⇒ R								
	RPF: ϕ = -ve ⇒ R								
	Decision	F	R	R	R	F	R	F	R
Proposed	$\lvert\Delta Z_1\rvert$ (in GCM only)	2.432	0.075	1.808	0.052				
	$\angle\Delta Z_1$ (both modes)	-111.45	76.006	88.31	76.52	-129.6	36.88	-137.7	41.31
	Decision	F	R	F	R	F	R	F	R

FPF-Forward Power Flow, RPF-Reverse Power Flow, F-Forward Fault, R-Reverse Fault, SI PSQ - superimposed positive sequence

The proposed MPU technique is also compared with a transient energy (TE) based scheme [Bhatraj and Nayak (2019)] and positive sequence fault current (PSFC) based differential protection scheme [Gao et al. (2017)]. The transient energies (TE) are derived at both ends of feeder for each phase. If TE at both ends are negative (relays

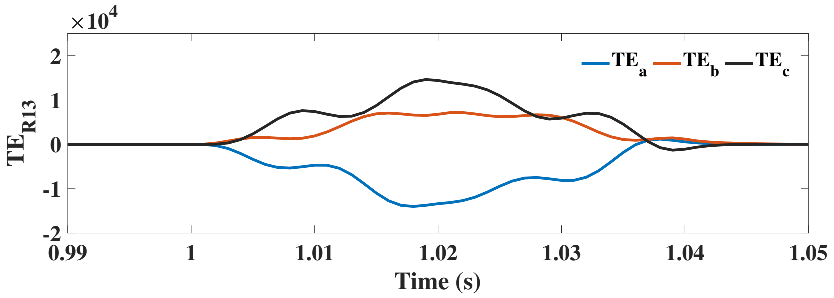

(a) Transient energy at R13 for an ACG fault at F_1 in GCM

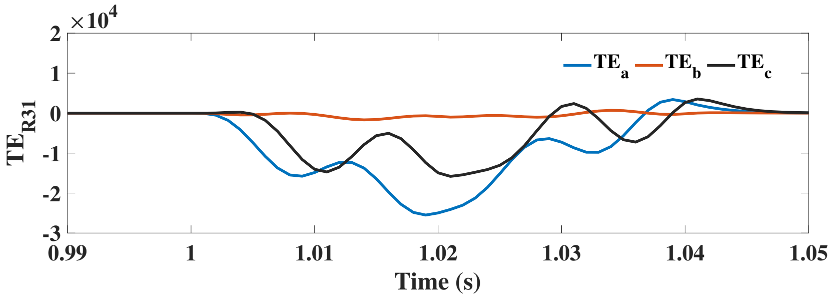

(b) Transient energy at R31 for an ACG fault at F_1 in GCM

Figure 4.14: Performance of TE based schemes

are directed towards the feeder) and exceeds a threshold, the corresponding phase of the feeder is identified as faulty. To evaluate its performance, an ACG fault with fault resistance 0.05Ω is simulated at F1 when BESS is charging and in GCM.

The fault currents at relay R_{31} are mainly contributed by the grid. The TE of faulted phases A and C exceeds the threshold and are negative as shown in Figure. 4.14b. Whereas the fault current at relay R_{13} is contributed by PQ controlled BESS. The TE of all phases exceeds the threshold and the TE of faulted phase C is positive as shown in Figure. 4.14a. Hence this method [Bhatraj and Nayak (2019)] find limitation with penetration of IIDGs. The performance comparison in Table. 4.3 confirms that proposed MPU technique is relatively faster and capable of detecting faults at all operating scenarios of a microgrid.

Table 4.3: Comparative Assessment for F1 fault with $R_f = 0.05\Omega$

Mode of operation	Fault instant	Fault Type	Proposed MPU	Diff scheme	TE based scheme		
					Ph A	Ph B	Ph C
Grid connected and BESS discharging	1s	ABCG	1.003s	1.006s	1.003s	1.003s	1.005s
	1s	BCG	1.003s	1.007s	-	1.002s	1.005s
	1s	BC	1.012s	1.006s	-	1.01s	1.009s
	1s	BG	1.003s	1.007s	-	1.002s	-
Grid connected and BESS charging	1s	ABCG	1.008s	1.006s	No Trip	No Trip	No Trip
	1s	BCG	1.005s	1.007s	-	1.002s	1.005s
	1s	BC	1.012s	1.007s	-	No Trip	No Trip
	1s	BG	1.004s	1.007s	-	1.002s	-
Islanded and BESS discharging	2.5s	ABCG	2.506s	2.509s	2.503s	2.503s	2.506s
	2.5s	BCG	2.503s	2.516s	-	2.503s	2.506s
	2.5s	BC	2.504s	2.513s	-	2.508s	2.51s
	2.5s	BG	2.509s	No Trip	-	2.503s	-
Islanded and BESS charging	2.5s	ABCG	2.503s	2.509s	2.503s	2.503s	2.506s
	2.5s	BCG	2.502s	2.516s	-	2.503s	2.506s
	2.5s	BC	2.503s	2.513s	-	2.508s	2.51s
	2.5s	BG	2.51s	No Trip	-	2.503s	-

Excluding communication delays

4.3 SUPERIMPOSED CURRENT BASED DIFFERENTIAL PROTECTION SCHEME

The adaptive schemes presented in the above section requires adaptive settings with different controls (grid following or grid forming) and voltage information. The next chapter will focus on the development of a current based differential relay that is not deterred by the microgrid topology, inverter control scheme, direction of power flow and type of fault.

4.3.1 Protection Principle

The relays are placed at either end of the protected feeder (MN) directed towards the feeder. During normal conditions, the relay currents are equal in magnitude and opposite in direction.

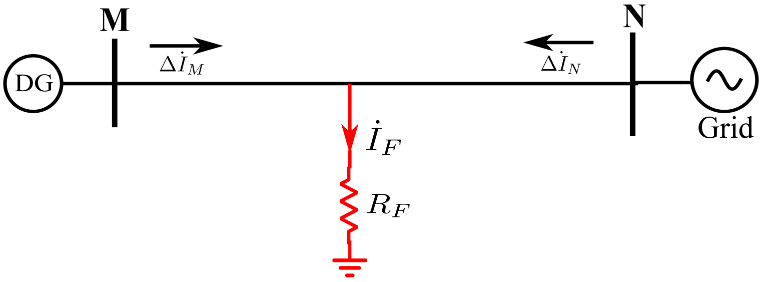

Figure 4.15: Internal fault in a microgrid feeder.

$$\dot{I}_{Mpre} + \dot{I}_{Npre} = 0 \tag{4.11}$$

where I_{Mpre}, I_{Npre} are the pre-fault currents. When an internal fault occurs in the feeder,

$$\dot{I}_{MF} + \dot{I}_{NF} = \dot{I}_F \tag{4.12}$$

I_{MF} and I_{NF} are the fault currents. The difference between fault and pre-fault currents are called incremental or superimposed currents. The fault current can be rewritten in terms of superimposed currents at buses M and N as in Eqn. 4.13.

$$\dot{I}_F = \Delta\dot{I}_M + \Delta\dot{I}_N \tag{4.13}$$

Park's transformation: Park's transformation is widely used in electrical machine models for the elimination of time-varying inductances. It achieves this by converting three-phase quantities (abc) to a rotating reference frame (dq0 frame) consisting of direct, quadrature, and zero axes components.

A set of balanced three-phase signals when passed through this transformation result in constant d and q-axes components, if the rotating reference frame is synchronized with the fundamental frequency of the signals. However, when Park's transformation is applied to an unbalanced system, the resultant dq components will oscillate at double frequency. These oscillations are due to the presence of negative sequence components.

The projection of symmetrical components in the locus diagram of an unbalanced system in dq0 coordinates is shown in Fig. 4.16 [O'Rourke et al. (2019)]. The positive sequence vector rotates in the same direction as the dq0 frame and hence its components appear as dc values. In contrast, the negative sequence vector rotates opposite to the dq0 frame. Its d and q components will show as second harmonic. The zero sequence component lies along 0 axis.

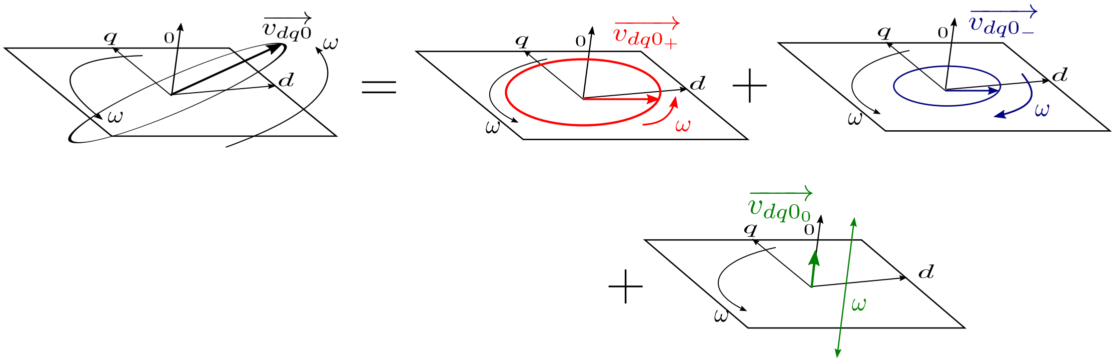
q
0
$\overrightarrow{v_{dq0}}$
ω
d
ω
=
q
0
$\overrightarrow{v_{dq0_+}}$
d
ω
ω
+
q
0
$\overrightarrow{v_{dq0_-}}$
d
ω
ω
+
$\overrightarrow{v_{dq0_0}}$
q
0
d
ω
ω

Figure 4.16: Locus diagram of an unbalanced system in rotating dq0 coordinates.

Park's transformation is applied to currents from a synchronous generator and an IIDG under steady-state and unsymmetrical fault conditions. It is clear from Fig. 4.17a and 4.17b that d, q axes currents stay constant till faults are applied, after which they start oscillating with double frequency. Since the fault currents from IIDGs are limited and lack negative sequence components, there are no appreciable disturbances in d-axis or q-axis currents as shown in Fig. 4.17b. The proposed differential relaying algorithm uses both d and q axes current components. The zero axis current is eliminated as it aligns with the zero sequence current. To enhance the sensitivity of the protection scheme even under weak infeed or high impedance fault(HIF), superimposed currents are used. Besides, they ensure that operating quantity is zero under steady-state conditions. The superimposed current phasor at each terminal is derived as

$$\dot{\Delta I} = \Delta I_d + j\Delta I_q = (\Delta I_d^{+} + \Delta I_d{}^{-}) + j(\Delta I_q^{+} + \Delta I_q^{-}) \tag{4.14}$$

Thus, a single phasor that encompasses both positive and negative sequence components (indicated by + and - superscripts in Eqn. 4.14) is achieved by Park's transformation. As the proposed method exchanges only this phasor between terminals, communication load is significantly reduced. Symmetrical and unsymmetrical faults can

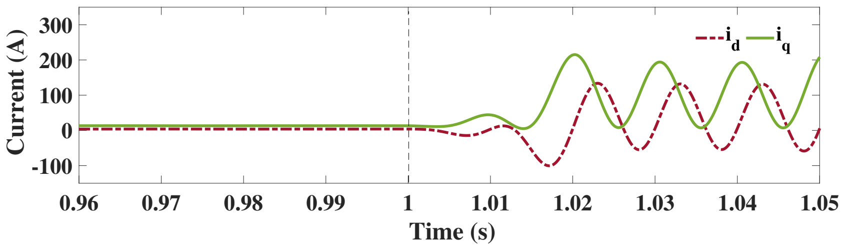

(a) Synchronous generators

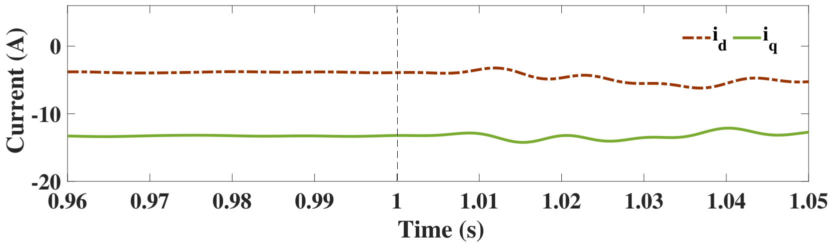

(b) Inverter Interfaced Distributed Generators

Figure 4.17: dq currents under HIF

be easily detected as the transmitted phasor preserves positive and negative sequence characteristics. The computation of operating and restraining currents for the proposed differential relay is detailed in the next section.

4.3.2 Proposed Protection Scheme

This subsection elaborates the differential relaying algorithm and its implementation. The schematic of proposed scheme is shown in Fig. 4.18.

4.3.2.1 Algorithm

The instantaneous phase current signals at each terminal are first passed through a low pass filter. To obtain the superimposed components, a delayed input signal is subtracted from the input signal itself.

$$\Delta i(t) = i(t) - i(t - 3N) \tag{4.15}$$

t is the sampling instant and N is the number of samples per cycle in Eqn. 4.15. $\Delta i(t)$ will be zero under steady state conditions and non zero during disturbances. Thus,

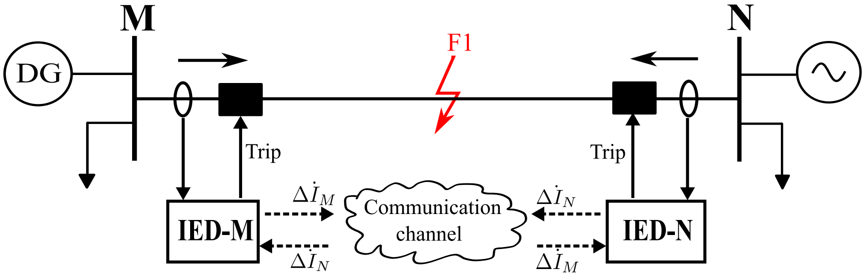

Figure 4.18: Schematic of proposed differential protection.

superimposed components offer a preliminary level of disturbance detection to the protection scheme.

The superimposed current signals (Δi_a, Δi_b, Δi_c) are then converted to dq frame by using Park's transformation in Eqn. 4.16.

$$\begin{bmatrix} \Delta I_d \\ \Delta I_q \end{bmatrix} = \frac{2}{3} \begin{bmatrix} cos\theta & cos(\theta - \frac{2\pi}{3}) & cos(\theta + \frac{2\pi}{3}) \\ -sin\theta & -sin(\theta - \frac{2\pi}{3}) & -sin(\theta + \frac{2\pi}{3}) \end{bmatrix} \begin{bmatrix} \Delta i_a \\ \Delta i_b \\ \Delta i_c \end{bmatrix} \tag{4.16}$$

where $\theta = wt$ and w is the angular frequency of fundamental wave.

Fundamental frequency superimposed current phasors at terminals M and N are then obtained as

$$\begin{aligned} \Delta\dot{I}_M &= \Delta I_{dM} + j\Delta I_{qM} \\ \Delta\dot{I}_N &= \Delta I_{dN} + j\Delta I_{qN} \end{aligned} \tag{4.17}$$

The operating and restraining currents of the proposed differential relay are calculated using Eqn. 4.18. If they are computed instantaneously, it would contain double frequency components. To eliminate it, a moving average approach is used to calculate the operating current $I_{op}(t)$ and restraining current $I_{res}(t)$.

$$\begin{aligned} I_{op}(t) &= \frac{\sum_{i=t-L+1}^{t} |\Delta\dot{I}_M(i) + \Delta\dot{I}_N(i)|}{L} \\ I_{res}(t) &= m \times \frac{\sum_{i=t-L+1}^{t} |\Delta\dot{I}_M(i) - \Delta\dot{I}_N(i)|}{L} \end{aligned} \tag{4.18}$$

where L is the data window length for computing moving average and m is the restraining coefficient. m value is chosen such that relay will not malfunction during external faults with CT saturation and its value ranges from 0.25 to 0.8 [Fletcher et al. (2014)]. The differential protection criterion is set as

$$I_{op}(t) > I_{res}(t) \tag{4.19}$$

As the end relays are directed towards the feeder, the operating current i.e. $(\Delta\dot{I}_M + \Delta\dot{I}_N)$ will be negligible for external faults and approximates fault current as in Eqn. 4.13 for internal faults.

4.3.2.2 Algorithm Implementation

The schematic of proposed differential protection is shown in Fig. 4.18. The differential protection algorithms (Equations. 4.18) are built in the terminal IEDs as in Fig. 4.19, which are time-synchronised by a GPS clock. The transmitted and received superimposed current phasors with the same timestamp are processed to calculate the operating

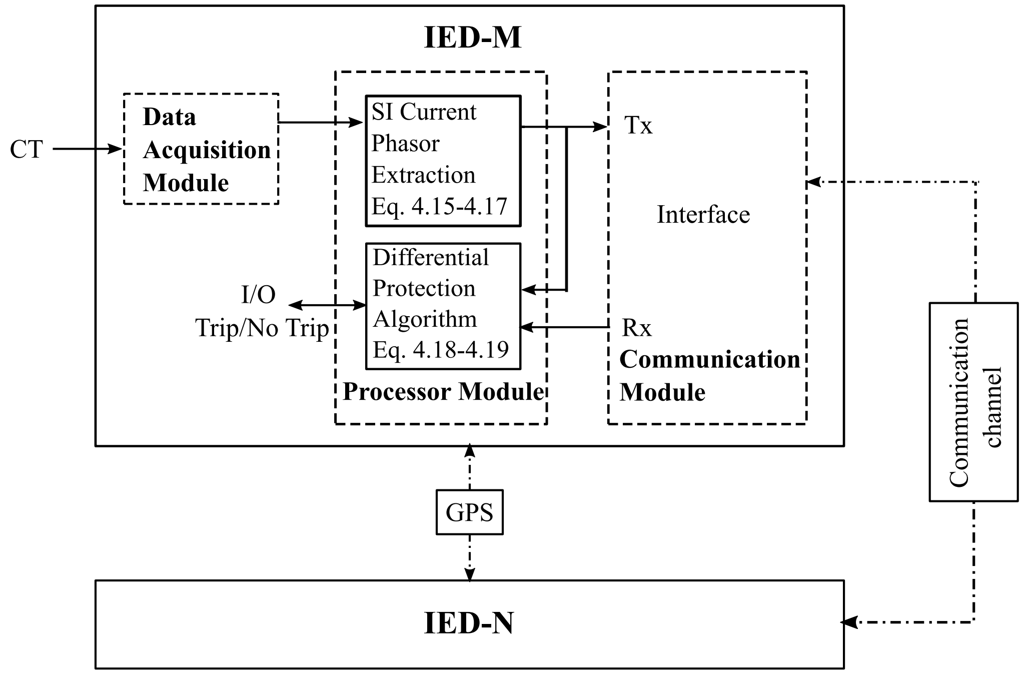
IED-M
CT
Data Acquisition Module
SI Current Phasor Extraction Eq. 4.15-4.17
Differential Protection Algorithm Eq. 4.18-4.19
I/O Trip/No Trip
Processor Module
Tx
Interface
Rx
Communication Module
Communication channel
GPS
IED-N

Figure 4.19: IED relay hardware architecture.

and restraining currents. When the protection criterion in Equation. 4.19 is met, the IEDs issue trip signals to their respective CBs.

4.3.2.3 Advantages of proposed protection scheme

- The proposed method offers high sensitivity. Sensitivity is the ability of the protection system to detect even the smallest faults within the protected zone. For the same restraining coefficient m, the ratio of operating to restraining currents for a SLG fault with $R_f = 3\Omega$ (HIF) is 1.41 for Gao's method, 1.405 for 87BD scheme and 3.922 for proposed method.

- Fault detection using phasor estimation methods such as Fourier requires one to two cycles. Whereas this method extracts fundamental frequency phasor very fastly using abc-dq transformation. As calculation of dq components does not require buffering of previous samples, storage and computation requirements are reduced significantly.

- High sampling frequency is not required as dq components are extracted at the fundamental frequency.

- Conversion to dq frame facilitates use of a single relay instead of three phase segregated relays in terms of phase a, b, and c currents. The communication load and associated circuitry cost reduce as a single phasor needs to be transmitted.

- Requires current measurements only.

- The estimated phasor using dq components contains both positive and negative sequence components. Inclusion of negative sequence components will increase the operating (differential) currents compared to methods which uses only positive sequence components [Gao et al. (2017)]. This will facilitate easy detection of faults, including high impedance(HIF).

- This method does not require any adaptive settings and valid for different microgrid topologies.

4.3.3 Results and Discussions

The performance of proposed differential scheme is analysed by simulating various faults and non-fault transients on the test microgrid shown in Fig. 4.20. The operation and control of microgrid is same as elaborated in Section. 3.2. The current signals are sampled at a frequency of 1 kHz (20 samples/cycle). As full cycle window(FCW) is chosen for moving average calculations, L is 20.

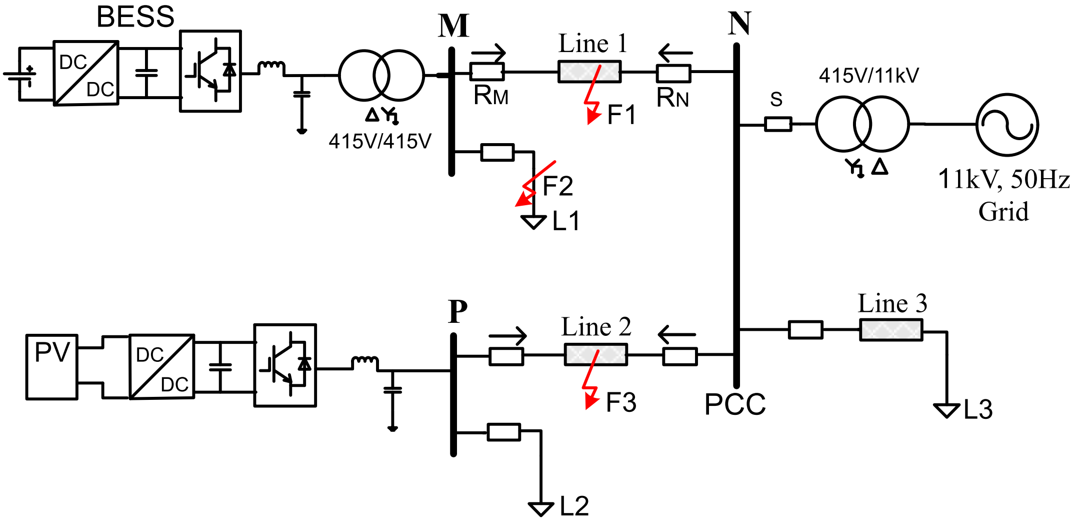

Figure 4.20: Microgrid topology.

The test fault scenarios are same as listed in Section. 4.2.3. The microgrid is operated in grid connected mode (GCM) up to 2s and after that in islanded mode (IM). The BESS operates as PQ-IIDG in GCM and V/F-IIDG in IM. Reverse power flow (battery charging) is attained by setting P setpoint negative in GCM and by adjusting load L3 in IM. Section MN in Fig. 4.20 is the protection zone of the test differential relay. The internal faults are simulated at location F1 at the middle of Line 1. Some extreme cases are demonstrated below:

4.3.3.1 Internal Faults

Case1: Forward power flow (BESS discharging) and Grid connected mode of operation

To validate the proposed scheme, a line to line (BC) fault with a fault resistance of 3Ω is simulated. The current at terminal M is contributed by PQ controlled BESS and current at terminal N is contributed by grid and PV(current controlled). The current seen by relay M (Fig. 4.21a) is limited and remains almost symmetrical. This is due to absence of zero sequence (fault does not involve ground) and negative sequence current components. On the other hand, current at relay N (Fig. 4.21b) exhibits voltage source characteristics. The operating and restraining currents calculated instantaneously contain double frequency components as shown in Fig. 4.21c. Hence, the proposed method uses one cycle average of the instantaneous values as in Equation. 4.18. The averaged operating and restraining currents of the proposed method is shown in Fig. 4.21d. Gao's method uses superimposed positive sequence components and 87BD scheme uses d-

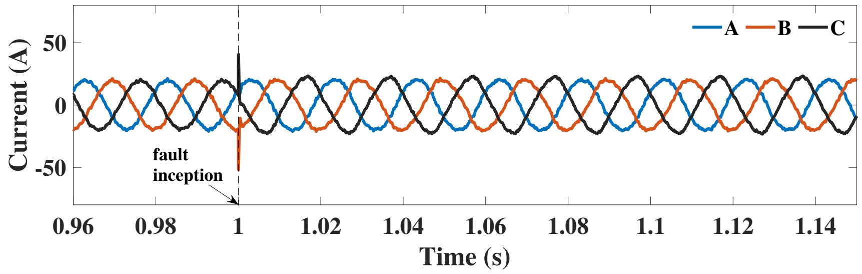

(a) R_M current

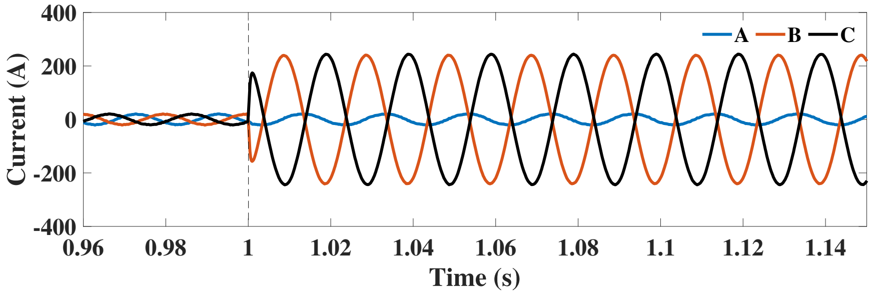

(b) R_N current

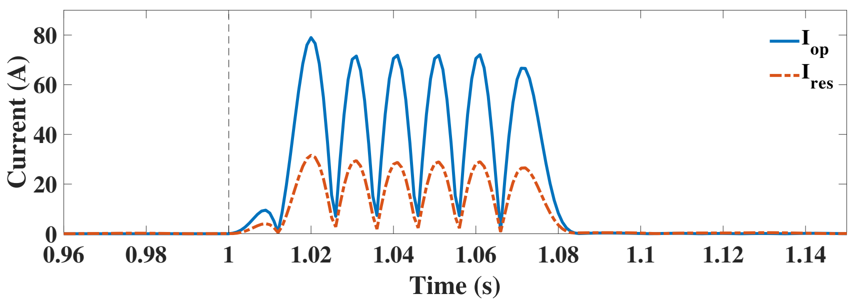

(c) Operating and restraining currents (Instantaneous) of proposed method

Figure 4.21: Case1: Internal BC fault in GCM

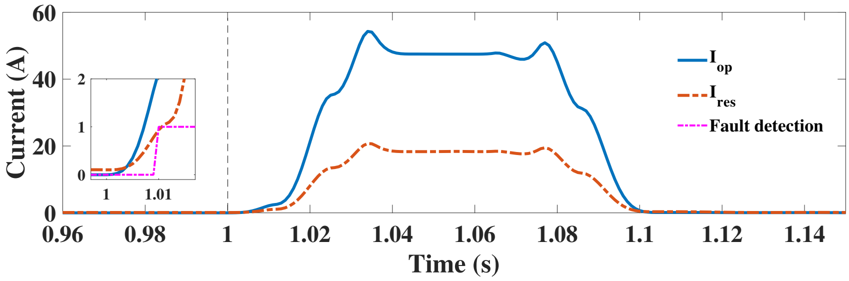

(d) Operating and restraining currents(Averaged) of proposed method

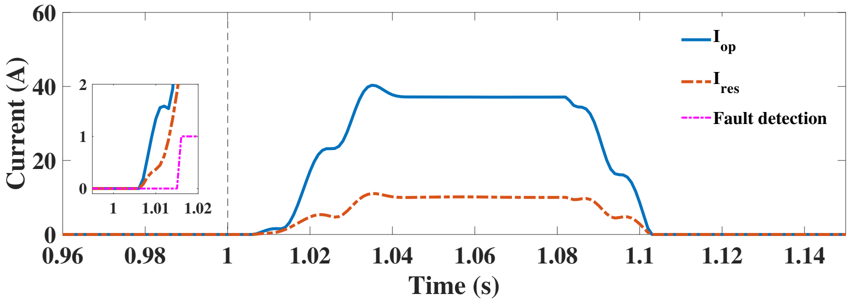

(e) Gao's method performance.

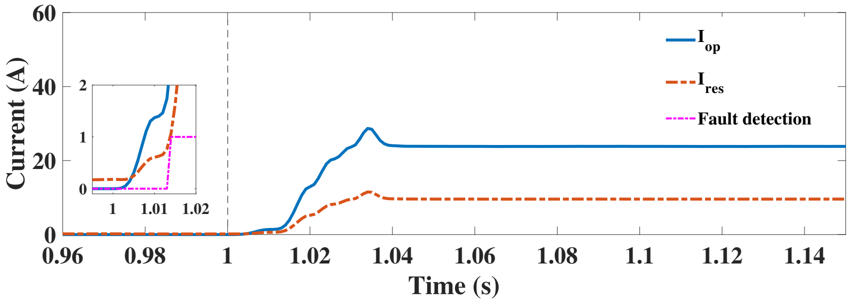

(f) 87BD scheme performance.

Figure 4.21: Internal BC fault in GCM

axis currents. Their performance is shown in Fig. 4.21e and Fig. 4.21f respectively. For a restraining coefficient of 0.4, the fault is detected by the proposed method in 9 ms, Gao's method in 15 ms and 87BD scheme in 13 ms.

Case2: Reverse Power Flow (BESS charging) and Islanded mode of operation

A line to ground (AG) fault is simulated at location F1 at 2.5s with fault resistance 1Ω. As BESS inverter is V/F controlled, its fault response (Fig. 4.22a) is similar to that of synchronous alternators. On the other hand, terminal N current (Fig. 4.22b) is contributed by current controlled PV. It possesses zero sequence components, but lacks negative sequence components.

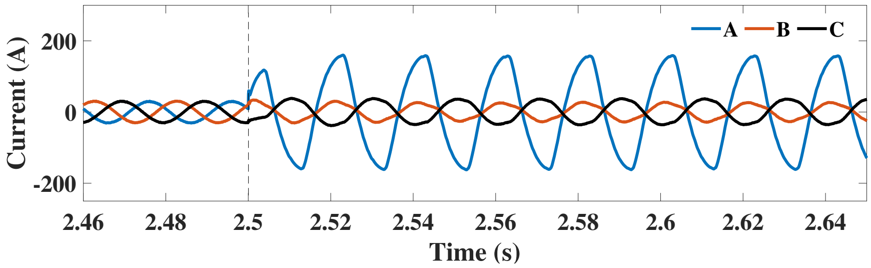

(a) R_M current

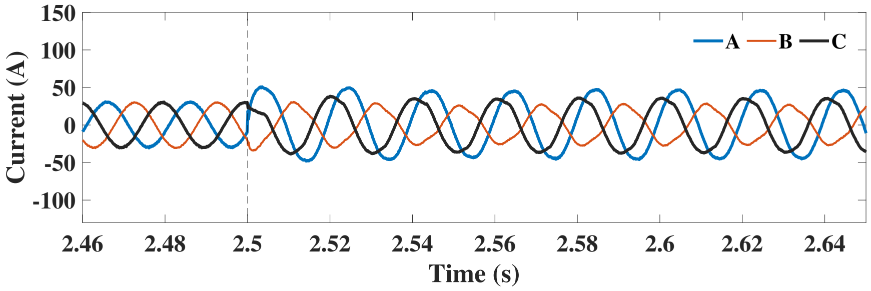

(b) R_N current

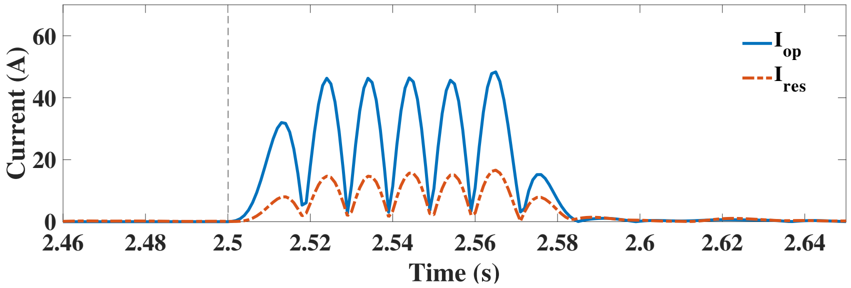

(c) Operating and restraining currents (Instantaneous) of proposed method

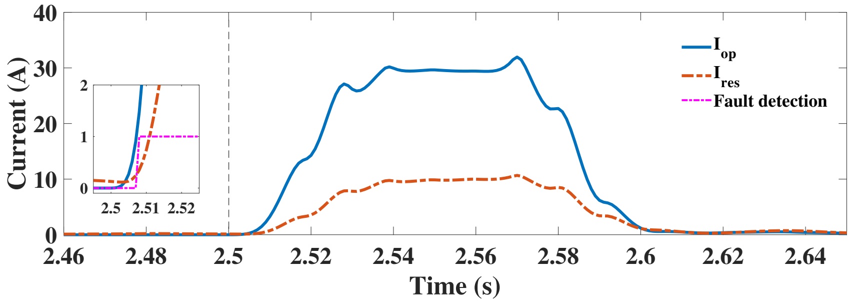

(d) Operating and restraining currents(Averaged) of proposed method

Figure 4.22: Case2: Internal AG fault in IM

The operating and restraining currents computed by proposed method, Gao's method and 87BD scheme are shown in Fig. 4.22d, 4.22e and 4.22f. As the fault currents are limited in IIDGs, differential schemes that operate only on magnitude of currents or positive sequence components may not detect HIF. The fault is detected by the proposed method in 7 ms, whereas Gao's method and 87BD scheme takes 18 ms and 20 ms respectively for fault detection.

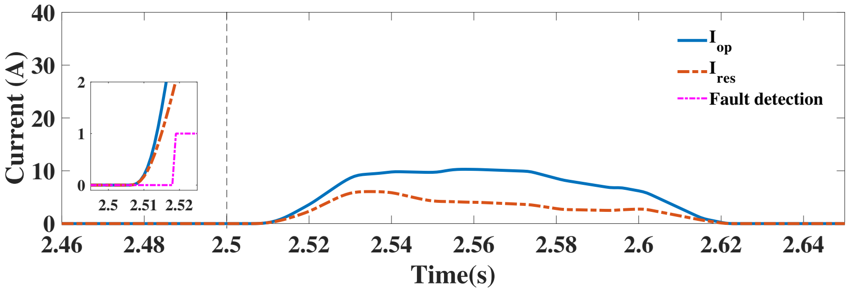

(e) Gao's method performance.

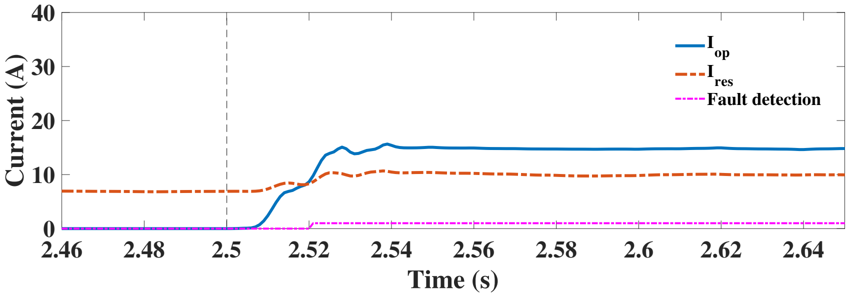

(f) 87BD scheme performance.

Figure 4.22: Case2: Internal AG fault in IM

Case3: Performance when BESS is voltage controlled and grid-connected

BESS inverters with grid forming control are finding application in VSM (Virtual Synchronous Machine) technology, as it provides virtual inertia and eliminates the need for changing inverter control during transitions between GCM and IM. To assess the performance of proposed protection scheme in such cases, a three phase fault is simulated at F1 with $R_f = 0.5\Omega$. Double frequency components are not present in the instantaneous currents, as negative sequence components are absent in symmetrical faults. The relay currents are shown in Fig. 4.23a and Fig. 4.23b. The fault is confirmed by the proposed method in 5 ms as shown in Fig. 4.23c.

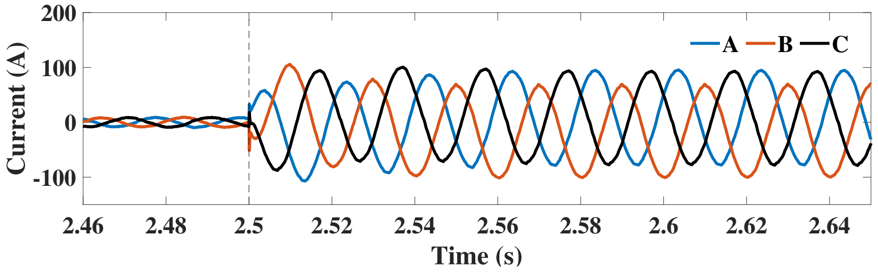

(a) R_M current

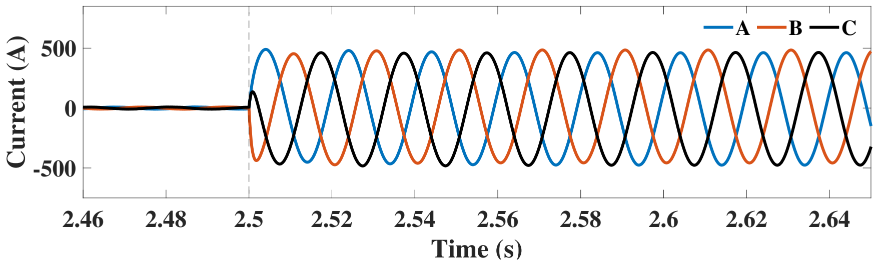

(b) R_N current

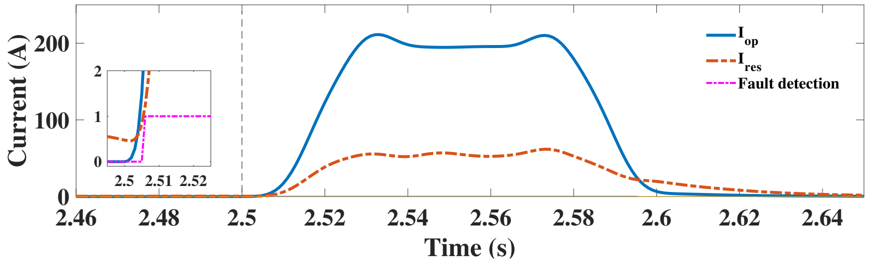

(c) Operating and restraining currents(Averaged) of proposed method

Figure 4.23: Case3: Internal ABCG fault when BESS is voltage controlled and grid connected

Case4: Performance in the presence of decaying DC component

To illustrate the performance of the proposed scheme in the presence of a decaying DC component, a single line to ground fault with fault resistance $R_f = 0.001\Omega$ has been simulated. The BESS is charging, voltage controlled and in the islanded mode of operation. Fig. 4.24a shows the current waveforms at R13. It can be observed that a significant decaying DC component is present in the current waveform after the fault inception. The response of the differential scheme for the aforementioned scenario is shown in Fig. 4.24b. It is noted that that the differential component rises just after the fault inception and the internal fault is detected in 7ms.

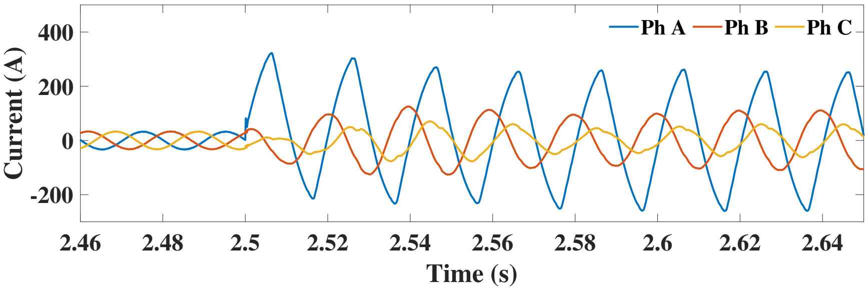

(a) R13 current waveform

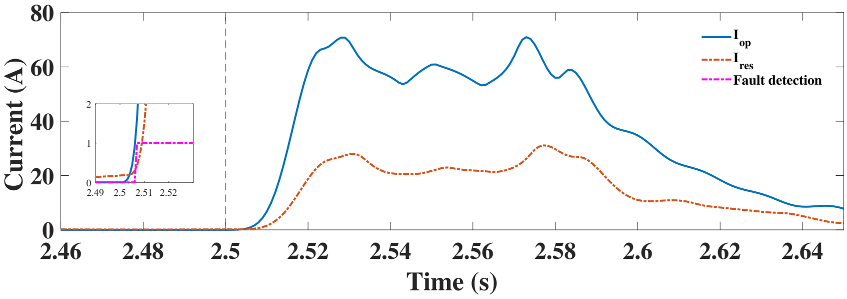

(b) $\angle\Delta Z_1$ of relays R13 and R31

Figure 4.24: Case4: Performance in the presence of decaying DC component

Case5: Performance under far and near end faults

An LLLG fault with Rf=0.05Ω is simulated on Line 1 at a distance of 10m from the relay R13. This can be considered as a near-end (close-in) fault with respect to relay R13 and a far-end (remote bus) fault for relay R31 present at the other end of the line. The BESS is PQ controlled and hence the fault current response at relay R13 is as shown in Fig. 4.25a. The current at relay R31 is mainly contributed by the grid and shown in

Fig. 4.25b. When the fault occurs in Line 1, Relay R13 sees a forward fault and relay R31 sees a reverse fault. The fault is detected in 6 ms.

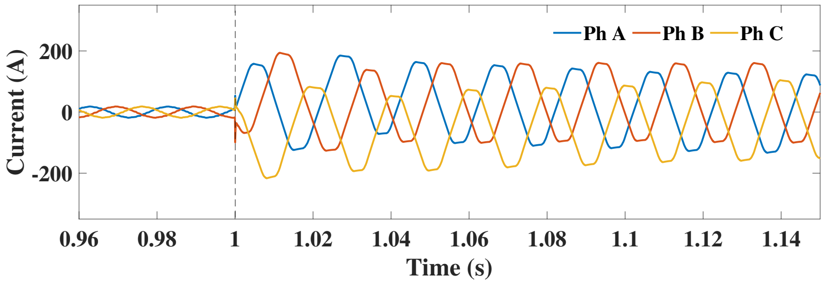

(a) R13 fault current

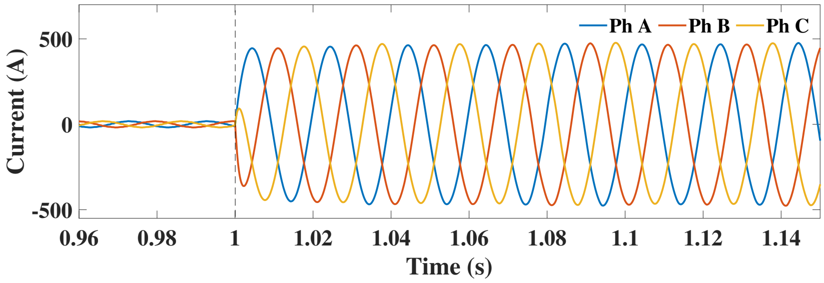

(b) R31 fault current

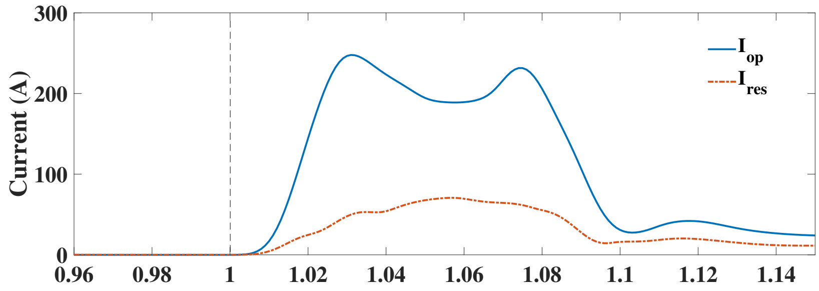

(c) $\angle \Delta Z_1$ of relays R13 and R31

Figure 4.25: Case5: Performance under far and near end faults

Case6: Performance under high resistance and high impedance faults

To evaluate the performance of the protection scheme under high resistance and high impedance faults, medium-voltage (MV) microgrid shown in Fig. 4.9 is chosen. But, relays R_M and R_N are aligned towards the protected circuit. The high resistance SLG fault ($R_f = 50\Omega$) simulated at location F was assessed by the proposed scheme in 4.16 ms.

In the HIF model of 4.10, Rp was varied between 300-900 Ω and Rn between

350-1050 Ω. The variable sources are Vp=4 kV, Vn=4.5 kV. The relay M and relay N currents are shown in Fig. 4.26a and Fig. 4.26b below. As the operating current is higher than the restraining current after fault initiation, the fault was detected in 7 ms.

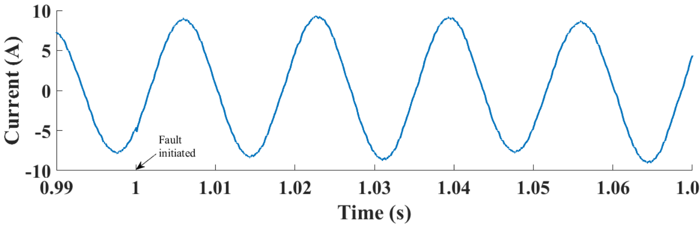

(a) R13 fault current

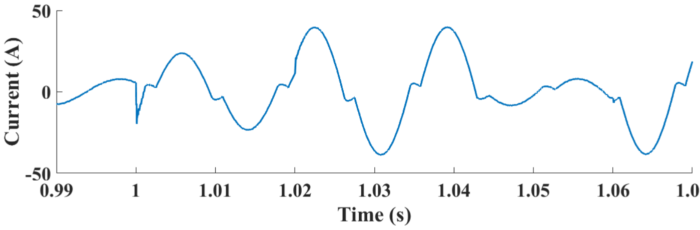

(b) R31 fault current

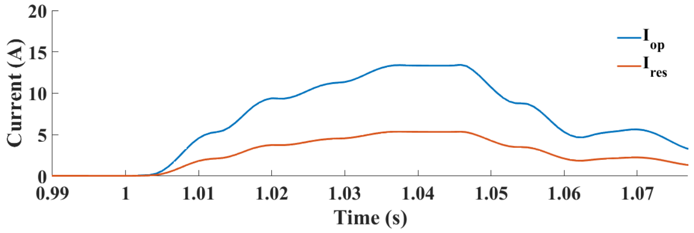

(c) $\angle \Delta Z_1$ of relays R13 and R31

Figure 4.26: Case6: Performance under HIF

4.3.3.2 External Faults

To test the efficacy of proposed protection scheme under external faults with CT saturation, a line to ground (AG) fault with a fault resistance of 0.1 Ω is simulated at location F2. Line 1 is the protected feeder. The burden on terminal N CT secondary is increased to replicate the CT saturation. The phase A currents seen by relays R_M and R_N are shown in Fig. 4.27a. Though the relay operating current increases upon external fault, it is well below the restraining current as shown in Fig. 4.27c. Thus, the differential relay abstains from tripping.

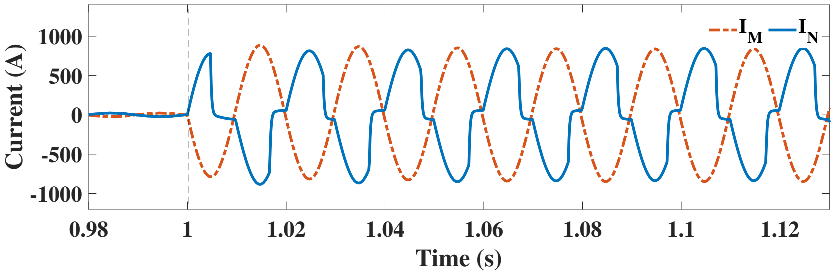

(a) Relay R_M and R_N phase A currents

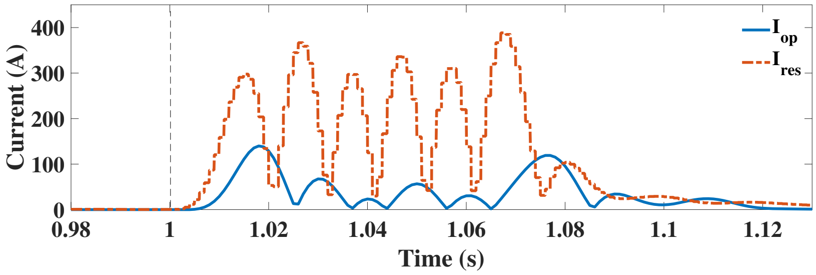

(b) Operating and restraining currents(Instantaneous

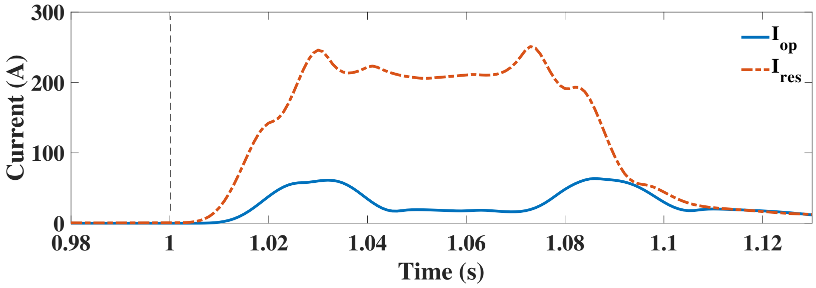

(c) Operating and restraining currents(Averaged)

Figure 4.27: External fault with CT saturation

4.3.3.3 Effect of Fault Inception Angle

The proposed method is not affected by the angle of fault inception. The operating and restraining currents for an internal AG fault occurring at 0^0, 45^0 and 225^0 fault inception angle of A phase is shown in Figure. 4.28.

4.3.3.4 Effect of varying DG penetration

To confirm that proposed method is independent of DG penetration levels, PV irradiance is varied from 400-1000 W/m^2. For each irradiance level, an AG fault with fault resistance of 0.1Ω is simulated at location F3. Line 2 is the zone of protection. The

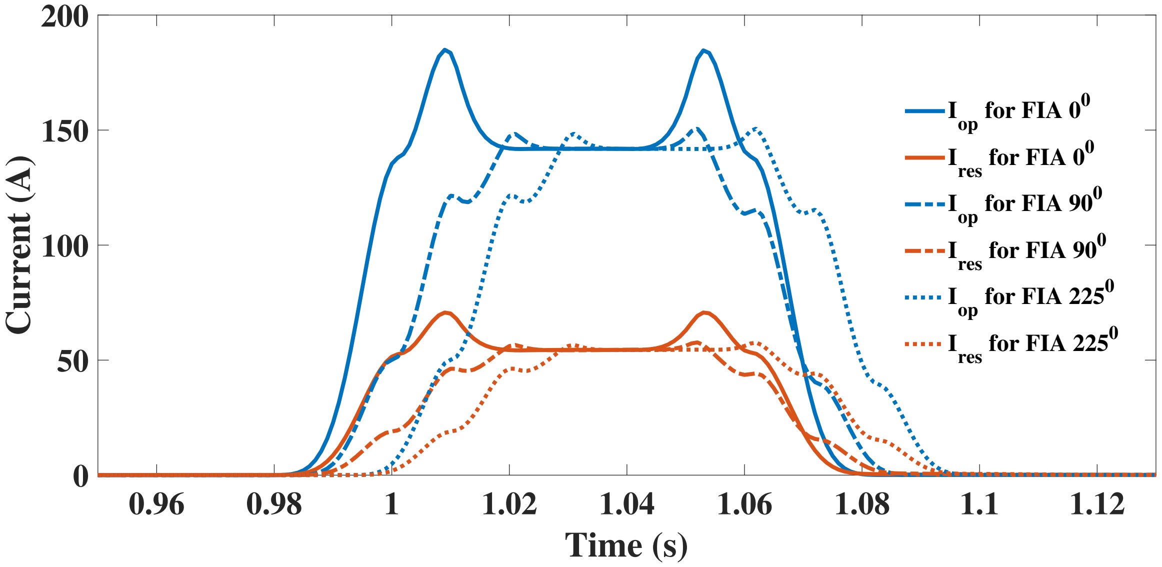

Figure 4.28: Internal AG fault with different inception angles.

operating and restraining currents of differential relays under different PV penetration levels are plotted in Fig. 4.29. This method remains robust under varying DG penetration levels, unlike differential energy based methods which require different threshold settings for different power outputs.

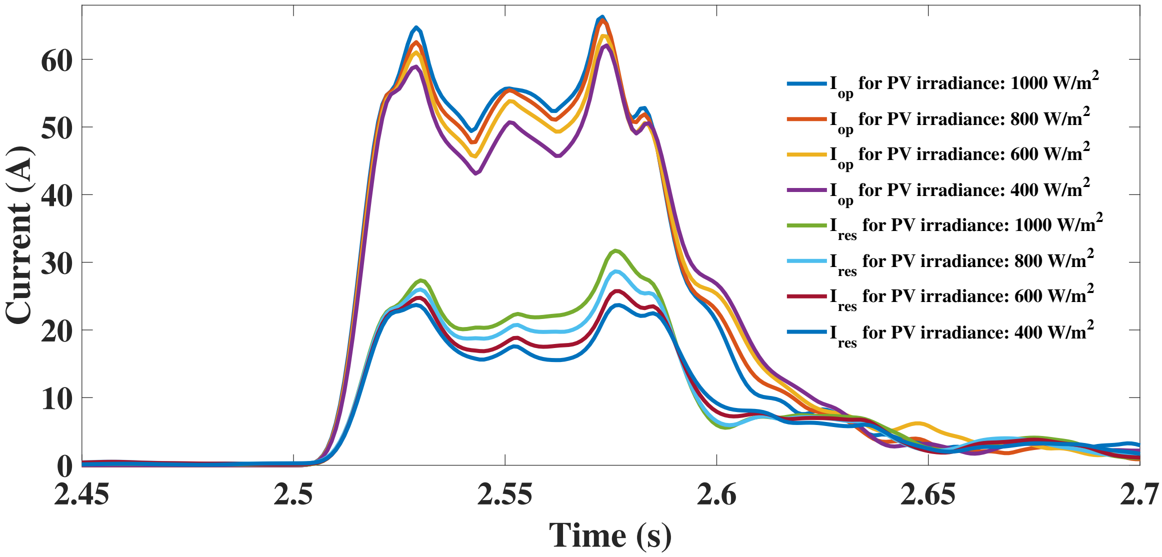

Figure 4.29: Internal AG fault with varying PV penetration levels.

4.3.3.5 Performance under non-fault disturbances

Several system disturbances are simulated to ascertain the efficacy of proposed method. At t=2 s, the microgrid transits from grid connected to islanded mode accompanied by current reversal in line MN. Similarly, a 200% load change is simulated in islanded mode of operation at t=2.2s. In both cases, the differential currents remain zero as in Fig. 4.30c and thus relays are not activated.

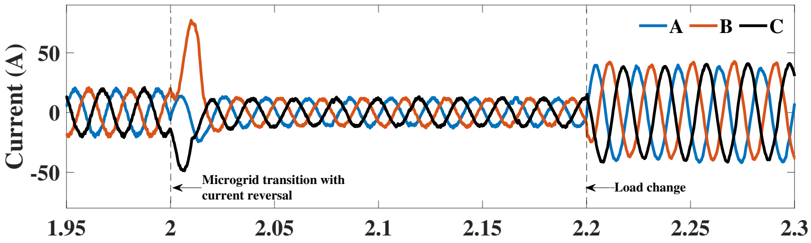

(a) R_M current

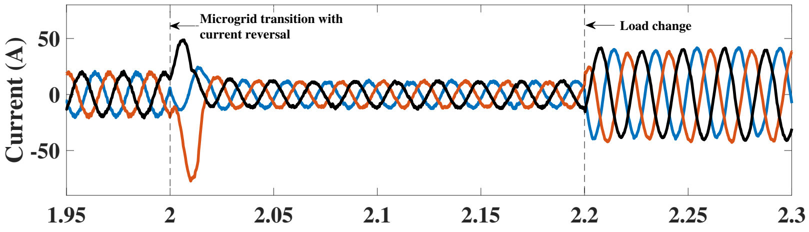

(b) R_N current

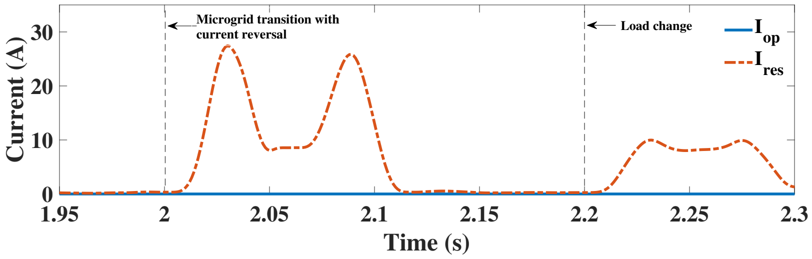

(c) Operating and restraining currents(Averaged)

Figure 4.30: Non-fault disturbances

Table 4.4: Comparison of differential schemes

Microgrid mode	Fault type	Fault resistance (Ω)	Fault instant	Fault detection time PSFC method	NSIA method	Proposed method (HCW)	(FCW)
Grid Connected	SLG	0.5	1s	1.011s	1.005s	1.005s	1.006s
	SLG	10	1s	1.02s	1.016s	1.009s	1.011s
	LL	0.5	1s	1.012s	1.006s	1.005s	1.006s
	LL	10	1s	1.023s	1.016s	1.013s	1.016s
	LLLG	0.5	1s	1.01s	fails	1.004s	1.005s
	LLLG	10	1s	1.017s	fails	1.008s	1.01s
Islanded mode	SLG	0.5	2.5s	2.514s	2.507s	2.506s	2.507s
	SLG	10	2.5s	fails	2.517s	2.508s	2.511s
	LL	0.5	2.5s	2.517s	2.505s	2.5s	2.51s
	LL	10	2.5s	fails	2.517s	2.511s	2.513s
	LLLG	0.5	2.5s	2.513s	fails	2.506s	2.507s
	LLLG	10	2.5s	2.521s	fails	2.508s	2.51s

4.3.3.6 Comparative evaluation of the proposed superimposed current based relay with existing differential schemes

Figures. 4.21d - 4.21f and 4.22d - 4.22f clearly show that the operating current rises rapidly during faults and is much higher in proposed method, leading to quick fault detection. This is due to inclusion of both d-axis and q-axis superimposed current components. A comparison of the proposed scheme with existing differential schemes for various faults is presented in Table. 4.4. Gao's method fails during SLG faults, as there is negligible variation in positive sequence currents. NSIA method cannot be relied upon for symmetrical fault detection. The proposed method is capable of detecting both symmetrical and unsymmetrical faults.

Since the operating and restraining current oscillate with double frequency, a half cycle data window length(HCW) can also be chosen. The speed of operation can be further increased if a half-cycle window is used instead of full cycle(FCW) for computing average. The variation in operating current with change in window length (L=20 for FCW and L=10 for HCW) is shown in Fig. 4.31.

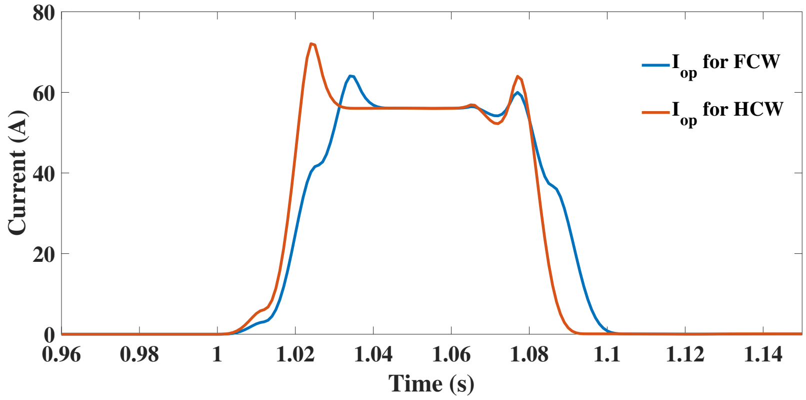

Figure 4.31: Operating currents with different window lengths.

4.4 INFERENCES

Conventional direction relaying schemes may fail in feeders integrating PQ controlled IIDGs with reverse power flow capability such as BESS. A modified criterion is proposed for assessing fault direction in Section. 4.2 of this chapter. The MPU uses the direction estimated by the feeder end relays for detecting an internal fault. The AOC scheme is proposed as a backup to the MPU. The proposed direction assessment schemes possess excellent selectivity and have provision for backup. However, these schemes requires adaptive settings with different controls (grid following or grid forming) and voltage information.

A differential relay using dq components of superimposed currents is presented in Section. 4.3 of this chapter. This scheme does not require adaptive settings and voltage information. However, this scheme is restricted to internal feeder faults only and cannot offer backup. As, Park's transformation is used for phasor estimation, the proposed scheme has a faster response time. The operating current superimposes both positive and negative sequence components. Hence this scheme assures reliable operation for all types of fault with improved sensitivity compared to other differential relays. The communication requirements and computation complexity are also minimal in the proposed differential relay.

The proposed methods are validated with different DG controllers(PQ and V/F) and not deterred by direction of power flow, fault type or fault impedance. The simulation results confirm that the proposed relays has an edge over conventional schemes in fault detection of microgrid feeders. Therefore, the suggested schemes can be envisaged for the protection of microgrids.

Chapter 5

Development of an Incremental Transient Power Based Protection Scheme for a DC Microgrid

5.1 INTRODUCTION

A key step in the realization of DC microgrids is the development of robust protection schemes. Bidirectional power flow in ring-type configurations makes protection design too complicated. This chapter presents an algorithm for selective fault location and isolation of faulty parts in the transient stage itself. At the onset of a fault, the proposed scheme computes incremental transient power (ΔP) from initial changes in voltage and current. The sign of ΔP captured by different IEDs is compared to determine the fault location. Though the scheme is designed for the unit protection of feeders, it is also capable of locating and isolating external faults accurately. A backup scheme using local measurements is provided, in case of communication failure. The schemes are simulated using extensive simulations in MATLAB/SIMULINK platform. The results confirm that the proposed protection design operates within a few milli seconds, highly selective and stable.

5.2 MICROGRID TOPOLOGY

A ring type bipolar DC microgrid comprising of a Solar Photovoltaic (PV) employing MPPT control, Battery Energy Storage unit (BESS) and loads are chosen for the study. The DC microgrid is grid interfaced via a two level VSC as shown in the Fig. 5.1. The VSC is current controlled in synchronous reference frame. Thus the DC voltage is maintained by the VSC in grid connected mode and by the BESS in islanded mode. The length of each cable is 4 km. IED x.y represents an IED relay in the feeder x-y. IED x.y.p refers to an IED connected in the positive pole of feeder aligned from bus x to bus y. IED x.y.n refers to an IED connected in the negative pole of the feeder.

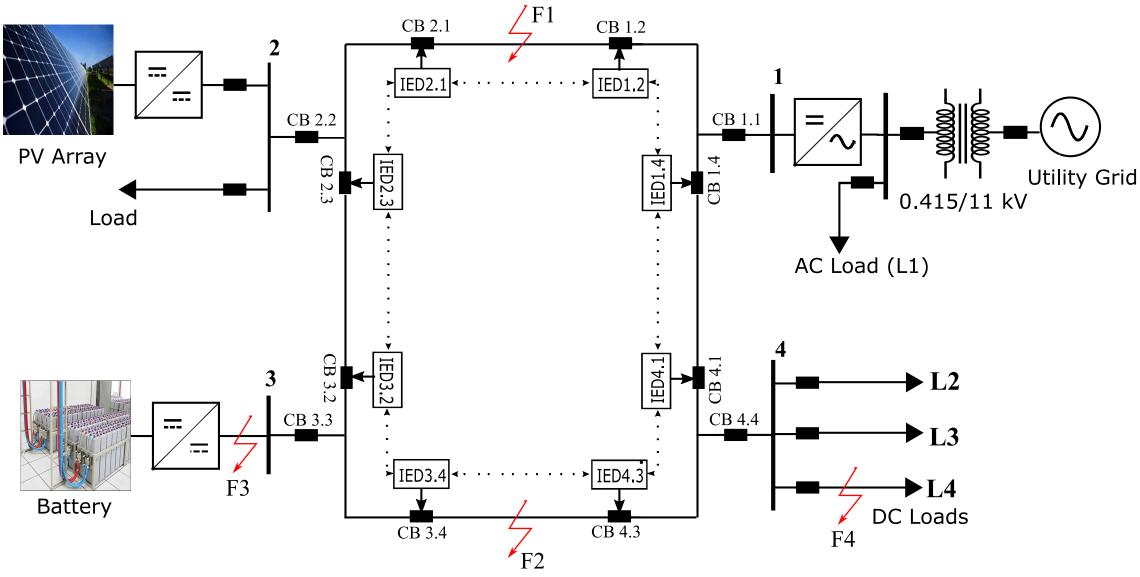
PV Array
Load
2
CB 2.1
F1
CB 1.2
IED2.1
IED1.2
CB 2.2
CB 2.3
IED2.3
IED1.4
CB 1.4
1
CB 1.1
Utility Grid
0.415/11 kV
AC Load (L1)
4
CB 4.1
IED4.1
CB 4.4
L2
L3
L4
DC Loads
F4
Battery
3
CB 3.2
IED3.2
CB 3.3
F3
IED3.4
IED4.3
CB 3.4
CB 4.3
F2

Figure 5.1: DC Microgrid Topology.

5.3 FAULT ANALYSIS

The fault response of a VSC interfaced grid or a DC-DC converter interfaced DER occurs in three stages: Capacitor discharging (i_C), Diode freewheeling (i_{FD}) and Grid or source feeding (i_{grid}). Stages 1 and 2 are referred as the transient stages and stage 3 as the steady state stage. The equivalent circuit of a VSC under short circuit fault is shown in Fig. 5.2 and fault responses in Fig. 5.3a. Because of the large DC link capacitors and short cable lengths, the initial fault response in DC microgrids will be dominated by the capacitor discharge [Fletcher (2013)]. The cable grounding capacitance is omitted here, considering the dominant role of DC link capacitor C1 [Shuai et al. (2019)]. Neglecting initial currents, the current and voltage during capacitor discharging stage can be expressed in time domain as

$$i_F(t) = \frac{v_c(0)}{Lw_d}e^{-\alpha t}sin(w_d t) \tag{5.1}$$

$$v_F(t) = v_c(0)e^{-\alpha t}[cos(w_d t) + \frac{\alpha}{w_d}sin(w_d t)] \tag{5.2}$$

where α is the damping factor, w_0 is the resonant radian frequency and w_d is the damped resonant frequency. $\alpha = \frac{R}{2L}$, $w_0 = \frac{1}{\sqrt{LC}}$, $w_d = \sqrt{w_0^2 - \alpha^2}$, R and L are the equivalent resistance and inductance between the discharging capacitor and fault. The time taken to reach the peak value of fault current is

$$t_{peak} = \frac{1}{w_d}\arctan(\frac{w_d}{\alpha}) \tag{5.3}$$

The capacitor discharge stage is followed by diode freewheeling stage. The magnetic energy stored in the line inductance drives high current through the antiparallel diodes of VSC or converter diode. However this stage will be present only if the DC bus voltage drops to zero. Hence this stage will absent in pole to ground faults. The fault analysis during freewheeling operation is detailed in Yang et al. (2012) for VSC based and in Mohanty and Pradhan (2019) for DC-DC converters. This is then followed by the source or grid feeding stage. The protection devices at AC side can identify the fault only at this stage. The freewheeling diodes of VSC are exposed to very high currents

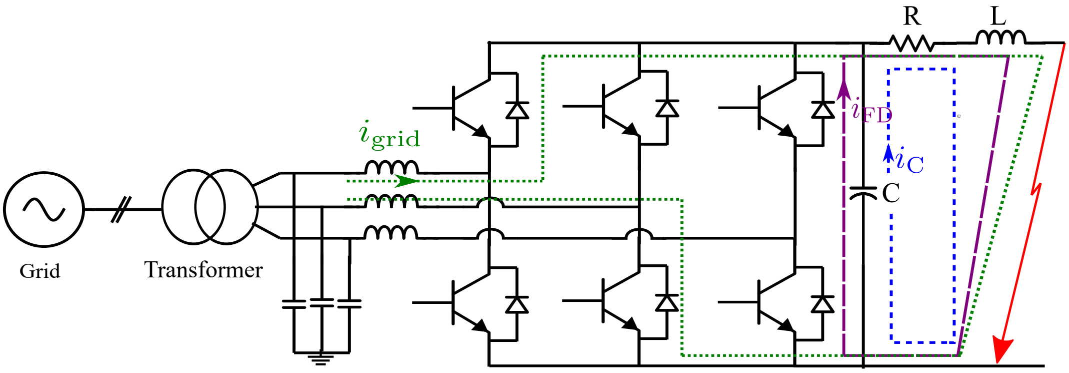

Figure 5.2: Equivalent Circuit of a VSC under fault.

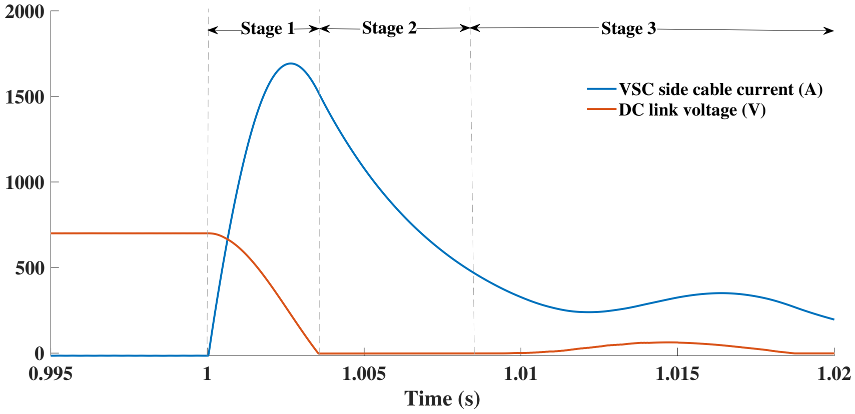

(a) VSC side DC link voltage and cable current

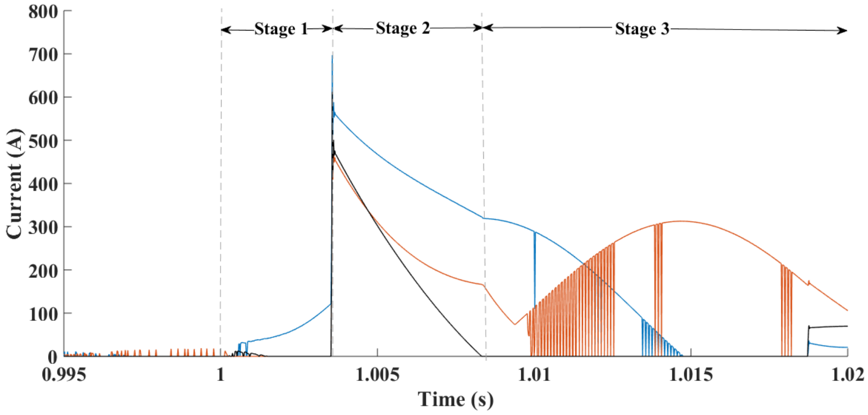

(b) VSC freewheeling diode currents

Figure 5.3: DC Fault Response of VSC

in stages 2 and 3 as seen from Fig. 5.3b. Similarly, converter diodes will be exposed to high currents in these stages. Hence the designed protection must act in the capacitor discharging stage itself; preferably before t_{peak} is reached.

The responses at various DG buses for a pole-pole (PP) fault with fault resistance 0.05Ω at location F1 (midpoint of 4km line 1-2) is shown in Fig. 5.4. The DC link capacitors of all the DGs, ESS and loads contribute to the fault in DC cable or bus almost simultaneously. However, the fault response is dependent on the fault impedance, fault type (Pole-Pole or Pole-Ground) and location of the fault. Since the BESS is located far away from the fault, its response is relatively slow. It is seen that the PV response (at steady state) is limited by the short circuit current of PV. Whereas, BESS and grid contribute large fault currents in the steady state also.

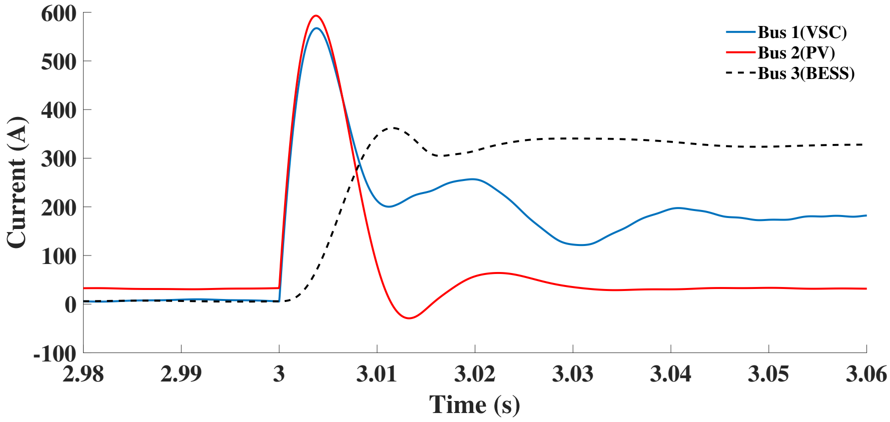

Figure 5.4: Fault responses at various DG buses for F1 fault

5.4 PROPOSED PROTECTION SCHEME

The proposed algorithm uses incremental or superimposed quantities for fault detection and fault direction assessment. The superimposed quantities are obtained by subtracting a N-sample delayed signal (prefault) from the signal (post fault) itself. These computations are instantaneous as it uses a previously stored signal. The superimposed voltage and current can be written as

$$\Delta v(t) = v_{post}(t) - v_{pre}(t) \tag{5.4}$$

$$\Delta i(t) = i_{post}(t) - i_{pre}(t) \tag{5.5}$$

5.4.1 Startup Unit

The superimposed voltages and currents are zero under normal operation. Upon fault occurrence or any other disturbances like load or DG switchings, the currents and voltages seen by IEDs deviate from their prefault quantities. The proposed scheme monitors Δv and Δi continuously using a quantity *Incremental Transient Power* which is defined as,

$$\Delta P = \frac{\sum\limits_{n=1}^{N} (\Delta v.\Delta i)_n}{N} \tag{5.6}$$

When ΔP exceeds a set threshold *Th*, a disturbance is detected and the protection unit becomes active. Unlike other thresholds like Δv, Δi and di/dt, ΔP is more reliable. This is because the DC link capacitors maintain the DC link voltage well within limits and hence ΔP remains negligible during non fault disturbances. The purpose of this threshold setting is not just disturbance detection. The sign of ΔP is also captured, at its threshold crossing.

5.4.2 Direction Identification Unit

Intelligent Electronic Devices (IED) are placed on either ends of all the feeders in the DC microgrid. The placement of IED relays on the positive and negative poles are as indicated in Fig. 5.5. IEDs are directed towards the feeder in the positive pole. Since the current directions are opposite in the positive and negative poles, the IED relays on negative poles are installed in the reverse direction. i.e., IEDs on negative poles are directed away from the feeder. This arrangement is for facilitating unit protection scheme.

Considering the power flow direction as indicated in the Fig. 5.5, the superimposed components are derived for forward fault (F1) and reverse fault (F2) for IED 1.2.p. Since the capacitors acts as initial fault current sources, the analysis is restricted to capacitor discharging stage.

Forward Fault(FF) The F1 fault components are primarily determined by the capacitor discharge of C1.

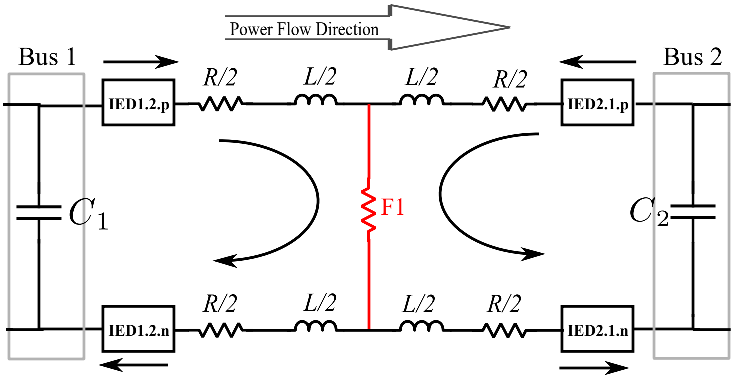

Figure 5.5: Forward Fault with respect to IED 1.2.p.

$$\begin{aligned}\Delta v_{F1} &= v_{post} - v_{pre} \\ &= \left\{ v_{C1}(0)e^{-\alpha t}[cos(w_{d1}t) + \frac{\alpha}{w_{d1}} sin(w_{d1}t) \right\} - v_{C1}(0)\end{aligned} \tag{5.7}$$

$$\begin{aligned}\Delta i_{F1} &= i_{post} - i_{pre} \\ &= \left\{ \frac{v_{C1}(0)}{Lw_{d1}} e^{-\alpha t} sin(w_{d1}t) \right\} - \left\{ \frac{v_{C1}(0) - v_{C2}(0)}{R} \right\}\end{aligned} \tag{5.8}$$

where $\alpha = \frac{R}{2L}$, $w_{01} = \frac{1}{\sqrt{LC1}}$, $w_{d1} = \sqrt{w_{01}^2 - \alpha^2}$

From the above equations it is clear that Δv_{F1} is negative and Δi_{F1} is positive (until t_{peak}) for a forward fault.

Reverse Fault(RF) During F2 fault, the fault current component seen by IED 1.2.p is determined by the capacitor C2 discharge. On account of IED direction, the F2 fault current is taken negative. However the fault voltage is primarily determined by C1. Hence Δv_{F2} remains same as Δv_{F1}

$$\Delta i_{F2} = -\left\{ \frac{v_{C2}(0)}{L_{eq}w_{d2}} e^{-\alpha_2 t} sin(w_{d2}t) \right\} - \left\{ \frac{v_{C1}(0) - v_{C2}(0)}{R} \right\} \tag{5.9}$$

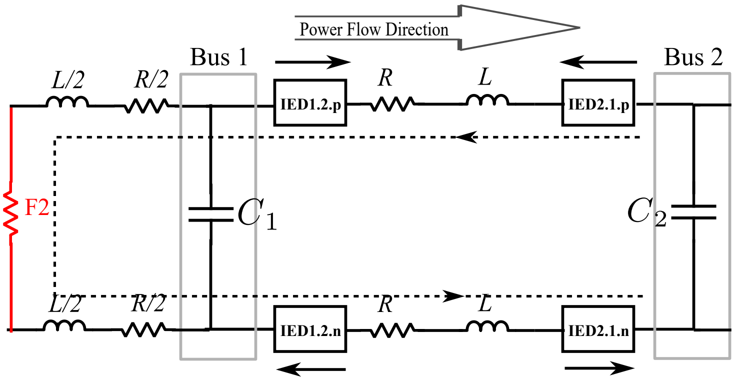

Figure 5.6: Reverse Fault with respect to IED 1.2.p.

where $R_{eq} = 3R$, $L_{eq} = 3L$, $\alpha_2 = \frac{R_{eq}}{2L_{eq}}$, $w_{02} = \frac{1}{\sqrt{L_{eq}C_{eq}}}$, $w_{d2} = \sqrt{w_{02}^2 - \alpha_2^2}$. Thus both Δv_{F2} and Δi_{F2} are negative for a reverse fault.

The sign of incremental transient power (ΔP) can be utilised to arrive at the direction decision, irrespective of the initial power flow direction. Δv and Δi have opposite signs in the initial stages for a forward fault which implies that ΔP sign is negative for a forward fault. Similarly, ΔP sign is positive during a reverse fault as Δv and Δi have similar signs. The sign of ΔP at its threshold crossing is captured for direction decision.

5.4.3 Fault Localisation

5.4.3.1 Internal (Feeder) Faults

When both IEDs of a feeder indicates a forward fault, an internal fault is identified and trip signals are issued to SSCBs (solid state circuit breaker)of the feeder. This scheme as shown in Fig. 5.7 requires communication. In case there is a communication failure and voltage at the relay point remains less than 85% of nominal voltage (v_n) for 10 ms, local protection method becomes active. The under voltage criterion in combination with the assessed fault direction can be used to trip the SSCB at fault location. The logic flow of local protection schemes are shown in Fig. 5.8

Negative Pole Faults: Similar logic can be implemented for detection, location and isolation of faults involving negative pole. The operating parameters are pole to pole voltage and current in the negative pole. When an internal fault occurs, ΔV decreases and ΔI increases (see Fig. 5.5). Thus ΔP is negative indicating forward fault.

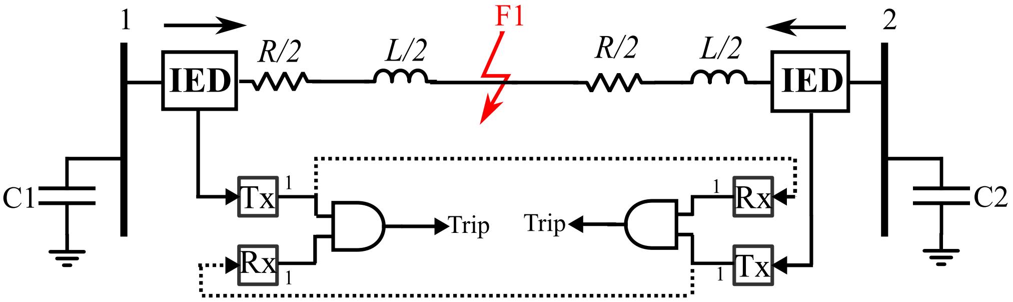

Figure 5.7: Schematic of the feeder protection scheme.

For example, if there is a NPG fault on feeder 1-2, IEDs 1.2.n and 2.1.n on the negative pole of the feeder, indicate FF and hence trip signal is issued to SSCBs on negative pole of the feeder 1-2. In bipolar schemes, this arrangement will help to maintain supply to loads connected in the healthy pole.

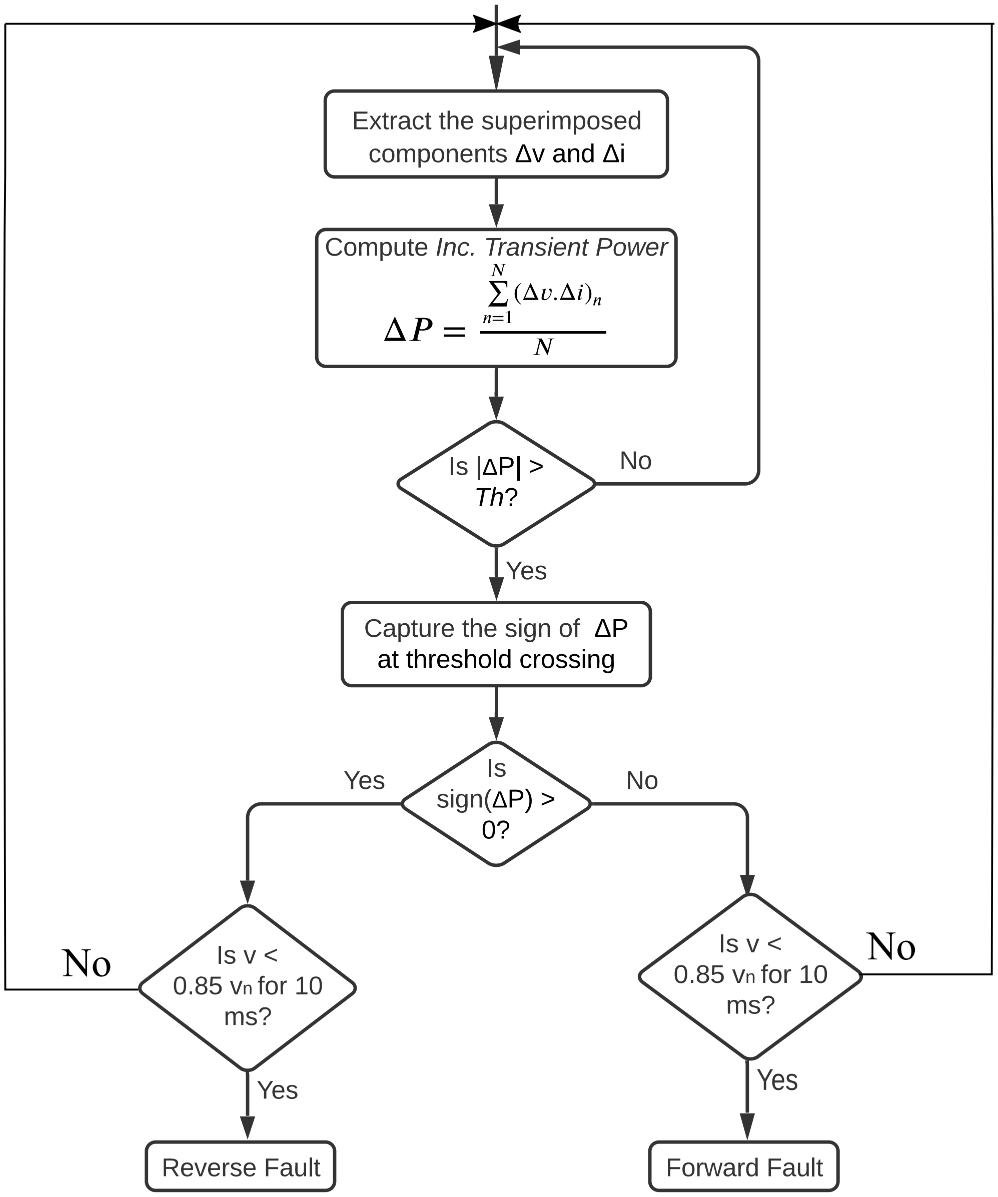
Extract the superimposed components Δv and Δi
Compute Inc. Transient Power
$\Delta P = \frac{\sum_{n=1}^{N} (\Delta v . \Delta i)_n}{N}$
Is |ΔP| > Th?
No
Yes
Capture the sign of ΔP at threshold crossing
Is sign(ΔP) > 0?
Yes
No
No
Is v < 0.85 vn for 10 ms?
Is v < 0.85 vn for 10 ms?
No
Yes
Yes
Reverse Fault
Forward Fault

Figure 5.8: Flow chart of the local measurement scheme.

5.4.3.2 External Faults

Unit protection schemes are designed for external faults also. If all the relays attached to a bus indicate a reverse fault, SSCB of that bus can be tripped.

If IED 1.2 == RF && IED 1.4 == RF ⇒ Trip CB 1.1
If IED 2.1 == RF && IED 2.3 == RF ⇒ Trip CB 2.2
If IED 3.2 == RF && IED 3.4 == RF ⇒ Trip CB 3.3
If IED 4.1 == RF && IED 4.3 == RF &&
$v < 0.85\ v_n$ for t_d s ⇒ Trip CB 4.4

The load bus CB 4.4 is tripped only if IEDs 4.3 and 4.1 indicate a RF and if the voltage at the bus stays below 85 % of nominal voltage for t_d s. This will ensure that the breaker is not tripped during load changes and will provide a coordination time with the individual PDs of loads. Thus, a comprehensive protection scheme is designed for a ring type DC microgrid.

5.5 RESULTS AND DISCUSSIONS

The signals are sampled at a rate of 4 kHz. All the faults are applied at t=3 s. For clarity of fault behaviour, the trip signals are not applied to the CBs and hence fault is remaining in the system.

5.5.1 Selection of Inc. Transient Power Threshold

The variation of incremental transient power seen by IED 3.4 for F2 fault with different fault resistances is shown in Fig. 5.9. For setting the threshold, various system disturbances are simulated. A far end fault (with respect to IED 3.4) is simulated at location F1. Further, different worst case scenarios in the normal operation are also simulated. The battery current is switched from -15A to 15A; thus $\Delta i = 30A$. Nevertheless, ΔP is negligible. A 200% load change with $\Delta i = 50$A is simulated at load bus 4 and ΔP is as shown in Fig. 5.9. Based on the simulations, a threshold setting of 200W is chosen.

5.5.2 Effect of fault on various line segments

A P-P fault is simulated at location F1 in the middle of line segment 1-2. The current and voltage seen by various IEDs along with their incremental transient powers

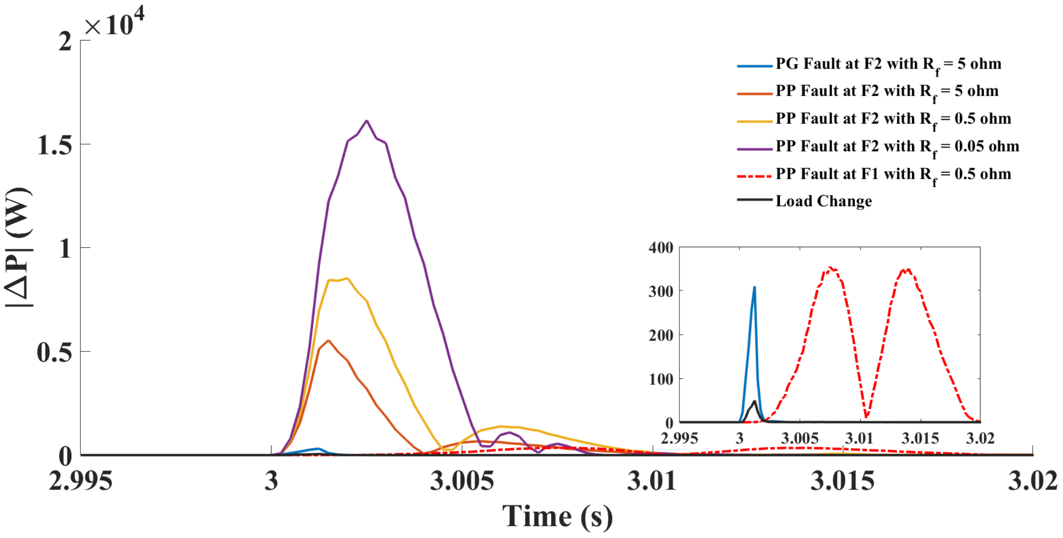

Figure 5.9: $|\Delta P|$ computed by IED 3.4 for various disturbances.

is shown in Fig. 5.10a-5.10l. The transient powers of IED 1.2 and IED 2.1 relays (in both poles) are negative at set threshold which indicate a forward fault. The fault current takes 5ms to reach its peak value. However, the fault is detected at 0.75ms. For the same fault the IED 2.3 indicate a RF (Fig. 5.10j) and IED 3.2 a FF (Fig. 5.10l)

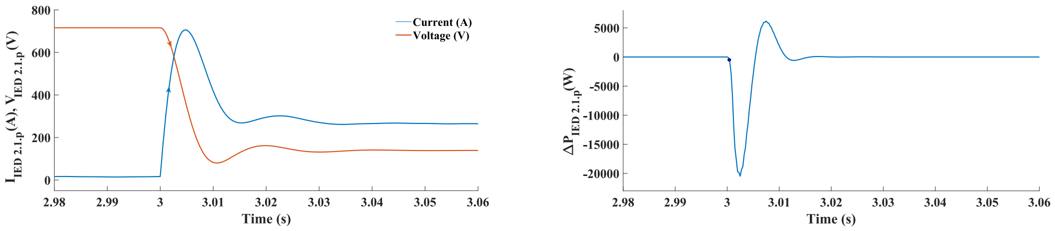

(a) I,V of IED 2.1.p

(b) ΔP of IED 2.1.p

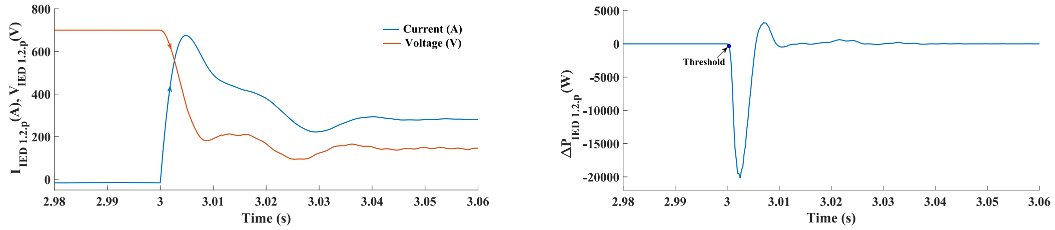

(c) I,V of IED 1.2.p

(d) ΔP of IED 1.2.p

Figure 5.10: I,V and ΔP seen by various relays for a PP fault at F1

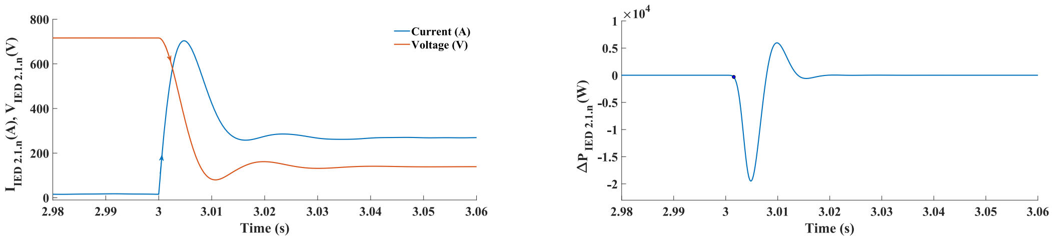

(e) I,V of IED 2.1.n **(f)** ΔP of IED 2.1.n

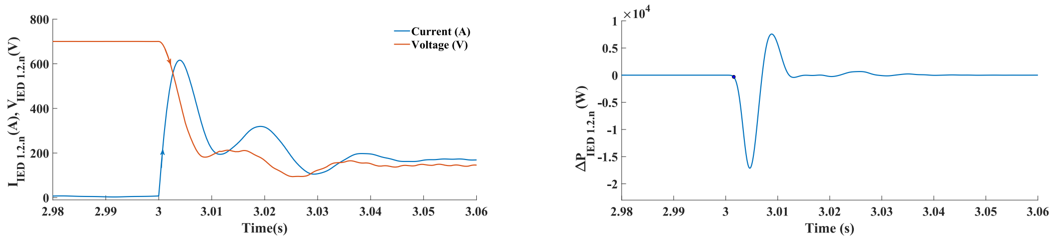

(g) I,V of IED 1.2.n **(h)** ΔP of IED 1.2.n

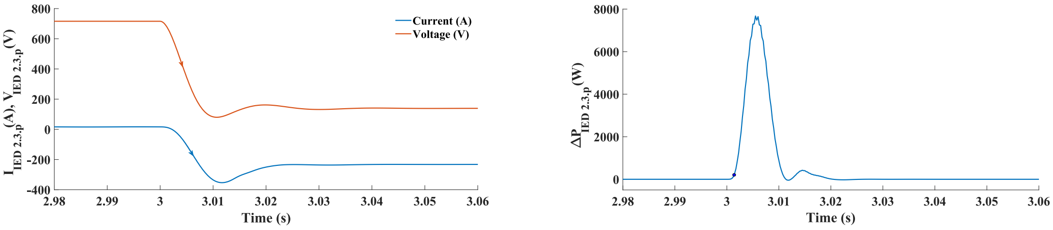

(i) I,V of IED 2.3.p **(j)** ΔP of IED 2.3.p

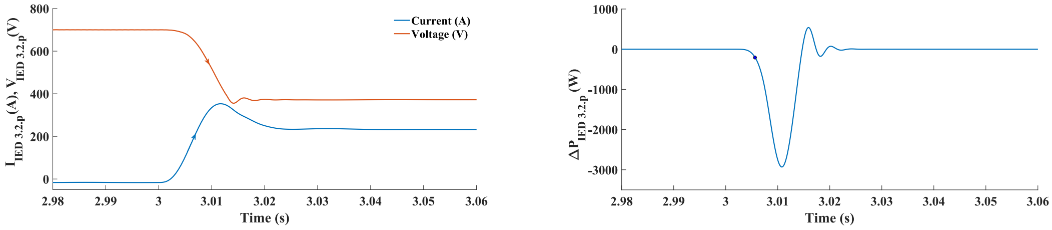

(k) I,V of IED 3.2.p **(l)** ΔP of IED 3.2.p

Figure 5.10: I,V and ΔP seen by various relays for a PP fault at F1

5.5.3 Performance under Close-In Faults

The performance of IED 2.1.p is investigated for close-in faults. During such faults, voltage may drop to near zero. Some relays cannot give reliable decision under close-in faults. A PP fault with $R_f = 0.01$ is simulated at a distance of 0.5 m in front and back of IED 2.1.p. The transient powers computed by the relay for forward and reverse faults are shown in Fig. 5.11. Since superimposed voltages are used, the relay decisions are not affected by close-in faults. The forward fault is detected in 2 ms, while

$t_{peak} = 2.5ms.$

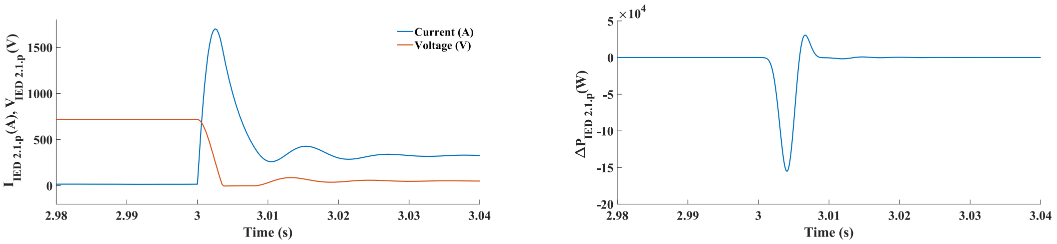

(a) I,V of IED 2.1.p **(b)** ΔP of IED 2.1.p

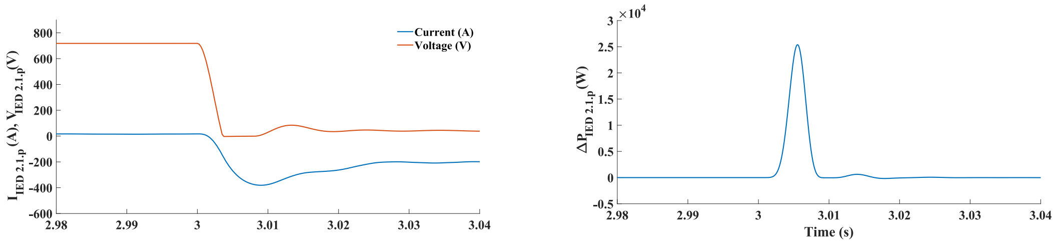

(c) I,V of IED 2.1.p **(d)** ΔP of IED 2.1.p

Figure 5.11: Forward Close-in Faults: (a) & (b) and Reverse Close-in Faults: (c) & (d)

5.5.4 Performance under High Impedance Faults (HIF)

Pole to ground faults are more common in DC microgrids and less severe compared to pole to pole faults. The sensitivity of relay may be impaired under pole to ground faults with high fault resistances. A fault resistance of 5Ω is considered as high impedance in a DC microgrid [Mohanty and Pradhan (2018b)]. A positive pole to ground fault with $R_f = 5\Omega$ is simulated at F1 and results shown in Fig. 5.12.

As the fault resistance and fault distance increases, the time taken to reach the threshold transient power increases and hence the fault detection time increases. It is

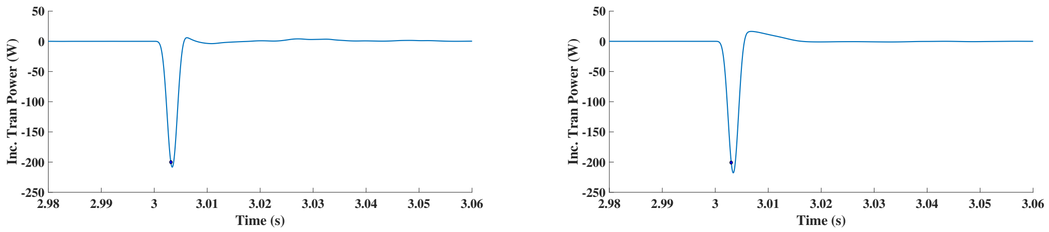

(a) IED 1.2.p **(b)** IED 2.1.p

Figure 5.12: High Impedance Faults.

also noted that faults involving single pole are taking more detection time when compared to PP faults. The performance of the proposed scheme with variation in fault resistance and type is shown in Table 5.3 and distance in Table 5.2.

Table 5.1: Performance of the proposed scheme with different fault types and fault resistances

Fault Location	Fault Type	Fault Resistance (Ω)	Operating IEDs and their assessed directions		Detection time (ms)
F1	PP	0.001	1.2 - FF	2.1 - FF	0.75
	PP	0.05	1.2 - FF	2.1 - FF	1.5
	PP	2	1.2 - FF	2.1 - FF	2
	PP	5	1.2.p - FF	2.1.p - FF	2.75
	PPG	0.05	1.2.p - FF	2.1.p - FF	1.75
	PPG	2	1.2.p - FF	2.1.p - FF	3.25
	NPG	0.05	1.2.n - FF	2.1.n - FF	1.75

PP-pole to pole, PPG- positive pole to ground, NPG- negative pole to ground

Table 5.2: Performance of the proposed scheme with different fault distances

Fault Location	Fault Type & Resistance	Distance from Bus 1 (km)	Operating IEDs and their assessed directions		Detection time (ms)
F1	PP 0.01Ω	0.005	1.2 - FF	2.1 - FF	2
		0.05	1.2 - FF	2.1 - FF	2
		0.5	1.2 - FF	2.1 - FF	1.75
		1	1.2 - FF	2.1 - FF	1.75
		2	1.2 - FF	2.1 - FF	1.5

5.5.5 Performance with Noisy Signals

Real DC microgrids are susceptible to noise. To ascertain whether the proposed protection is affected by noise, the current and voltage signals of IED 1.2.p are contaminated with white noise of a standard deviation of 3%. A P-G fault F1 of $R_f = 1\Omega$ is simulated at t=3s. It is seen from Fig. 5.13c that ΔP remains almost zero during normal conditions and exceeds the threshold during fault. Since it is a forward fault, ΔP is negative. The fault is detected in 2.25ms.

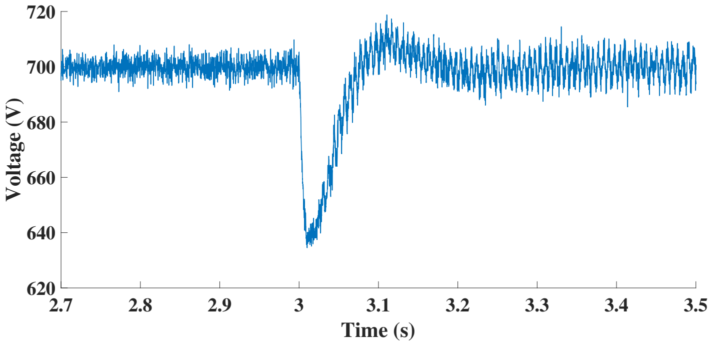

(a) Noisy voltage signal of IED 1.2.p

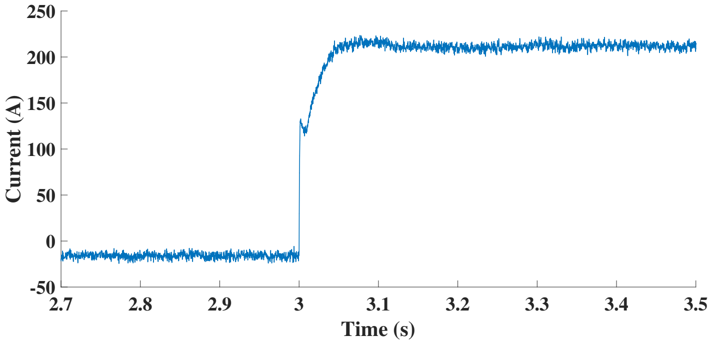

(b) Noisy current signal of IED 1.2.p

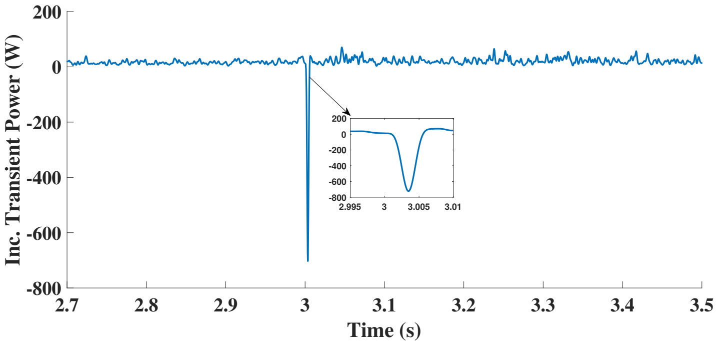

(c) Inc. Transient Power computed by IED 1.2.p

Figure 5.13: Effect of noisy signals.

5.5.6 Performance under External Faults

To validate the efficacy of the proposed protection scheme, faults are simulated at the terminals of bidirectional converter of BESS (F3), VSC, boost converter of PV and load (F4). During an external fault F3 (see Fig. 5.1), Δi seen by IEDs 3.2.p and 3.4.p are negative, as they are directed away from bus 3. Δv being negative due to sudden discharge of DC link capacitor, ΔP becomes positive as shown in Fig. 5.14 indicating

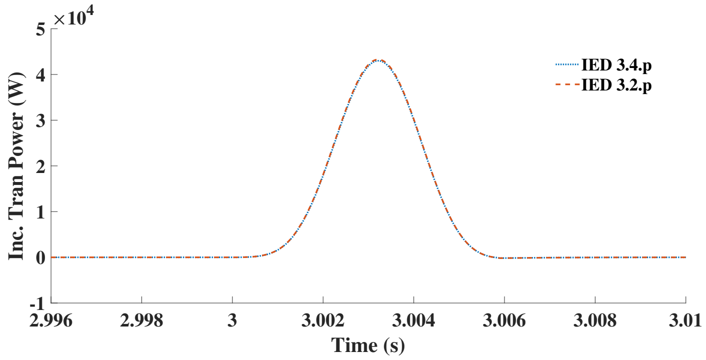

Figure 5.14: ΔP of IEDs 3.2.p and 3.4.p for F3 (External) fault.

reverse faults. When IEDs 3.2.p and 3.4.p detect a RF, trip signal is issued to CB 3.3. The fault is detected in 0.75 ms. Even the SC faults occuring within PE converters which provides a discharge path for the capacitor, can be detected by this method.

5.5.7 Performance under No Fault cases

The following disturbances other than faults were also simulated. (a) Variations in PV radiation (b)load changes (c) battery mode transitions (d) Grid connected to islanded mode and (e) network changes by switching off PV unit. Under these conditions, the voltage variations will be suppressed by the DC link capacitors. Hence in most cases the starting unit itself is not activated. Since the fault is identified by direction criteria, lower threshold settings can be chosen. A lower threshold will also help in faster decision.

Table 5.3: Performance of the proposed schemes for faults at various locations

Fault	Type	Distance from Bus 1 (km)	Fault Type	Fault Resistance (Ω)	Operating IEDs and their assessed directions	Detection time (ms)	Remarks
F2	Internal	2	PPG	0.05	3.4.p - FF 4.3.p - FF	1.75	Power flow Bus 3$\rightarrow$ 4
	Internal	2	PPG	0.05	3.4.p - FF 4.3.p - FF	1.75	Power flow Bus 4$\rightarrow$ 3
F3	External	2	PP	0.001	3.2 - RF 3.4 -RF	0.75	
F4	External	2	PPG	0.05	4.1 - RF 4.3 - RF	10	with delay $t_d = 10ms$

5.5.8 Comparative evaluation of the proposed scheme with existing methods

A comparison of the proposed method with existing techniques is presented in Table. 5.4. This method uses an average of three samples at a sampling frequency of 4kHz for computing incremental transient power. The protection decision is not arrived on a sample basis as in Fletcher et al. (2014) or Meghwani et al. (2017) and hence may take up to 3.5 ms for HIF detection. Thus this method is more robust in the presence of spurious signals or noise.

Unlike differential current schemes Fletcher et al. (2014) where currents are communicated for comparison, this scheme communicates a single bit, i.e, the sign of incremental transient power. The sign is captured when the set threshold is crossed and it indicates the direction of the fault. Hence, communication requirements are minimum. Differential relays cannot tolerate communication delays and require time synchronisation. Suppose there is a communication delay at a feeder end or a synchronisation error in the IEDs. In that case, the operating current can exceed the threshold, causing the differential relay to mal-operate. Whereas the proposed method is based on fault direction and hence not affected by communication delays.

The disadvantage of $\frac{di}{dt}$ based method is that it does not guarantee selectivity. A threshold of 39A/250μs is computed as per Meghwani et al. (2017). When a PP fault with $R_f = 0.01\Omega$ is simulated at F1, IEDs at the adjacent segments 2.3, 3.2, 1.4 and 4.1 also operate. The parameter method in Mohanty and Pradhan (2018a) detects a forward fault if the estimated value of inductance is negative. The estimated inductance by IED 2.1 for a PP fault with $R_f = 0.01\Omega$ at F1 location is -0.085 mH, which indicates a forward fault. This method thus requires advanced processors with high precision. Further, the estimated inductance relies on fault distance and fault resistance. The parameter 'threshold robustness' in Table. 5.4 is kept low in Meghwani et al. (2017) due to the selectivity issue, in Fletcher et al. (2014) due to relay mal-operation under communication delays and in Mohanty and Pradhan (2018a) due to chances of mal-operation during de-energisation of adjacent lines.

Table 5.4: Comparison of proposed method with existing protection schemes

Parameters	Methods			
	Proposed	Mohanty et al. 2018a	Meghwaniet et al. 2017	Fletcher et al. 2014
Operating time	<4 ms	<4 ms	1.5 ms	0.1 ms
Threshold robustness	High	Low	Low	Low

To validate the selectivity of proposed protection scheme, a PP fault with $R_f = 0.001\Omega$ is simulated at F1. A delay time of 1 ms is considered for communication. The faulty segment(line 1-2) is isolated in 1.75 ms. The currents in various segments of the microgrids are shown in Fig. 5.15. The slight transients are due to the opening of SSCBs in the faulted segment.

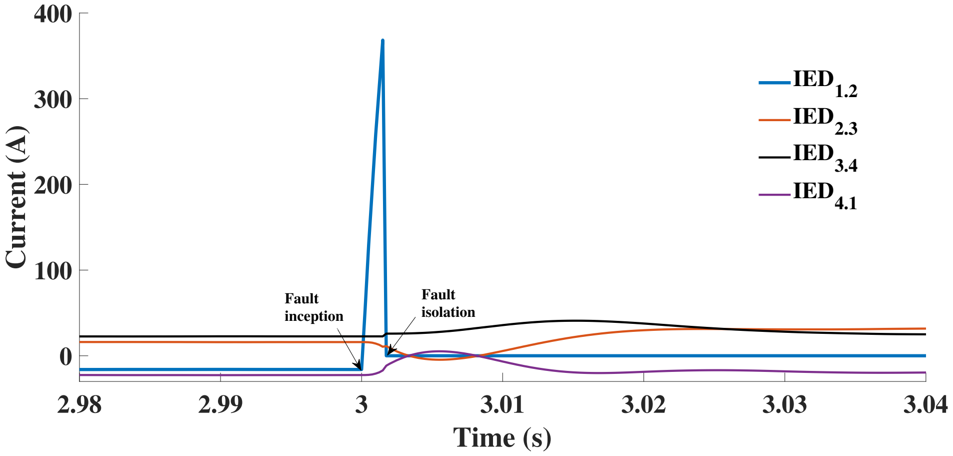

Figure 5.15: Validation of proposed scheme.

5.6 INFERENCES

An effective protection scheme based on incremental transient power for a ring type DC microgrid is presented in this chapter. This scheme identifies and interrupts PP, PPG and NPG faults accurately. Also, the developed scheme can precisely locate both internal and external faults. A backup for feeder protection is also included, in the event of communication failure. The proposed method detects all faults within 4 ms, even for worst cases. This scheme neither requires time based synchronisation nor high bandwidth communication. Since incremental quantities are used instead of derivatives, this scheme is least affected by noise which is a big concern in DC microgrids. This scheme can be adapted to other configurations of DC microgrids.

Chapter 6

Conclusive Remarks and Scope for Future Work

6.1 KEY POINTS EMPHASIZED IN THE THESIS

The following conclusions are drawn from the research work presented in this thesis.

- Microgrids are gaining immense popularity due to their environmental and economic benefits. However, there are many technical challenges concerning control, stability and protection in microgrids.
- The conventional schemes cannot assure reliable protection in microgrids mainly due to the integration of intermittent RES and ESS, bidirectional power flow, dynamic loads and different fault current levels. The fault current is impacted by the microgrid operating mode, control strategy, DER type, fault type, fault resistance, distance of fault and grounding schemes.
- Most of the recently proposed protection schemes did not specify the microgrid control techniques and were validated on microgrids with machine based DGs. The fault currents from IIDGs are entirely different from machine based DGs. The fault behaviour of PQ controlled ESS, when set power is negative (charging)

is not addressed in any literature.

- The inverter controller determines the fault current in IIDGs. During faults, the grid following controller (current or PQ) tries to keep the output current at the target level by adjusting the internal voltage of inverter. Hence the fault current from such inverters is limited and balanced even for asymmetrical faults. Whereas grid forming controller (V/F, droop, VSM etc.) attempts to keep the voltage at desired level by adjusting the fault current. Therefore, the fault current (from grid forming controllers) possesses a higher peak value, contains an exponential damping dc component, and remains unbalanced for asymmetrical faults. Thus inverter controllers impact either output voltages or currents during faults.

- The conventional direction schemes may maloperate in feeders integrating PQ controlled IIDGs with reverse power flow capability such as BESS. When set powers are negative, the DER cannot dissipate into a fault due to the stringent PQ controller. To overcome this flaw, an adaptive direction estimation scheme is proposed for AC microgrids in Chapter 4. Based on the simulation studies, the magnitude and phase angle of superimposed positive sequence impedance were chosen as the direction estimation parameters. Positive sequence impedance was selected as it is not affected by inverter controller or grounding scheme and exists for all types of faults. The cosine of the argument of superimposed impedance correctly assesses the fault direction in most cases. The magnitude criterion is incorporated in feeders integrating PQ controlled DERs only. In the absence of grid, the magnitude criterion is eliminated, as impedances can vary abruptly. Thus an adaptive directional scheme that relies on both magnitude and angle criteria with PQ control and only on angle criterion with voltage control is proposed for BESS feeders. Besides, this thesis proposed unit and backup protection schemes for microgrid feeders. The unit scheme compares the assessed direction at either end of the feeder for fault detection. An adaptive backup overcurrent relay that calculates the pickup current dynamically in current controlled mode and uses fixed settings in voltage controlled mode is also presented.

- Though the above schemes could locate the fault correctly, they require adaptive settings and rely on both current and voltage. Hence, a current only differential protection scheme that does not require any adaptive settings is also presented in Chapter 4. The operating current phasor is computed from dq components of superimposed currents. This method is faster than conventional differential schemes as it does not rely on Fourier based algorithms for phasor estimation. Another highlight of this method is that it requires communication of a single phasor instead of three or more phasors in legacy schemes. The computed phasor was shown to encompass both positive and negative sequence components. Hence this method can detect any faults, irrespective of microgrid mode, inverter controller, DER type, or grounding scheme.

- The DC fault response from a converter (VSC or DC-DC) interfaced DER comprises three stages - capacitor discharging, diode freewheeling and grid or source feeding stage. Though during faults, the self protection circuits in converters can lock the gate signals to the main switches, a discharge loop will be formed between converters and fault points through diodes leading to its damage. Hence the fault must be located and interrupted in capacitor discharging stage itself. The proposed scheme in Chapter 5 captures the sign of incremental transient power at its threshold crossing. The captured sign is compared with adjacent IEDs for exact fault localisation (both external and internal faults). This scheme does not require high bandwidth time synchronised communication and is capable of fault isolation in the transient period itself.

.

6.2 MAJOR CONTRIBUTIONS

The major contributions of the thesis are listed as follows:

- Modelled and simulated a low voltage microgrid with a centralised Battery Energy Storage System (BESS).

- Transient behavioral studies on microgrid under AC and DC faults were done and the challenges in developing suitable protection schemes were identified.

- Following protection schemes for feeders integrating IIDGs or BESS were proposed.
  - An adaptive direction assessment scheme that uses magnitude and angle of positive sequence impedance was proposed. The assessed directions are then compared to devise a unit protection scheme for microgrid feeders.
  - An adaptive overcurrent relay for backup protection was also proposed.
  - A current only differential protection scheme without any adaptive settings is also proposed in this thesis.

  The proposed schemes are validated for both charging and discharging modes of BESS and for different microgrid operation modes.

- A protection scheme for identifying the fault location in DC microgrids using incremental quantities was presented. The scheme is validated on ring type bipolar dc microgrids.

6.3 SCOPE OF FUTURE WORK

Future works may be carried out to address the following issues

- Development of a fault type classifier for an AC microgrid with IIDGs only.
  The existing fault classification techniques are based on magnitude of fault current or sequence components. The fault current from current controlled inverters lack negative sequence components and behave aberrantly. The healthy phases are also affected by the fault and may even indicate a higher current than faulty phases. Hence fault classification is challenging in IIDG microgrids and may require an intelligent technique that process multiple features to arrive at a correct decision. Further works may be taken to develop a classifier capable of accurately classifying the faults in both modes of microgrid operation.

- The proposed protection schemes were validated on microgrids with two widely used control strategies - current control (PQ and DC link voltage) and voltage control (V/F). However, many multi agent control strategies (like SOC weighted droop control) are being proposed for microgrids with distributed ESS. Future studies may be taken up to investigate the impact of such control on protection schemes and its coordination.

- The performance of the proposed methods with distribution automation strategies such as reclosers, sectionalizers and capacitor banks were not investigated. Future works may include such studies as the penetration of microgrid feeders into distribution systems is increasing.
- Selection of a suitable threshold in DC microgrid protection is difficult as there is huge variations in transient monitors with different fault type and fault resistance. Development of an adaptive threshold setting for the startup unit may be taken as future work.

References

(2018). Ieee standard for interconnection and interoperability of distributed energy resources with associated electric power systems interfaces. *IEEE Std 1547-2018 (Revision of IEEE Std 1547-2003)*, pages 1–138.

(2018). Ieee standard for the specification of microgrid controllers. *IEEE Std 2030.7-2017*, pages 1–43.

Al-Nasseri, H., Redfern, M., and O'Gorman, R. (2005). Protecting micro-grid systems containing solid-state converter generation. In *2005 International Conference on Future Power Systems*, pages 5 pp.–5.

Alexandre, R. A., Pinto, S. F., and Santana, J. J. (2016). Energy storage system for grid connection and island operation. In *2016 IEEE International Smart Cities Conference (ISC2)*, pages 1–6.

Augustine, S., Reno, M. J., Brahma, S. M., and Lavrova, O. (2020). Fault current control and protection in a standalone dc microgrid using adaptive droop and current derivative. *IEEE Journal of Emerging and Selected Topics in Power Electronics*, pages 1–1.

Basit, S., Bukhari, A., Saeed, M., Zaman, U., Haider, R., Oh, Y.-s., and Kim, C.-h. (2017). A protection scheme for microgrid with multiple distributed generations using superimposed reactive energy. *International Journal of Electrical Power and Energy Systems*, 92:156–166.

Bayati, N., Hajizadeh, A., and Soltani, M. (2018). Protection in dc microgrids: a comparative review. *IET Smart Grid*, 1(3):66–75.

Beheshtaein, S., Cuzner, R. M., Forouzesh, M., Savaghebi, M., and Guerrero, J. M. (2019). Dc microgrid protection: A comprehensive review. *IEEE Journal of Emerging and Selected Topics in Power Electronics*, pages 1–1.

Bhargav, R., Bhalja, B. R., and Gupta, C. P. (2019). Algorithm for fault detection and localisation in a mesh-type bipolar dc microgrid network. *IET Generation, Transmission and Distribution*, 13(15):3311–3322.

Bhargav, R., Bhalja, B. R., and Gupta, C. P. (2020). Novel fault detection and localization algorithm for low-voltage dc microgrid. *IEEE Transactions on Industrial Informatics*, 16(7):4498–4511.

Bhatraj, A. and Nayak, P. K. (2019). Transient energy-based combined fault detector and faulted phase selector for distribution networks with distributed generators. *International Transactions on Electrical Energy Systems,*, 30.

Biswas, S. and Nayak, P. K. (2021). A fault detection and classification scheme for unified power flow controller compensated transmission lines connecting wind farms. *IEEE Systems Journal*, 15(1):297–306.

Brahma, S. and Girgis, A. (2004). Development of adaptive protection scheme for distribution systems with high penetration of distributed generation. *IEEE Transactions on Power Delivery*, 19(1):56–63.

Bui, D. M., Chen, S.-L., Lien, K.-Y., Chang, Y.-R., Lee, Y.-D., and Jiang, J.-L. (2017). Investigation on transient behaviours of a uni-grounded low-voltage ac microgrid and evaluation on its available fault protection methods: Review and proposals. *Renewable and Sustainable Energy Reviews*, 75:1417–1452.

Carminati, M., Ragaini, E., Grillo, S., and Tironi, E. (2014). Currents, potentials towards ground and fault protection in dc microgrids. In *2014 AEIT Annual Conference - From Research to Industry: The Need for a More Effective Technology Transfer (AEIT)*, pages 1–6.

Casagrande, E., Woon, W. L., Zeineldin, H. H., and Svetinovic, D. (2014). A differential sequence component protection scheme for microgrids with inverter-based distributed generators. *IEEE Transactions on Smart Grid*, 5(1):29–37.

Che, L., Khodayar, M. E., and Shahidehpour, M. (2014). Adaptive protection system for microgrids: Protection practices of a functional microgrid system. *IEEE Electrification Magazine*, 2(1):66–80.

Chmiel, Z. and Bhattacharyya, S. C. (2015). Analysis of off-grid electricity system at isle of eigg (scotland): Lessons for developing countries. *Renewable Energy*, 81:578–588.

Costa, F. B., Monti, A., and Paiva, S. C. (2017). Overcurrent protection in distribution systems with distributed generation based on the real-time boundary wavelet transform. *IEEE Transactions on Power Delivery*, 32(1):462–473.

Cuzner, R. M., Palaniappan, K., Sedano, W., Hoeft, N., and Qi, M. (2017). Fault characterization and protective system design for a residential dc microgrid. In *2017 IEEE 6th International Conference on Renewable Energy Research and Applications (ICRERA)*, pages 642–647.

Cuzner, R. M. and Venkataramanan, G. (2008). The status of dc micro-grid protection. In *Industry Applications Society Annual Meeting*, pages 1–8.

Dai, Z., Liu, N., Zhang, C., Pan, X., and Wang, J. (2020). A pilot protection for hvdc transmission lines based on transient energy ratio of dc filter link. *IEEE Transactions on Power Delivery*, 35(4):1695–1706.

Dang, K., He, X., Bi, D., and Feng, C. (2011). An adaptive protection method for the inverter dominated microgrid. In *2011 International Conference on Electrical Machines and Systems*, pages 1–5.

de Souza, A. C. Z. and Castilla, M. (2019). *Microgrids Design and Implementation*. Springer Nature.

Dewadasa, M., Ghosh, A., and Ledwich, G. (2011). Protection of microgrids using differential relays. In *AUPEC 2011*, pages 1–6.

Dubey, K. and Jena, P. (2020). Impedance angle-based differential protection scheme for microgrid feeders. *IEEE Systems Journal*, pages 1–10.

Emhemed, A. A. S., Fong, K., Fletcher, S., and Burt, G. M. (2017). Validation of fast and selective protection scheme for an lvdc distribution network. *IEEE Transactions on Power Delivery*, 32(3):1432–1440.

Fang, Y., Jia, K., Yang, Z., Li, Y., and Bi, T. (2019). Impact of inverter-interfaced renewable energy generators on distance protection and an improved scheme. *IEEE Transactions on Industrial Electronics*, 66(9):7078–7088.

Farrokhabadi, M., König, S., Cañizares, C. A., Bhattacharya, K., and Leibfried, T. (2018). Battery energy storage system models for microgrid stability analysis and dynamic simulation. *IEEE Transactions on Power Systems*, 33(2):2301–2312.

Fathima, A. H., Prabaharan, N., Palanisamy, K., Kalam, A., Mekhilef, S., and Justo, J. J. (2018). *Hybrid-Renewable Energy Systems in Microgrids Integration, Developments and Control*. Woodhead Publishing Series in Energy.

Feng, X., Qi, L., and Pan, J. (2017). A novel fault location method and algorithm for dc distribution protection. *IEEE Transactions on Industry Applications*, 53(3):1834–1840.

Fletcher, S. (2013). *Protection of Physically Compact Multiterminal DC Power Systems*. PhD thesis, University of Strathclyde.

Fletcher, S. D. A., Norman, P. J., Fong, K., Galloway, S. J., and Burt, G. M. (2014). High-speed differential protection for smart dc distribution systems. *IEEE Transactions on Smart Grid*, 5(5):2610–2617.

Fletcher, S. D. A., Norman, P. J., Fong, K., Galloway, S. J., and Burt, G. M. (2014). High-speed differential protection for smart dc distribution systems. *IEEE Transactions on Smart Grid*, 5(5):2610–2617.

Fletcher, S. D. A., Norman, P. J., Galloway, S. J., Crolla, P., and Burt, G. M. (2012).

Optimizing the roles of unit and non-unit protection methods within dc microgrids. *IEEE Transactions on Smart Grid*, 3(4):2079–2087.

Gao, H., Li, J., and Xu, B. (2017). Principle and implementation of current differential protection in distribution networks with high penetration of dgs. *IEEE Transactions on Power Delivery*, 32(1):565–574.

Guo, W.-M., Mu, L.-H., and Zhang, X. (2017). Fault models of inverter-interfaced distributed generators within a low-voltage microgrid. *IEEE Trans. on Power Delivery*, 32(1):453–461.

Gururani, A., Mohanty, S. R., and Mohanta, J. C. (2016). Microgrid protection using hilbert–huang transform based-differential scheme. *IET Generation, Transmission & Distribution*, 10:3707–3716.

Halabi, N., Shen, C., Yin, X., Liu, X., and Shen, Z. J. (2011). Current phase comparison pilot scheme for distributed generation networks protection. *Applied Energy*, 18(12):4563–4569.

Hashemi, S. M., Hagh, M. T., and Seyedi, H. (2013). Transmission-line protection: A directional comparison scheme using the average of superimposed components. *IEEE Transactions on Power Delivery*, 28(2):955–964.

Hirose, K. (2013). Behavior of the sendai microgrid during and after the 3.11 great east japan disaster. In *Proc. 35th IEEE Int. Telecommun. Energy Conf. (INTELEC), Hamburg, Germany*, pages 1–6.

Hong, Y.-Y. and Cabatac, M. T. A. M. (2020). Fault detection, classification, and location by static switch in microgrids using wavelet transform and taguchi-based artificial neural network. *IEEE Systems Journal*, 14(2):2725–2735.

Hooshyar, A. and Iravani, R. (2017). Microgrid protection. *Proceedings of the IEEE*, 105(7):1332–1353.

Hooshyar, A. and Iravani, R. (2018). A new directional element for microgrid protection. *IEEE Trans. on Smart Grid*, 9(6):6862–6876.

Jain, R., Lubkeman, D. L., and Lukic, S. M. (2019). Dynamic adaptive protection for distribution systems in grid-connected and islanded modes. *IEEE Transactions on Power Delivery*, 34(1):281–289.

Jia, K., Wang, C., Bi, T., Zhu, R., and Xuan, Z. (2019a). Transient current waveform similarity based protection for flexible dc distribution system. *IEEE Transactions on Industrial Electronics*, 66(12):9301–9311.

Jia, K., Yang, Z., Fang, Y., Bi, T., and Sumner, M. (2019b). Influence of inverter-interfaced renewable energy generators on directional relay and an improved scheme. *IEEE Transactions on Power Electronics*, 34(12):11843–11855.

Jiang, S., Fan, C., Huang, N., Zhu, Y., and He, M. (2019). A fault location method for dc lines connected with dab terminal in power electronic transformer. *IEEE Transactions on Power Delivery*, 34(1):301–311.

Kar, S. and Samantaray, Rajan, S. (2014). Time-frequency transform-based differential scheme for microgrid protection. *IET Generation, Transmission and Distribution*, 8(2):310–320.

Kar, S., Samantaray, S. R., and Zadeh, M. D. (2017). Data-mining model based intelligent differential microgrid protection scheme. *IEEE Systems Journal*, 11(2):1161–1169.

Kavi, M., Mishra, Y., and Vilathgamuwa, M. (2018). Morphological fault detector for adaptive overcurrent protection in distribution networks with increasing photovoltaic penetration. *IEEE Transactions on Sustainable Energy*, 9(3):1021–1029.

Kim, J.-Y., Jeon, J.-H., Kim, S.-K., Cho, C., Park, J. H., Kim, H.-M., and Nam, K.-Y. (2010). Cooperative control strategy of energy storage system and microsources for stabilizing the microgrid during islanded operation. *IEEE Transactions on Power Electronics*, 25(12):3037–3048.

Kocer, M. C., Cengiz, C., Gezer, M., Gunes, D., Cinar, M. A., Alboyaci, B., and Onen, A. (2019). Assessment of battery storage technologies for a turkish power network. *Sustainability*, 11(13).

Kumar, D., Zare, F., and Ghosh, A. (2017). Dc microgrid technology: System architectures, ac grid interfaces, grounding schemes, power quality, communication networks, applications, and standardizations aspects. *IEEE Access*, 5:12230–12256.

Laaksonen, H. J. (2010). Protection principles for future microgrids. *IEEE Trans. on Power Electronics*, 25(12):2910–2918.

Liu, J., Miura, Y., and Ise, T. (2016). Comparison of dynamic characteristics between virtual synchronous generator and droop control in inverter-based distributed generators. *IEEE Transactions on Power Electronics*, 31(5):3600–3611.

Ma, J., Ma, W., Wang, X., and Wang, Z. (2013). A new adaptive voltage protection scheme for distribution network with distributed generations. *Canadian Journal of Electrical and Computer Engineering*, 36(4):142–151.

Mahamedi, B., Zhu, J., Eskandari, M., Fletcher, J., and Li, L. (2018). Protection of inverter-based microgrids from ground faults by an innovative directional element. *IET Generation, Transmission and Distribution*, 12(22):5918–5927.

Mahat, P., Chen, Z., Bak-Jensen, B., and Bak, C. L. (2011). A simple adaptive overcurrent protection of distribution systems with distributed generation. *IEEE Transactions on Smart Grid*, 2(3):428–437.

Manson, S. and McCullough, E. (2021). Practical microgrid protection solutions: Promises and challenges. *IEEE Power and Energy Magazine*, 19(3):58–69.

Meghwani, A., Gokaraju, R., Srivastava, S. C., and Chakrabarti, S. (2020). Local measurements-based backup protection for dc microgrids using sequential analyzing technique. *IEEE Systems Journal*, 14(1):1159–1170.

Meghwani, A., Srivastava, S., and Chakrabarti, S. (2017). A non-unit protection scheme for dc microgrid based on local measurements. *IEEE Trans. on Power Delivery*, 32(1):172–181.

Mishra, D. P., Samantaray, S. R., and Joos, G. (2016). A combined wavelet and data-mining based intelligent protection scheme for microgrid. *IEEE Transactions on Smart Grid*, 7(5):2295–2304.

Mishra, P., Pradhan, A. K., and Bajpai, P. (2020). A positive sequence relaying method for solar photovoltaic integrated distribution system. *IEEE Transactions on Power Delivery*, pages 1–1.

Mobarrez, M., Fregosi, D., Bhattacharya, S., and Bahmani, M. (2017). Grounding architectures for enabling ground fault ride-through capability in dc microgrids. In *2017 IEEE Second International Conference on DC Microgrids (ICDCM)*, pages 81–87.

Mohan, M. and Vittal, K. (2019). Dc fault protection in multi-terminal vsc-based hvdc transmission systems with current limiting reactors. *J. Electr. Eng. Technol. 14*, pages 1–12.

Mohanty, R. and Pradhan, A. K. (2018a). Protection of smart dc microgrid with ring configuration using parameter estimation approach. *IEEE Transactions on Smart Grid*, 9(6):6328–6337.

Mohanty, R. and Pradhan, A. K. (2018b). A superimposed current based unit protection scheme for dc microgrid. *IEEE Transactions on Smart Grid*, 9(4):3917–3919.

Mohanty, R. and Pradhan, A. K. (2019). Dc ring bus microgrid protection using the oscillation frequency and transient power. *IEEE Systems Journal*, 13(1):875–884.

Mohanty, R., Sahoo, S., Pradhan, A. K., and Blaabjerg, F. (2021). A cosine similarity-based centralized protection scheme for dc microgrids. *IEEE Journal of Emerging and Selected Topics in Power Electronics*, 9(5):5646–5656.

Monadi, M., Amin Zamani, M., Ignacio Candela, J., Luna, A., and Rodriguez, P. (2015). Protection of ac and dc distribution systems embedding distributed energy resources: A comparative review and analysis. *Renewable and Sustainable Energy Reviews*, 51:1578–1593.

Moon, W., Won, J., Huh, J., and Kim, J. (2013). A study on the application of a superconducting fault current limiter for energy storage protection in a power distribution system. *IEEE Transactions on Applied Superconductivity*, 23(3):5603404–5603404.

Muda, H. and Jena, P. (2017a). Sequence currents based adaptive protection approach for dns with distributed energy resources. *IET Generation, Transmission and Distribution*, 11:154–165.

Muda, H. and Jena, P. (2017b). Superimposed adaptive sequence current based microgrid protection: A new technique. *IEEE Transactions on Power Delivery*, 32(2):757–767.

Naveen, P. and Jena, P. (2017). A review on issues and coordination strategies for over current protection in microgrid. In *2017 14th IEEE India Council International Conference (INDICON)*, pages 1–6.

Naveen, P. and Jena, P. (2021). Adaptive protection scheme for microgrid with multiple point of common couplings. *IEEE Systems Journal*, 15(4):5618–5629.

Nimpitiwan, N., Heydt, G. T., Ayyanar, R., and Suryanarayanan, S. (2007). Fault current contribution from synchronous machine and inverter based distributed generators. *IEEE Transactions on Power Delivery*, 22(1):634–641.

Nsengiyaremye, J., Bikash, P. C., and Begovic, M. M. (2021). Low-cost communication-assisted line protection for multi-inverter based microgrids. *IEEE Transactions on Power Delivery*, 36(6):3371–3382.

Nsengiyaremye, J., Pal, B. C., and Begovic, M. M. (2020). Microgrid protection using low-cost communication systems. *IEEE Transactions on Power Delivery*, 35(4):2011–2020.

O'Rourke, C. J., Qasim, M. M., Overlin, M. R., and Kirtley, J. L. (2019). A geometric interpretation of reference frames and transformations: dq0, clarke, and park. *IEEE Transactions on Energy Conversion*, 34(4):2070–2083.

Papaspiliotopoulos, V., Kleftakis, V., Kotsampopoulos, P., Korres, G., and Hatziargyriou, N. (2014). Hardware-in-the-loop simulation for protection blinding and sympathetic tripping in distribution grids with high penetration of distributed generation. In *MedPower 2014*, pages 1–6.

Park, J. and Candelaria, J. (2013). Fault detection and isolation in low-voltage dc-bus microgrid system. *IEEE Transactions on Power Delivery*, 28(2):779–787.

Park, J., Candelaria, J., Ma, L., and Dunn, K. (2013). Dc ring-bus microgrid fault protection and identification of fault location. *IEEE Transactions on Power Delivery*, 28(4):2574–2584.

Patrao, I., Figueres, E., Garcerá, G., and González-Medina, R. (2015). Microgrid architectures for low voltage distributed generation. *Renewable and Sustainable Energy Reviews*, 43:415 – 424.

Rakhra, P. (2017). *On the Protection of Compact DC Power Systems with High-Power Energy Storage*. PhD thesis, University of Strathclyde.

Rocabert, J., Luna, A., Blaabjerg, F., and Rodríguez, P. (2012). Control of power converters in ac microgrids. *IEEE Transactions on Power Electronics*, 27(11):4734–4749.

Sagiraju, D. K. V., Obulesu, Y., and Choppavarapu, S. B. (2017). Dynamic performance improvement of standalone battery integrated pmsg wind energy system using proportional resonant controller. *Engineering Science and Technology, an International Journal*, 20(4):1353–1365.

Salomonsson, D., Soder, L., and Sannino, A. (2009). Protection of low-voltage dc microgrids. *IEEE Transactions on Power Delivery*, 24(3):1045–1053.

Satpathi, K., Yeap, Y. M., Ukil, A., and Geddada, N. (2018). Short-time fourier transform based transient analysis of vsc interfaced point-to-point dc system. *IEEE Transactions on Industrial Electronics*, 65(5):4080–4091.

Shahidehpour, M. (2014). Microgrids for enhancing the economics, reliability, and resilience of smart cities – an iit experience. In *2014 Smart Grid Conference (SGC)*, pages 1–1.

Shamsoddini, M., Vahidi, B., Razani, R., and Mohamed, Y. A.-R. I. (2020). A novel protection scheme for low voltage dc microgrid using inductance estimation. *International Journal of Electrical Power and Energy Systems*, 120:105992.

Sharma, N. K. and Samantaray, S. R. (2020). Pmu assisted integrated impedance angle-based microgrid protection scheme. *IEEE Transactions on Power Delivery*, 35(1):183–193.

Shuai, Z., He, D., Xiong, Z., Lei, Z., and John Shen, Z. (2019). Comparative study of short-circuit fault characteristics for vsc-based dc distribution networks with different distributed generators. *IEEE Journal of Emerging and Selected Topics in Power Electronics*, 7(1):528–540.

Shuai, Z., Member, S., Shen, C., Yin, X., Liu, X., and Shen, Z. J. (2018). Fault Analysis of Inverter-Interfaced Distributed Generators. *IEEE Transactions on Power Delivery*, 33(3):1223–1235.

Singh, M. and Basak, P. (2019). Adaptive protection methodology in microgrid for fault location and nature detection using q0 components of fault current. *IET Generation, Transmission and Distribution*, 13(6):760–769.

Sufyan, M., Rahim, N. A., Aman, M. M., Tan, C. K., and Raihan, S. R. S. (2019). Sizing and applications of battery energy storage technologies in smart grid Sizing and applications of battery energy storage technologies in smart grid system : A review. (February).

Teimourzadeh, S., Aminifar, F., Davarpanah, M., and Shahidehpour, M. (2019). Adaptive protection for preserving microgrid security. *IEEE Transactions on Smart Grid*, 10(1):592–600.

Telukunta, V., Pradhan, J., Agrawal, A., Singh, M., and Srivani, S. G. (2017). Protection challenges under bulk penetration of renewable energy resources in power systems: A review. *CSEE Journal of Power and Energy Systems*, 3(4):365–379.

Tselepis, S. (2012). 12 years operation of the gaidouromantra microgrid in kythnos island. In *5th International Conference on Integration of RES and DER, Hamburg, Berlin*.

Ukil, A. (2016). Detection of direction change in prefault current in current-only directional overcurrent protection. In *IECON 2016 - 42nd Annual Conference of the IEEE Industrial Electronics Society*, pages 3829–3833.

Ukil, A., Deck, B., and Shah, V. H. (2010). Smart distribution protection using current-only directional overcurrent relay. In *2010 IEEE PES Innovative Smart Grid Technologies Conference Europe (ISGT Europe)*, pages 1–7.

Ukil, A., Member, S., Deck, B., and Shah, V. H. (2012). Current-Only Directional Overcurrent Protection for Distribution Automation : Challenges and Solutions. *IEEE Transactions on Smart Grid*, 3(4):1687–1694.

Ustun, T. S., Ozansoy, C., and Ustun, A. (2013). Fault current coefficient and time delay assignment for microgrid protection system with central protection unit. *IEEE Transactions on Power Systems*, 28(2):598–606.

Voima, S. and Kauhaniemi, K. (2014). Using distance protection in smart grid environment. In *IEEE PES Innovative Smart Grid Technologies, Europe*, pages 1–6.

Voima, S., Laaksonen, H., and Kauhaniemi, K. (2014). Adaptive protection scheme for smart grids. In *12th IET International Conference on Developments in Power System Protection (DPSP 2014)*, pages 1–6.

Yang, J., Fletcher, J. E., and O'Reilly, J. (2012). Short-circuit and ground fault analyses and location in vsc-based dc network cables. *IEEE Transactions on Industrial Electronics*, 59(10):3827–3837.

Yap, K. Y., Sarimuthu, C. R., and Lim, J. M.-Y. (2019). Virtual inertia-based inverters for mitigating frequency instability in grid-connected renewable energy system: A review. *Applied Sciences*, 9(24).

Yeap, Y. M., Geddada, N., and Ukil, A. (2017). Analysis and validation of wavelet transform based dc fault detection in hvdc system. *Applied Soft Computing*, 61:17 – 29.

Zamani, M. A. (2012). *Protection and Control of Active Distribution Networks and Microgrids*. PhD thesis, The University of Western Ontario.

Zamani, M. A., Sidhu, T. S., and Yazdani, A. (2014). Investigations into the control and protection of an existing distribution network to operate as a microgrid: A case study. *IEEE Transactions on Industrial Electronics*, 61(4):1904–1915.

Zhang, L., Shi, H., Sun, K., Xiao, X., and Lu, X. (2016). A smooth switch method for battery energy storage systems between vf mode and pq mode by utilizing electromagnetic relay. In *2016 IEEE 8th International Power Electronics and Motion Control Conference (IPEMC-ECCE Asia)*, pages 3702–3707.

Zuo, Y., Yuan, Z., Sossan, F., Zecchino, A., Cherkaoui, R., and Paolone, M. (2021). Performance assessment of grid-forming and grid-following converter-interfaced battery energy storage systems on frequency regulation in low-inertia power grids. *Sustainable Energy, Grids and Networks*, 27:100496.

Appendix A

AC Microgrid Parameters

Grid	Nominal voltage	11 kV
	Rated frequency	50 Hz
Transformer	Rated capacity	250 kVA
	Transformation ratio	11/0.415 kV
Loads	L1 & L2	10 kW, 5 kVAR
	L3 (variable)	40 kW, 20 kVAR
BESS	Li-ion battery	
	Rated voltage	360 V
	Rated capacity	160 Ah
	Interface converter	Buck Boost
PV System	Generation Capacity	40 kW
	Voltage at MPP	580 V
	Current at MPP	58A
	Interface converter	Boost
DC bus	Voltage	700 V
	Capacitance	5 mF
VSI	Rated voltage	415 V
	Interface inductance	2.5 mH
	Ripple filter	$C_f = 10\mu F$; $R_f = 5\Omega$
Lines	Resistance per km	0.315Ω
	Reactance per km	0.074Ω
	Length of lines 1-3	2 km

Appendix B

DC Microgrid Parameters

AC System	MV Utility voltage	11 kV
	Rated frequency	50 Hz
	MV/LV transformer power	250 kVA
	LVAC voltage	415 V
VSC	DC-link voltage	700 V
	DC link capacitance	6 mF
	Grid interfacing inductance	5 mH
	Switching frequency	10 kHz
BESS	Li-ion battery	
	Rated voltage	360 V
	Rated capacity	160 Ah
PV System	Generation Capacity	30 kW
	Voltage at MPP	580 V
	Current at MPP	53A
Cable	Resistance per km	0.125Ω
	Inductance per km	0.56mH
BESS Converter	Buck Boost	
	DC link capacitance	6 mF
	Inductance	0.8 mH
	Switching frequency	10 kHz
PV Converter	Boost	
	DC link capacitance	6 mF
	Inductance	2 mH
	Switching frequency	10 kHz
Loads	L1	25 kW, 5kVAR
	L2 & L5 (P-P)	30 Ω
	L3 & L4 (P-G)	15 Ω

Appendix C

List of Publications

INTERNATIONAL JOURNALS

1. Ann Mary Joshua, K Panduranga Vittal, “ Protection schemes for a battery energy storage system based microgrid,” **Electric Power Systems Research (Elsevier), SCIE Indexed**, 2022.
   DOI:204.107701.10.1016/j.epsr.2021.107701

2. Ann Mary Joshua, K Panduranga Vittal, “Incremental transient power-based protection scheme for a DC microgrid,” **Electrical Engineering (Springer), SCI Indexed**, 2022
   DOI:10.1007/s00202-021-01461-9

3. Ann Mary Joshua, K Panduranga Vittal, “Superimposed Current Based Differential Protection Scheme for AC Microgrid Feeders,” Accepted in **Applied Energy (Elsevier), SCI Indexed**.

INTERNATIONAL CONFERENCE PROCEEDINGS

1. Ann Mary Joshua, K Panduranga Vittal,“Transient behavioural modelling of Battery Energy Storage System supporting Microgrid” **2020 IEEE International Conference on Power Electronics, Smart Grid and Renewable Energy (PESGRE 2020)**, Hotel Le Meridian, Cochin, Kerala, 2020.
   DOI:10.1109/PESGRE45664.2020.9070389.

Curriculum Vitae

Name : Ann Mary Joshua

Permanent Address : Kuzhiyilazhikathu (H),
Karickam P.O, Kottarakkara,
Kollam, Kerala, India – 691531.
Email : annmaryjoshua@gmail.com

Qualifications : **B.Tech.** (Electrical & Electronics Engg), 2005,
M. G. University, Kottayam, Kerala, India.

M.Tech. (Industrial Drives & Control), 2008,
M. G. University, Kottayam, Kerala, India.

Experience : **Lecturer,** (2008-2009)
Amal Jyothi College of Engineering, Kerala

Assistant Engineer, (May 2010 - Oct 2013)
Kerala State Electricity Board

Assistant Professor, (Oct 2013 - July 2018)
Department of Technical Education, Kerala

Research Scholar, (July 2018 - July 2021)
National Institute of Technology Karnataka, Surathkal

Assistant Professor, (July 2021 - till date)
Department of Technical Education, Kerala